THE DRAG AND LIFT CHARATERISTICS OF A CYLINDER PLACED NEAR A PLANE SURFACE

Selâhattin Göktun

NAVAL POSTGRADUATE SCHOOL
Monterey, California

THESIS

THE DRAG AND LIFT CHARACTERISTICS
OF A
CYLINDER PLACED NEAR A PLANE SURFACE

by

Selâhattin Göktun

December 1975

Thesis Advisor: T. Cooper

Approved for public release; distribution unlimited.

REPORT DOCUMENTATION PAGE

READ INSTRUCTIONS BEFORE COMPLETING FORM

1. REPORT NUMBER	2. GOVT ACCESSION NO. / 3. RECIPIENT'S CATALOG NUMBER
4. TITLE (and Subtitle): The Drag and Lift Characteristics of a Cylinder Placed Near a Plane Surface	5. TYPE OF REPORT & PERIOD COVERED: Master's Thesis; December 1975
	6. PERFORMING ORG. REPORT NUMBER
7. AUTHOR(s): Selâhattin Göktun	8. CONTRACT OR GRANT NUMBER(s)
9. PERFORMING ORGANIZATION NAME AND ADDRESS: Naval Postgraduate School, Monterey, California 93940	10. PROGRAM ELEMENT, PROJECT, TASK AREA & WORK UNIT NUMBERS
11. CONTROLLING OFFICE NAME AND ADDRESS: Naval Postgraduate School, Monterey, California 93940	12. REPORT DATE: December 1975
	13. NUMBER OF PAGES: 114
14. MONITORING AGENCY NAME & ADDRESS (if different from Controlling Office)	15. SECURITY CLASS. (of this report): Unclassified
	15a. DECLASSIFICATION/DOWNGRADING SCHEDULE

16. DISTRIBUTION STATEMENT (of this Report)

Approved for public release; distribution unlimited.

17. DISTRIBUTION STATEMENT (of the abstract entered in Block 20, if different from Report)

18. SUPPLEMENTARY NOTES

19. KEY WORDS (Continue on reverse side if necessary and identify by block number)

Drag Coefficient
Lift Coefficient
Cylinder, Right Circular

20. ABSTRACT (Continue on reverse side if necessary and identify by block number)

Surface pressure, drag and lift coefficients have been experimentally determined for a right circular cylinder located near a plane surface and placed in a cross flow of air. Parametric studies were carried out for Reynolds number varying from 90,000 to 250,000, three plate lengths and a variety of cylinder to plate spacings. The variation of the drag coefficient as a function of gap size was found to exhibit an interesting and unexpected trend. The drag was a

(20. ABSTRACT Continued)

minimum when the cylinder was resting on the plate and was a maximum at a gap size of approximately one cylinder radius. Flow visualization studies together with detailed measurements of the vortex shedding frequency in the cylinder wake indicate that the plate interferes with the formation of the vortex street in the cylinder wake when it is located within a cylinder radius of the cylinder. This interference disturbs the cylinder base pressure which in turn influences the magnitude of the drag coefficient.

The Drag and Lift Characteristic of a Cylinder Placed Near a Plane Surface

by

Selâhattin Göktun
Lieutenant, Turkish Navy
B.S.M.E., Naval Postgraduate School, 1975

Submitted in partial fulfillment of the
requirements for the degree of

MASTER OF SCIENCE IN MECHANICAL ENGINEERING

from the

NAVAL POSTGRADUATE SCHOOL
December 1975

ABSTRACT

Surface pressure, drag and lift coefficients have been experimentally determined for a right circular cylinder located near a plane surface and placed in a cross flow of air. Parametric studies were carried out for Reynolds numbers varying from 90,000 to 250,000, three plate lengths and a variety of cylinder to plate spacings. The variation of the drag coefficient as a function of gap size was found to exhibit an interesting and unexpected trend. The drag was a minimum when the cylinder was resting on the plate and was a maximum at a gap size of approximately one cylinder radius. Flow visualization studies together with detailed measurements of the vortex shedding frequency in the cylinder wake indicate that the plate interferes with the formation of the vortex street in the cylinder wake when it is located within a cylinder radius of the cylinder. This interference disturbs the cylinder base pressure which in turn influences the magnitude of the drag coefficient.

TABLE OF CONTENTS

LIST OF ILLUSTRATIONS

ACKNOWLEDGMENT

I would like to express my sincere thanks and appreciation to my thesis advisor, Professor Thomas E. Cooper, whose professionalism, knowledge, and encouragement were inspirational to me throughout this entire endeavor.

Also, I would like to extend my appreciation to Professor Paul F. Pucci, who provided me with many helpful suggestions regarding the finalization of this work.

I. INTRODUCTION

In this study, the flow field, drag and lift characteristics of a cylinder placed in close proximity to a plane surface in a cross flow of air were investigated. Previous work of this nature has concentrated primarily on free cylinders.

This project is a follow-on study to an investigation originated by McComas [1] and continued by Gnerlich [2]. In both of these previous studies, primary emphasis was devoted to obtaining the heat transfer characteristics of a cylinder placed in proximity to a plane surface. Although surface pressure data were obtained in these studies, these data were not analyzed in detail. The present investigation has focused on obtaining drag and lift information on the cylinder as a function of the size of the gap between the cylinder and plate. A range of Reynolds numbers varying from 90,000 to 250,000 was investigated and the length of plate ahead of the cylinder was varied from 2.0 to 8.0 cylinder diameters. Also, the flow field surrounding the cylinder was studied in detail with the aid of a flow visualization technique and with a hotwire anemometer.

The present experiments were conducted using the Mechanical Engineering Department wind tunnel located in Building 500 and the water channel located in Building 234 on the Naval Postgraduate School campus. The wind tunnel,

described in detail in Section III, has a speed range of 15 to 250 ft/sec, and is equipped with a traversing mechanism and hotwire anemometer which can be used to obtain velocity information throughout the test section. The hotwire was also used to measure the vortex shedding frequency behind the cylinder.

Experiments were conducted in the wind tunnel at uncorrected free stream Reynolds numbers of 90,000, 153,000, 250,000 for plate to cylinder spacings of $d/r = 0.0$, 0.25, 0.5, 1.0, 2.0, 3.0, 4.0, 5.33, and 9.33 (no plate case) where d = gap size and r = cylinder radius (See Figure 1). For these studies the plate length ahead of the cylinder was four cylinder diameters ($L/D = 4.0$). Experiments were also performed at a free stream Reynolds number of 153,000 with the same d/r ratios but with plate leading edge lengths of 2.0 and 8.0 cylinder diameters ($L/D = 2.0$ and 8.0).

In calculating and plotting the pressure drag coefficient as a function of gap spacing an interesting and unexpected trend was revealed. Over the range of Reynolds numbers investigated, it was found that the minimum pressure drag coefficient occurred when the plate was attached to the cylinder. Further, these curves also indicated a maximum drag coefficient at $d/r = 1.0$. The lift coefficient was found to be a maximum when the plate and cylinder were in contact and continuously decreased as the gap size was increased. In order to provide a qualitative explanation

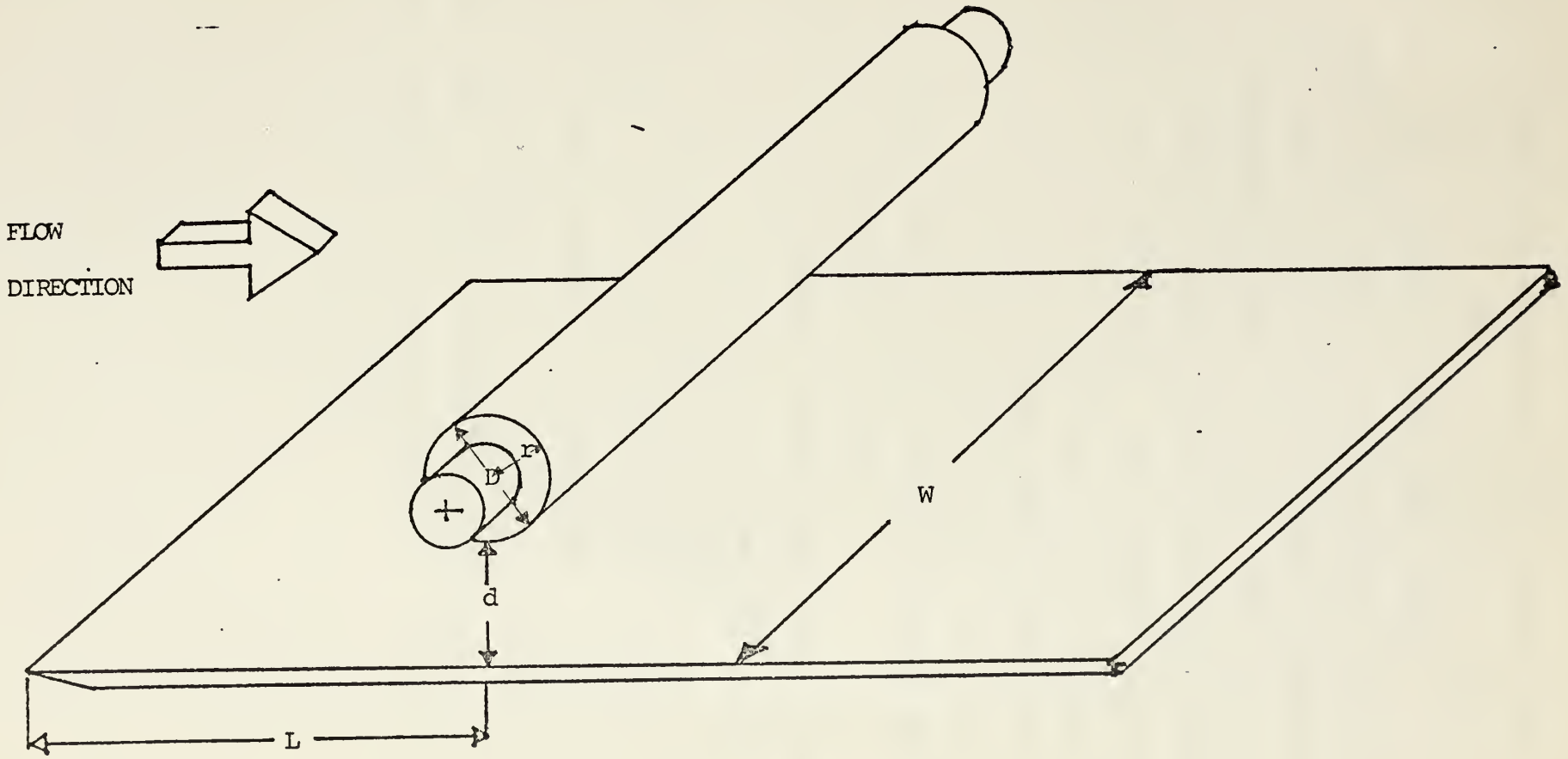

FIGURE 1. Schematic diagram of plate-cylinder arrangement

for the existence of a maximum in the pressure drag coefficient curve at $d/r = 1.0$, a flow visualization experiment was conducted in the water channel. In this water channel (See Section III for detailed description) a 14 inch long plexiglass flat plate and 1.5 inch diameter hollow plexiglass cylinder were used. The system was scaled for geometric similitude with the experimental apparatus in the wind tunnel. The cylinder was equipped with three dye ports and the space between the cylinder plate was varied using a lifting device which was attached to the plate. Due to limitations in the water pump, the maximum Reynolds number which could be attained with this apparatus was approximately 10,000.

The flow visualization revealed very clearly that in the range $0 \leq d/r < 1$ the plate was interfering with the formation of the vortex street that forms in the wake of a free cylinder. The surface pressure data indicated that this interference produced a significant effect on the cylinder base pressure and an attendant effect on the cylinder drag. Hotwire anemometer measurements of the vortex shedding frequency were also made in the cylinder wake and tend to substantiate this claim.

II. BACKGROUND

The present investigation of the flow field around a cylinder placed in proximity to a plane surface was conducted concurrently with an investigation by Kösemen [3] of the heat transfer characteristics of a heated cylinder located near a plane surface. Information obtained from the flow experiments proved useful in explaining the heat transfer trends observed by Kösemen. Likewise, Kösemen's measurements provided insight into a better understanding of the flow field.

Data relating to the drag and heat transfer characteristics of the cylinder-plate geometry under investigation were not found in the literature. Such information would be of obvious value in the design of heated piping systems located near walls and in heat exchanger design.

While numerous investigations have been conducted upon free cylinders having continuous surfaces and diverse shapes, few studies have been made of the flow patterns associated with a plate-cylinder system. Roshko [4] conducted an experiment using a splitter plate located at various locations behind a circular cylinder. He concluded that vortex dynamics were indeed important and that any interference with their formation would have a strong influence on the base pressure and drag of the cylinder. By placing a splitter plate along the centerline of the wake, it was found that the normal

periodic vortex formation was inhibited and the base pressure was found to be increased considerably. Roshko's investigation was very informative and provided insight into our investigation.

Another study which provided insight into our problem was an investigation by Spivak [5] of the characteristics of vortex formation in the wake behind a pair of cylinders located at various gap spacings in a cross flow. Spivak found:

a) When two cylinders located in cross flow are separated by a gap just smaller than a cylinder diameter, an instability in the wake vortex pattern occurs.

b) At larger gap sizes the cylinders behave like independent bodies.

c) At spacings less than one-half diameter a low gap vortex shedding frequency is observed. Between one-half and one diameter a high gap vortex shedding frequency is present decreasing to the independent cylinder value at a critical spacing of one cylinder diameter.

d) At very small gap sizes individual von Kármán vortex streets are not detached from each cylinder; instead, a coupled vortex street is formed by the overall system along with certain internal vortices that depend upon the gap. The internal vortices are generated in vortex sheets bordering a jet that emanates from the orifice formed by the adjacent sides of the two cylinders. Spivak's investigation was very informative and provided significant insights into our investigation.

III. EXPERIMENTAL APPARATUS

The wind tunnel, water channel, test cylinders and plates and their mounting are discussed in this section.

A. WIND TUNNEL

All data were collected in a subsonic, open circuit, wind tunnel manufactured by the Kenny Engineering Corporation of Monrovia, California. This tunnel was powered by a 75 HP, 1750 rpm variable-speed motor driving a 45 inch diameter adjustable pitch, vaneaxial fan (blower) capable of supplying air at 10,000 to 70,000 cubic feet per minute. The tunnel was equipped with six graded-mesh screens to control turbulence and a 24-inch manometer tube tapped into the stilling chamber and test section for velocity measurement. The tunnel was designed to operate at velocities ranging from approximately 15 ft/sec to 250 ft/sec. The turbulence intensity in the clear tunnel was measured as 0.2%.

The wind tunnel consists of the inlet section, test section (28" high x 20" wide x 6' long), diffuser and blower. The blower pulls air through the inlet past the test section. After passing the test section, the air enters the diffuser and then the blower. The blower then expels the air to the atmosphere. A schematic of the wind tunnel with pertinent dimensions is shown in Figure 2.

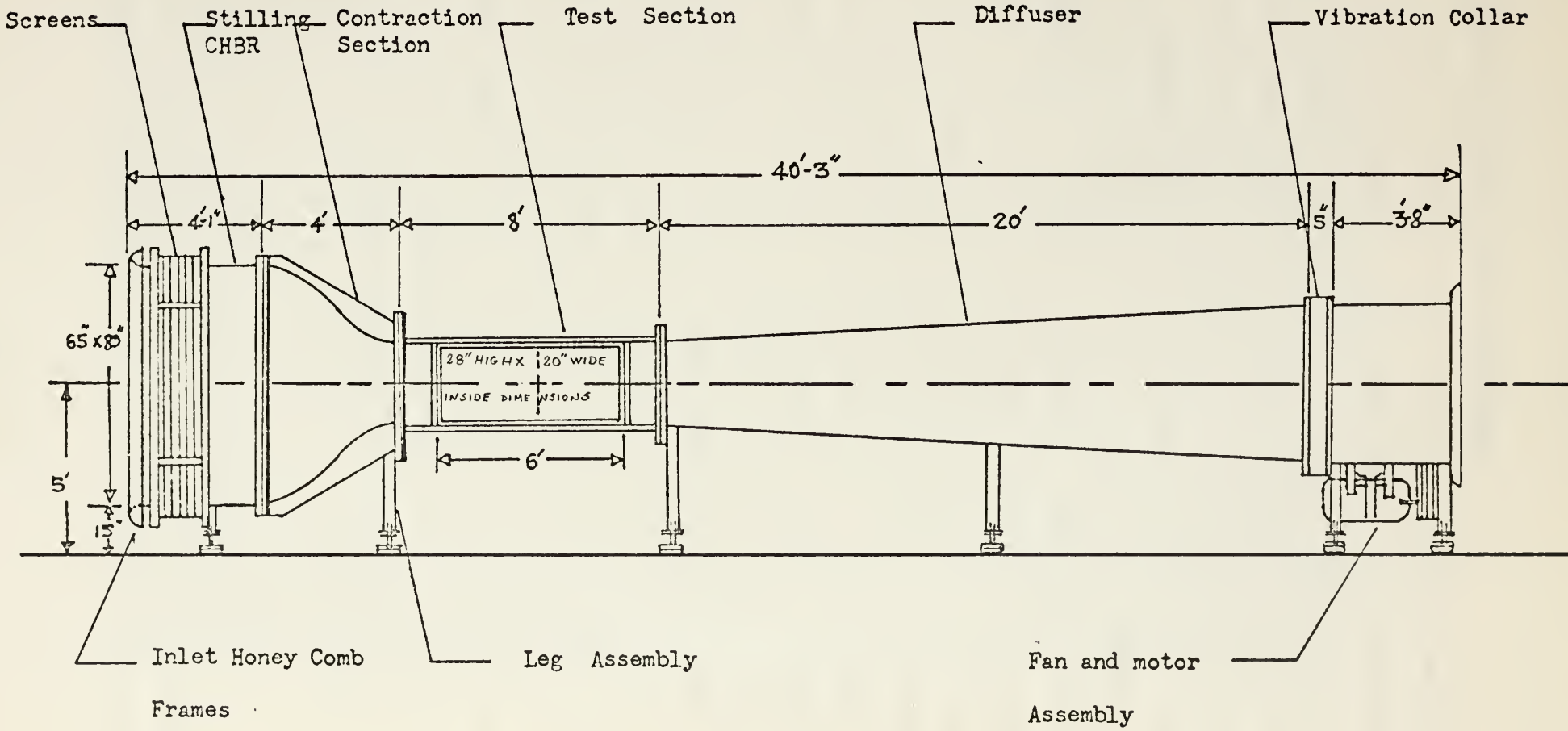

FIGURE 2. Schematic diagram of the wind tunnel

B. PRESSURE COEFFICIENT EXPERIMENT

In order to obtain static surface pressure measurements on a cylinder placed in this particular flow situation, a 3 inch diameter, 20 inch long, smooth, right circular cylinder constructed of aluminum was used. This cylinder was fitted with four 0.025 inch surface pressure taps located at the cylinder mid-point and spaced at 90-degree intervals around its circumference. The circumference of the cylinder was scribed in 5 degree increments. Reference lines were scribed on the test section wall at 90 degree intervals so that the matching of the scribe marks on the cylinder with these lines provided a means of accurately establishing the angular location of the pressure taps. The pressure cylinder is shown in Figure 3. The surface pressure taps were connected to a bank of 8 water filled manometer tubes by means of plastic tubing. Two tubes of the manometer bank were referenced against atmospheric pressure. The wind tunnel stilling chamber static pressure and test section (free stream) static pressure were measured on the same manometer bank through pre-existing connections on the wind tunnel. The experiments were performed to find the variation of the surface pressure around the circumference of the cylinder as a function of gap size, Reynolds number and plate length.

The plates used in these experiments were manufactured from 1/2 inch plexiglass. These plates were 40 inches, 46 inches, and 58 inches long, respectively. To minimize

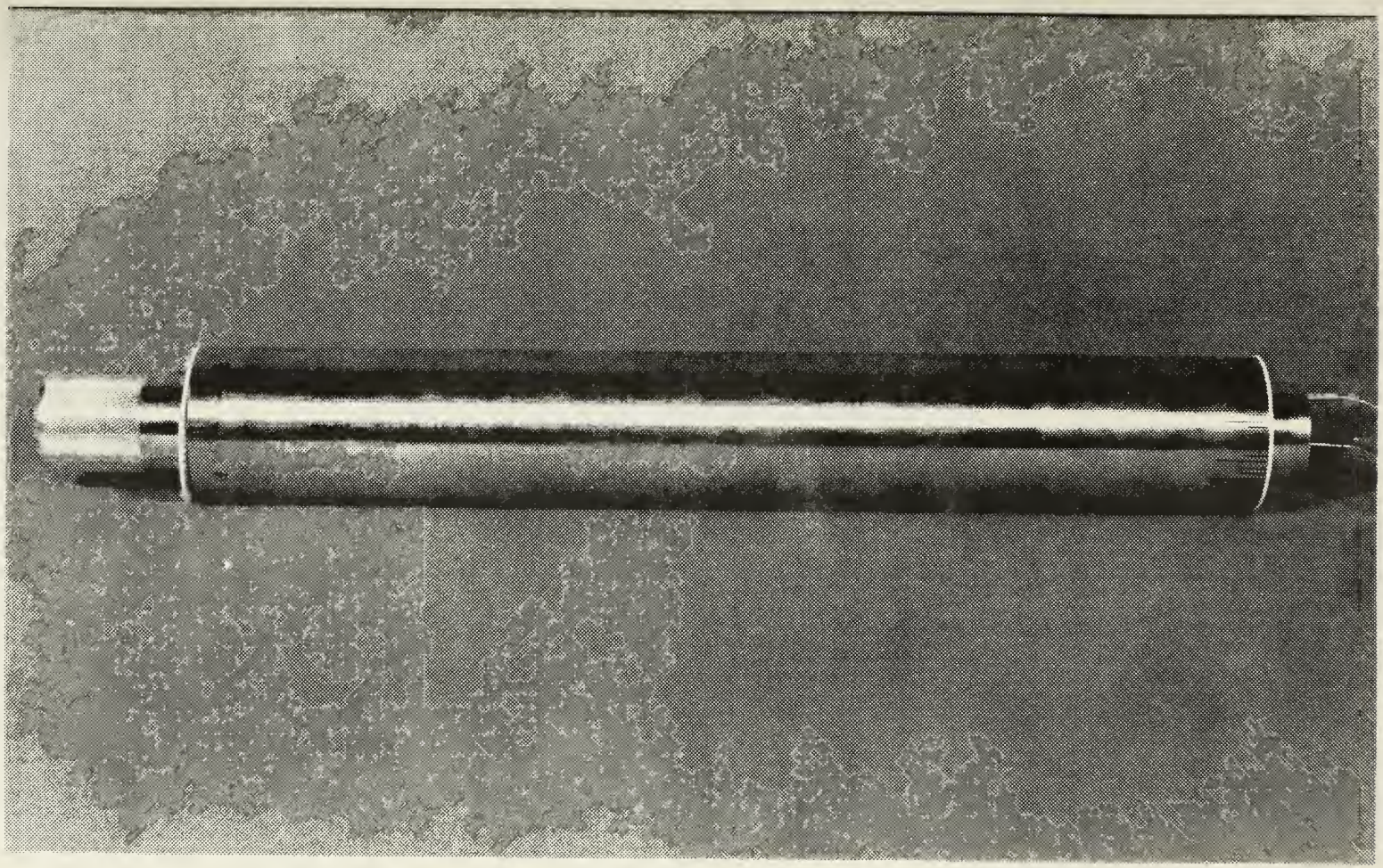

Figure 3 Photograph of the cylinder used to collect pressure data.

the influence of the downstream edge on the flow patterns around the cylinder, the trailing edge in all studies was maintained at a length of 34 inches. This provided leading edge lengths of 6 inches, 12 inches, and 24 inches, respectively. The width of the plates was 20 inches and they were beveled on the under side of the leading edge to a 12 degree angle.

The plates and cylinder were placed in the tunnel horizontally in such a way that the leading edge of the plates extended 2, 4, and 8 cylinder diameters ahead of the cylinder centerline. The plates were connected by means of two iron angles to a threaded rod extending through the tunnel floor which was capable of moving the plates vertically and a rear brace which locked in position by means of a split nut. A typical plate and cylinder arrangement is shown in Figure 4. It was possible to locate the plate at any position relative to the cylinder from attached to a maximum possible distance of 8 inches away.

C. FLOW VISUALIZATION EXPERIMENT

The apparatus used for flow visualization consisted of a converging wooden water channel 15 feet in length and 13 inches deep with a plexiglass test section 13 inches long, 12 inches wide, and 13 inches deep. A hollow, 1.5-inch diameter plexiglass cylinder was attached between the test section walls with its longitudinal axis located eight inches from the test section floor. In order to preserve geometric

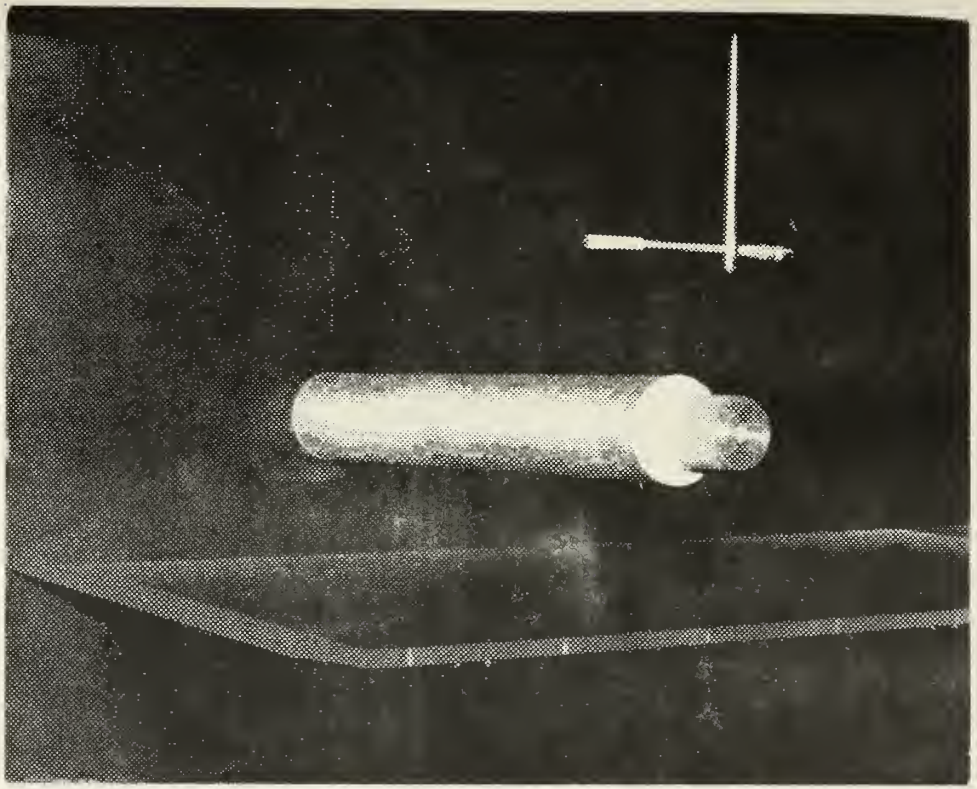

FIGURE 4. Photograph of the plate and cylinder arrangement in the wind tunnel

similitude, a 1/2 inch thick plexiglass flat plate was constructed to the scale of the ratio of the water channel cylinder diameter to the wind tunnel cylinder diameter (0.5:1). Thus, this plate was 14 inches long and 12 inches wide. The leading edge was beveled to a 12-degree angle as were the larger flat plates used in the wind tunnel. This flat plate was placed above the cylinder and was connected to an apparatus which raised or lowered the plate and also moved the plate to downstream and upstream directions horizontally. By moving the plate up and down and also horizontally, the desired gap sizes and L/D ratios were obtained.

The cylinder was fitted with three dye ports which were connected by polyethylene tubing to three separate dye reservoirs with individual valving located approximately three feet higher than the cylinder. This additional height insured that a constant head was maintained on the injection system, and the individual valving was necessary to allow each port to be operated separately in order that the flow field at various sections of the cylinder could be observed independently.

Water was pumped into the channel by means of an irrigation pump directly coupled to a Westinghouse Type SK dynamometer running as a motor. With the motor running at 1200 rpm, the pump output was approximately 1000 gallons per minute. Because of the limitation in the pump capacity, the highest Reynolds number which could be obtained in this

channel was approximately 10,000. The depth of water in the channel was controlled by a tilting weir at the end of the channel. For this particular experiment, the water depth was maintained at approximately 12 inches. This allowed the entire apparatus to be immersed to a depth sufficient to minimize free surface effects.

The cylinder and plate arrangement in the test section of the water channel is shown in Figure 5.

D. VORTEX FREQUENCY EXPERIMENT

The apparatus used to measure the vortex shedding frequency behind the cylinder in the wind tunnel consisted of the hotwire anemometer, TYPE 555 DUAL BEAM OSCILLOSCOPE with amplifier TYPE 1A1, KROHON-HETE MODEL 3100(R) Filter, and FLUKE 1950A Digital Counter.

The hotwire was attached to a tranversing mechanism by means of a narrow depth cantilever. The transversing mechanism allowed the hotwire to be moved to the desired locations during the experiments. The output of the hotwire anemometer was displayed on the oscilloscope. The Model 3100(R) filter is a solid state variable electronic band-pass filter which allows both high and low cut-off frequencies to be independently and continuously adjusted over a frequency range from 10 Hz to 1 MHz. The pass-band gain is unity (0 dB), with an attenuation rate of 24 dB per octave outside the pass-band, and a maximum attenuation of 80 dB. Using this filter the turbulent high frequency noise was cut-off at an

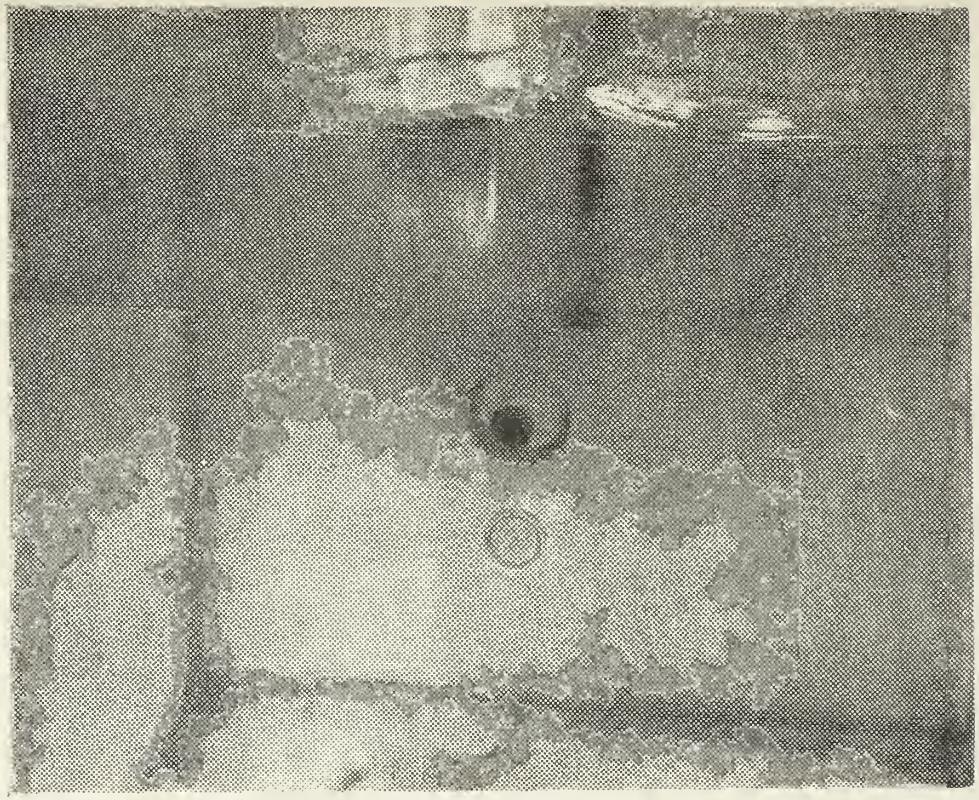

FIGURE 5. Photograph of the plate and cylinder arrangement in the water channel

output of less than 100 microvolts. This allowed the low shedding frequency to be obtained easily. The vortex shedding frequency was read in Hertz from the FLUKE 1950A Digital Counter.

IV. EXPERIMENTAL PROCEDURE

In order to ensure that significant and accurate data would be obtained, it was necessary to compare our initial results with previous work. Since Gnerlich [2] performed his experiment at a Reynolds number of 153,000 and $L/D = 4.0$, it was decided to check the apparatus at that Reynolds number. For this reason, an air stream speed of 98 ft/sec was used for comparative purposes. Experiments were then carried out using Reynolds numbers of 90,000 and 250,000 at $L/D = 4.0$. To examine the influence of the location of the plate leading edge, additional runs were also made at a Reynolds number of 153,000 and $L/D = 2.0$ and $L/D = 8.0$.

In the present work the Reynolds number is defined in the conventional fashion

$$Re = \frac{U_s \cdot D}{\nu}$$

where

Re = Reynolds number,

U_s = Free stream velocity at test section entrance, ft/sec (uncorrected for blockage),

D = Cylinder diameter, ft,

ν = Kinematic viscosity of air, ft^2/sec.

A. PRESSURE COEFFICIENT EXPERIMENT

Pressure data were obtained at Reynolds numbers of 90,000, 153,000, and 250,000. After considerable checks with the hotwire anemometer, it was decied to use the wall manometer to set the tunnel speeds of 98 ft/sec and 160 ft/sec for Reynolds numbers of 153,000 and 250,000. To accurately set a tunnel speed of 57.6 ft/sec, which yielded a Reynolds number 90,000, the hotwire anemometer was used.

Initially, all leads were checked for tightness and the manometer bank was leveled. The pressure taps were initially located at 0, 90, 180, and 270 degrees. The wind tunnel was started, and the velocity was increased to a predetermined value. The manometer readings were recorded for each pressure tap on the cylinder, the stilling chamber pressure, and the test section pressure. The cylinder was then rotated in five-degree increments, with data being recorded at each increment, until the entire circumference of the cylinder had been traversed. This procedure was repeated for all desired Reynolds numbers, d/r , and L/D spacings. For all experiments, data were then reduced to obtain pressure coefficient around the circumference of the cylinder. Also polar plots of the pressure coefficient versus angular location were obtained. The polar plots are shown in Figures 12 through 19 in Section V and Figures 28 through 59 in Appendix D. The pressure data and data reduction scheme used to obtain the pressure coefficient can be found in Appendix A.

The scheme used to calculate the pressure drag coefficient and lift coefficient from the pressure coefficient is described in Appendix B.

B. FLOW VISUALIZATION EXPERIMENT

Before starting the motor, the sump was completely filled with water. The motor was then started and brought up to a speed of 1200 rpm. The tilting weir was adjusted such that a height of water was obtained which completely submerged the plate and cylinder. The flow was allowed to steady out and the polyethylene tubes were checked for tightness. The dye was then injected through the top and bottom ports, which were 120-degrees apart from each other, in a trial and error fashion until the flow could be visualized clearly. This procedure was repeated for every desired gap spacing and plate leading edge length. As previously described, the gap spacing (d/r) and plate leading edge length (L/D) were 0.0, 0.25, 0.5, 1.0, 2.0, 3.0, 4.0, 5.33 and 2.0, 4.0 and 8.0, respectively. These quantities were obtained according to a scale which was attached to the water channel test section wall. Because of the limitation in the pump capacity, only one run was made with the highest Reynolds number of 10,000 which could be obtained in this experiment.

C. VORTEX FREQUENCY EXPERIMENT

In order to explain the trends which were observed in the drag curve, a vortex shedding frequency experiment was conducted in the wind tunnel at a Reynolds number of 153,000.

To start the experiment, the speed of the wind tunnel was set to 98 ft/sec (2.2 in-H_2O). The frequency measurements were made with a standard hotwire anemometer. Readings were taken at the cylinder mid-span at various locations in the wake behind the cylinder. Because of the limitation on the hotwire anemometer's transversing mechanism, measurements were restricted to a maximum downstream distance of 2.5 cylinder diameters.

The output of the hotwire anemometer was connected to a TYPE 1A1 amplifier which removed the mean velocity (D.C. level) and amplified the signal to a useful level. This amplifier was connected internally to an oscilloscope display which provided a visible signal for confirming the readings from the counter. Also, this amplifier was connected internally to a filter described in detail in Section III which was used to remove the noise and turbulence. This filter was connected to a TYPE 1A1 amplifier which amplified the signal to a useful level and passed it to the display. The second output of the last filter was connected to a precision counter which yielded the vortex shedding frequency.

Using the above electronic circuit and hotwire anemometer, the vortex shedding frequencies were obtained at $d/r = 0.0$, 0.25, 0.5, 1.0, 2.0, 3.0, 4.0, 5.33 and $L/D = 4.0$. The error of the frequency measurements was estimated to be two percent.

In exploring the flow in the cylinder wake, two different frequencies were observed for the same air speed when the gap spacing was small. These frequencies were observed over the top of the cylinder and between the cylinder and plate in the flow field. Results of the vortex shedding frequency measurements are shown in Section V.

V. RESULTS AND DISCUSSION

The results shown and discussed in this section are the cylinder surface pressure distributions, pressure drag and lift coefficients, qualitative observations from the flow visualization experiment, and the measurements of the vortex shedding frequency in the wake of the cylinder.

A. PRESSURE EXPERIMENT AND CYLINDER SURFACE PRESSURE DISTRIBUTIONS

Raw data for three typical pressure runs and a sample calculation of the pressure coefficient are contained in Appendix A. This section presents a graphical presentation of the pressure coefficient versus angular location on polar coordinates for:

(a) Reynolds numbers of 90,000, 153,000, 250,000 with no plate, Figures 9 through 11.

(b) Reynolds number of 153,000 with plate, L/D = 4.0 and d/r ranging from 0.0 to 5.33, Figures 12 through 19.

Polar plots for Reynolds numbers of 90,000 and 250,000 with plate L/D = 4.0 and d/r ranging from 0.0 to 5.33 are shown in Appendix D, Figures 28 through 43. Also Appendix D includes the polar plots for Reynolds number 153,000 with plate L/D = 2.0 and 8.0, and d/r ranging from 0.0 to 5.33, Figures 44 through 59.

All polar plots include Nusselt number versus angular location curves which were taken from Kösemen's [3] data. Again this study was a parallel study with Kosemen who used

the same Reynolds number range (except 250,000) and the same size cylinder to investigate the heat transfer characteristics of a heated cylinder. Because Kösemen's data indicate precise separation points and the flow characteristics on the top and bottom half of the cylinder, his data were found very informative and were plotted with the curves of pressure coefficients versus angular location.

The trend in the plots and the magnitude of the pressure coefficient for the no-plate case were found to agree well with published values in the literature [6] (within 2%). See Figures 9 through 11.

Before proceeding with an examination of the polar plots which are shown in Figures 12 through 19, a brief description of the classification of flow past a cylinder will be given. This description will help to explain our observations about the flow phenomena.

Flow is characterized by the nature of the separation of the boundary layer from the cylinder surface. Using the definitions employed by Achenbach [6]:

1. When the boundary layer separates laminarly, this state of flow is called subcritical flow. In subcritical flow, a laminar boundary layer develops at the forward stagnation point of the cylinder and grows to a maximum thickness at an angular location between 80 and 85 degrees. At 80 to 85 degrees, the kinetic energy of the moving fluid is no longer sufficient to overcome the adverse pressure gradient present on the cylinder's surface, and the laminar

boundary layer separates. Upon separation, a wake forms in the rear portion of the cylinder. A typical subcritical flow pattern is shown in Figure 6.

2. When a separation bubble, followed by a turbulent reattachment, occurs, this state of flow is called critical flow. In critical flow, the laminar boundary layer again grows from the forward stagnation point to the 80 to 85 degree point where laminar separation again occurs. But, unlike the subcritical flow case, a transition of the separated laminar layer to a turbulent state occurs which results in the reattachment of a turbulent boundary layer. This reattached turbulent boundary layer ultimately separates at a position further downstream. The region between the laminar separation point and the point of reattachment of the turbulent boundary layer is called a "separation bubble." A typical critical flow pattern is shown in Figure 7.

3. When an immediate transition from the laminar to the turbulent boundary layer occurs without separation, this state of flow is called supercritical flow. A typical supercritical flow pattern is shown in Figure 8.

In examining the polar plots which are shown in Figures 12 through 19 for significant trends or unusual phenomena, two items of interest were immediately apparent: one was the change from critical to subcritical flow, the other was a shift in the location of the stagnation point and the laminar separation points as the plate was moved away from the cylinder.

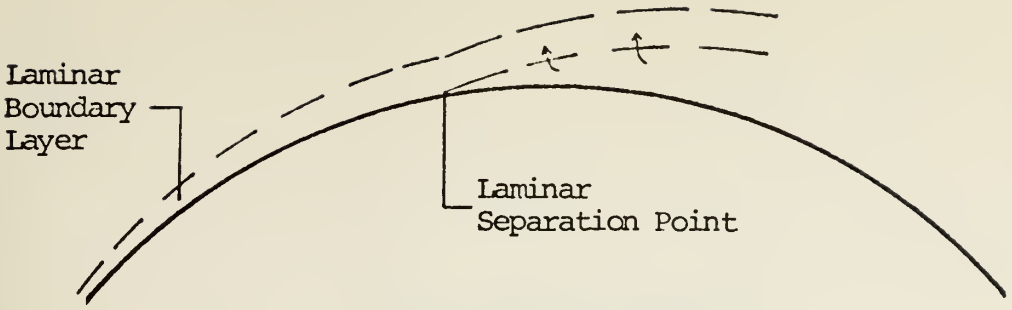

FIGURE 6. Sketch of a typical subcritical flow pattern on the surface of a cylinder

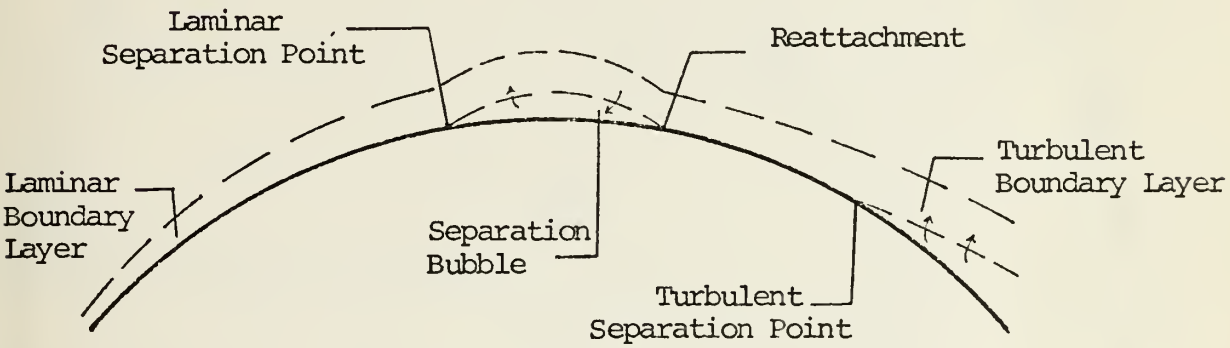

FIGURE 7. Sketch of a typical critical flow pattern on the surface of a cylinder

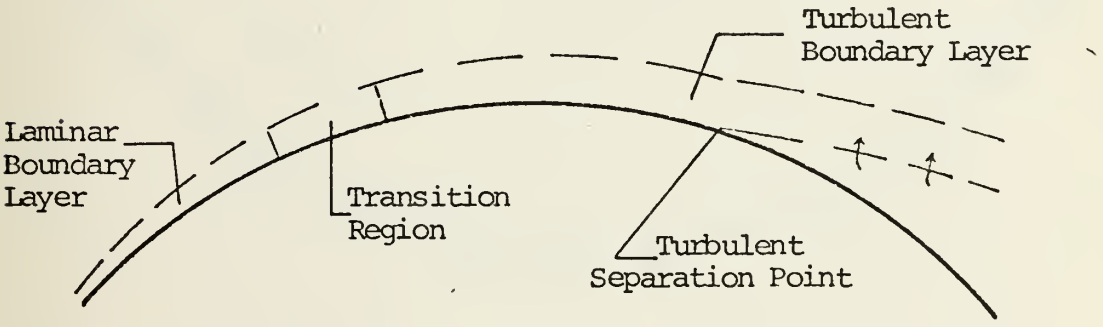

FIGURE 8. Sketch of a typical supercritical flow pattern on the surface of a cylinder

C_p x

Nu •

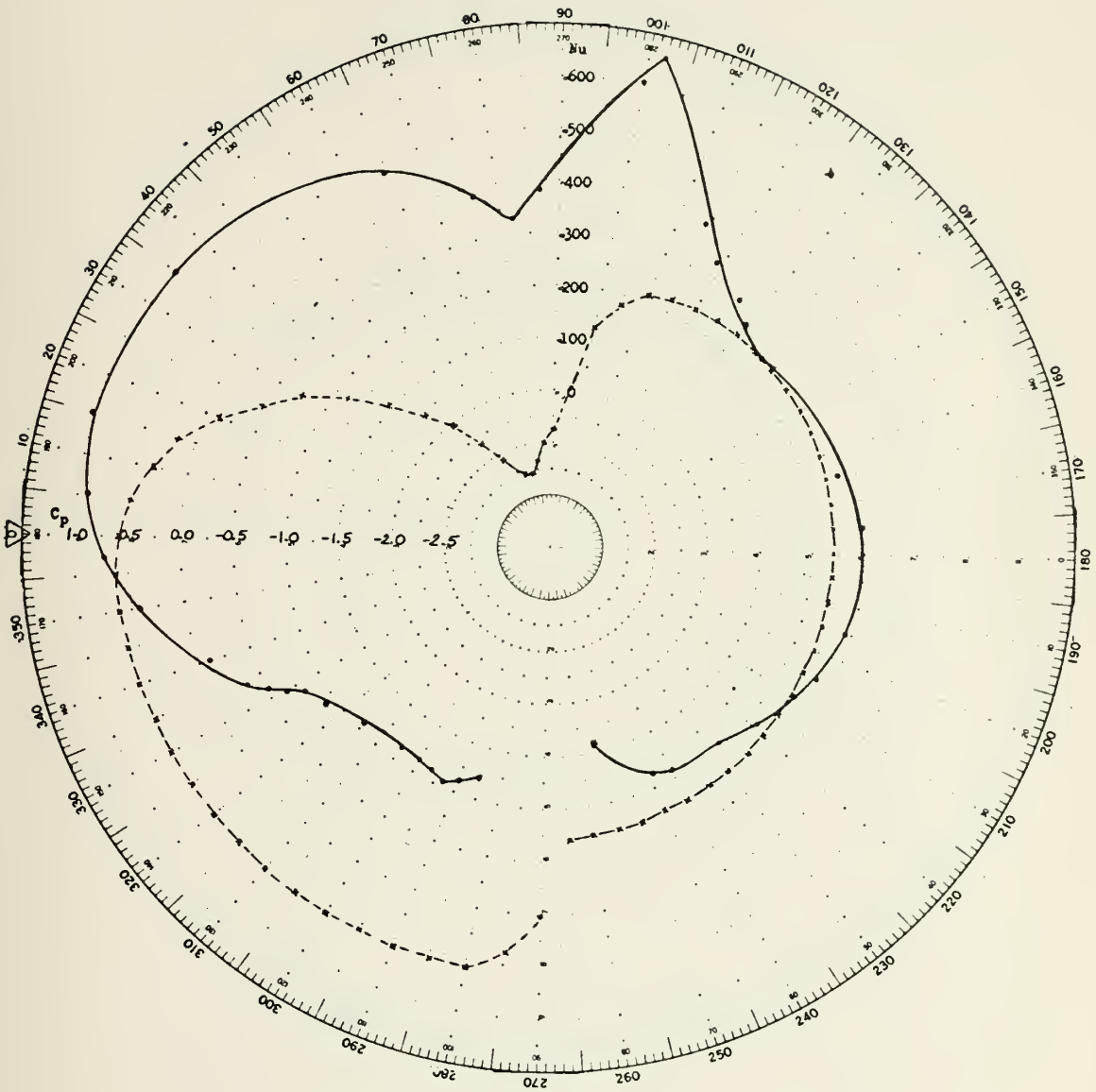

FIGURE 12. Pressure coefficient and local Nusselt number on the surface of a cylinder placed near a plane surface for:
Re = 153,000, L/D = 4.0, d/r = 0.0

C_p x

Nu .

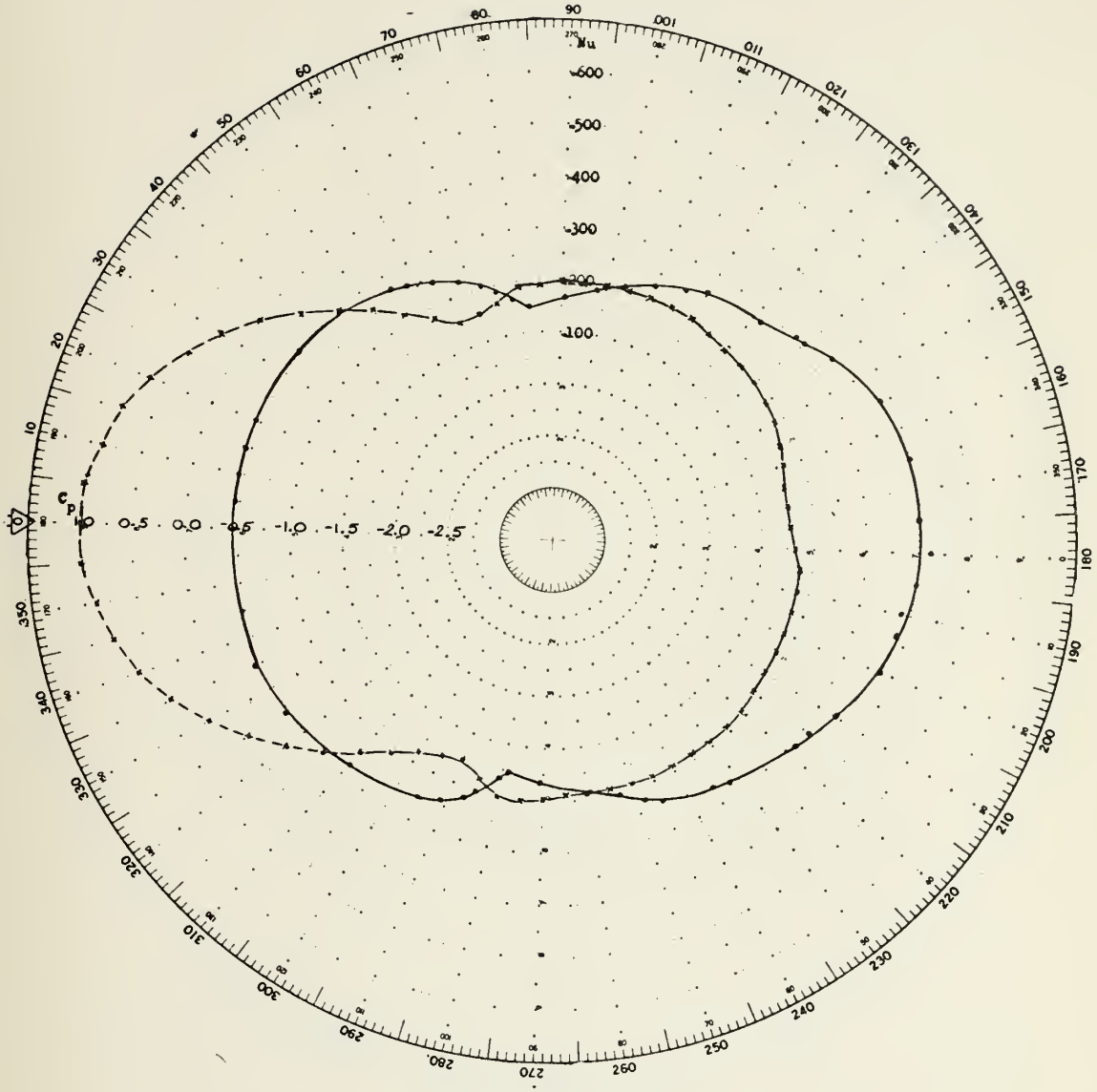

FIGURE 9. Pressure coefficient and local Nusselt number on the surface of a free cylinder for Re = 90,000

C_p x

Nu •

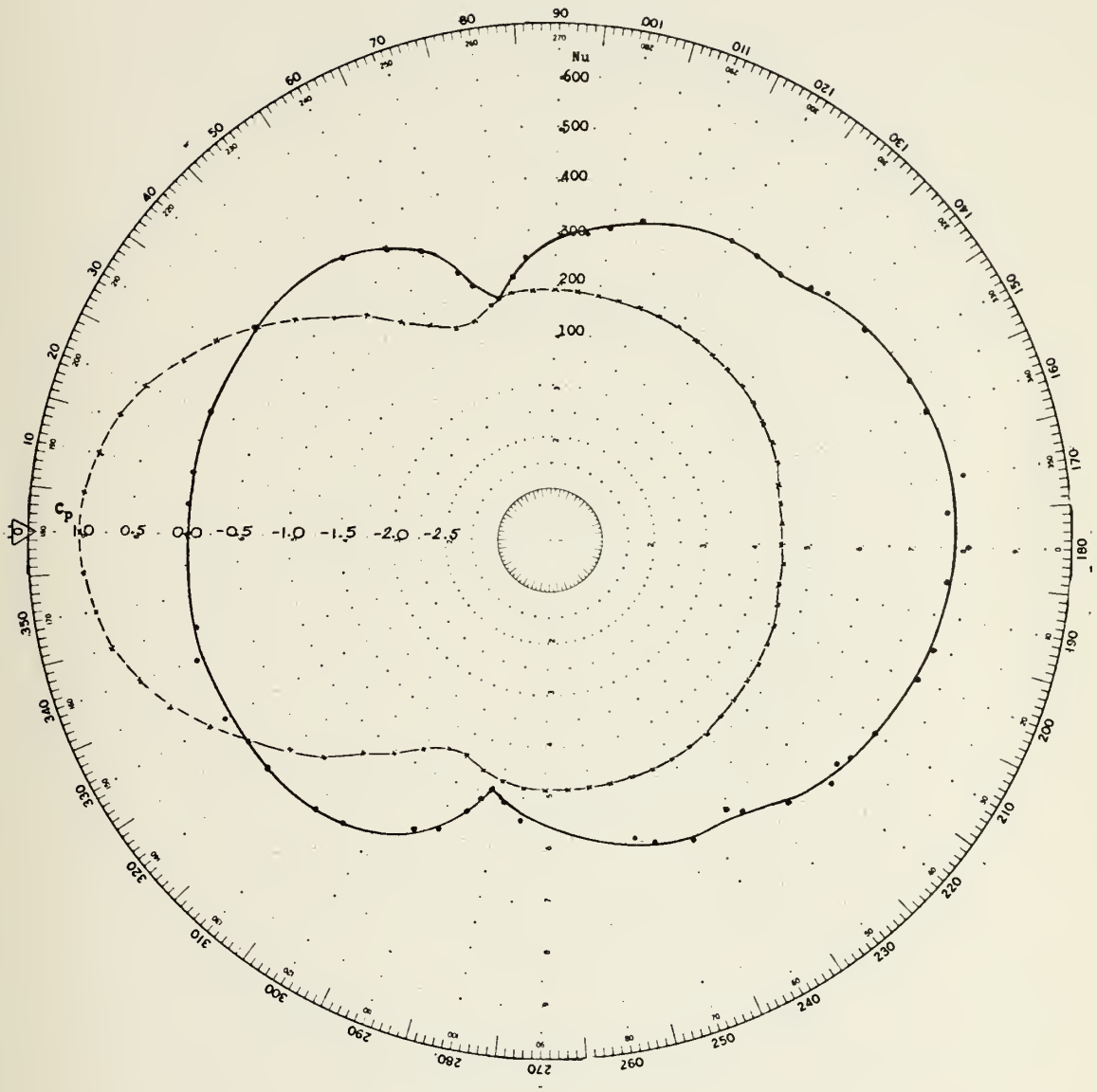

FIGURE 10. Pressure coefficient and local Nusselt number on the surface of a free cylinder for Re = 153,000

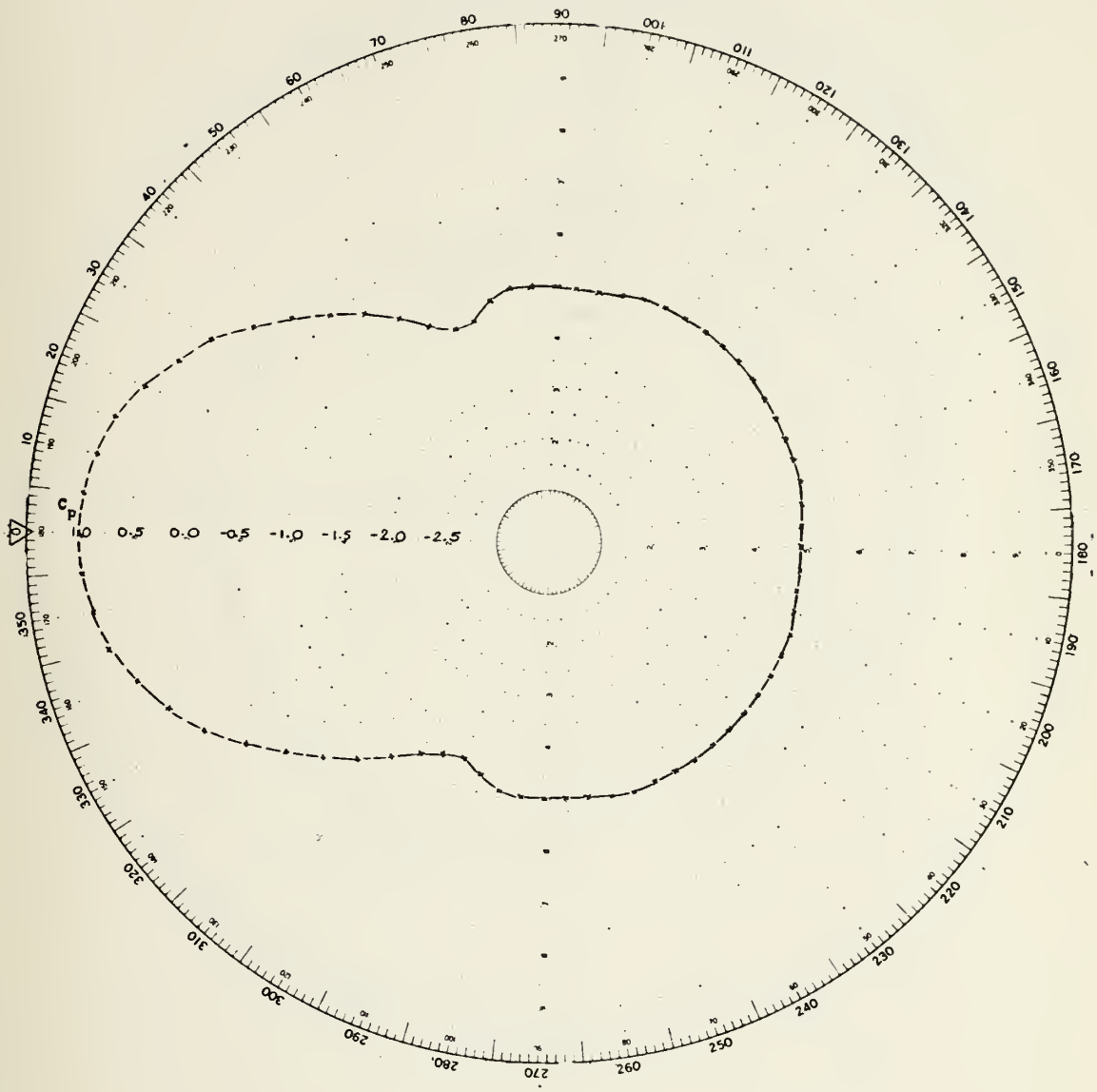

FIGURE 11. Pressure coefficient on the surface of a free cylinder for Re = 250,000

C_p x

Nu •

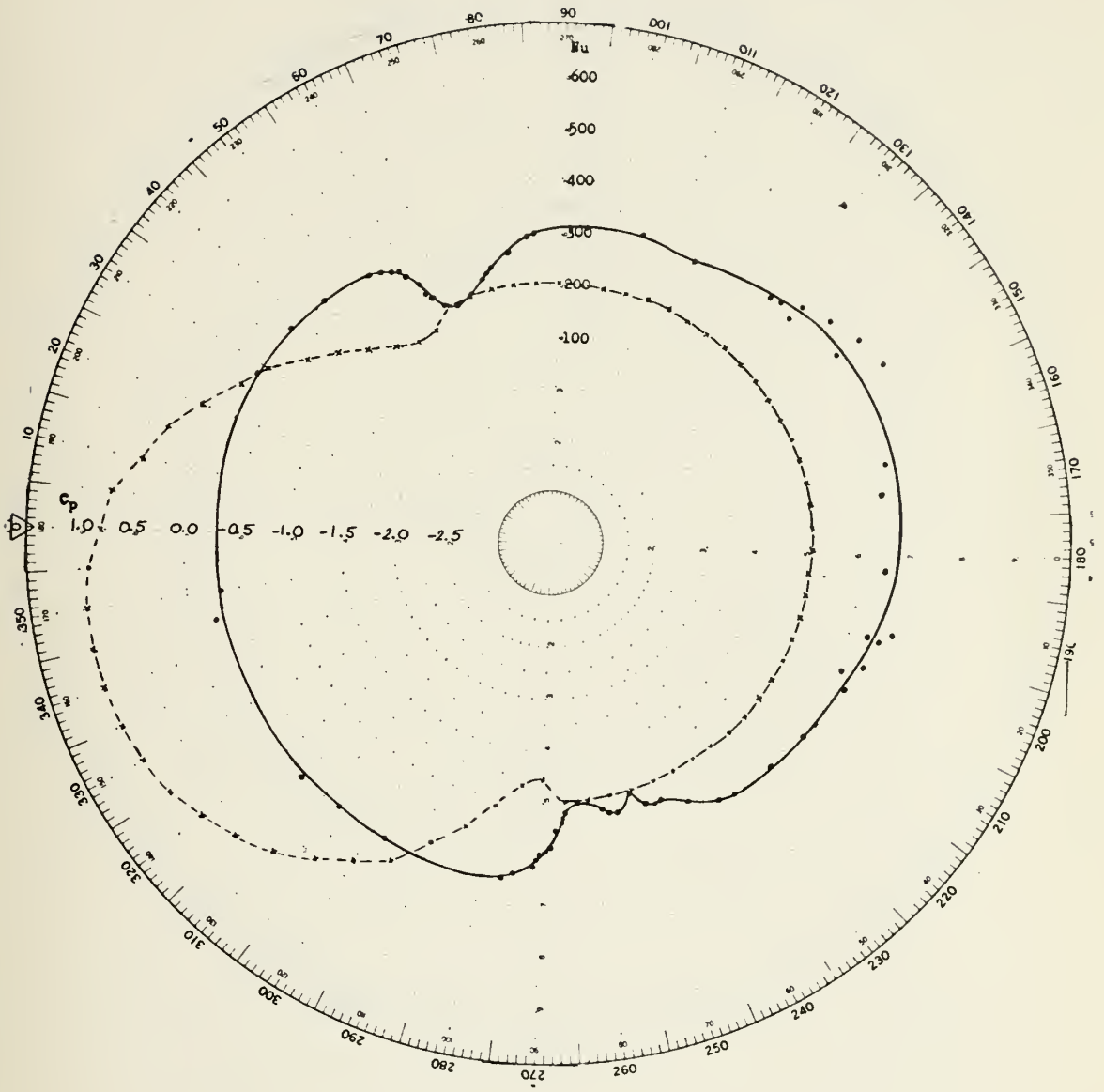

FIGURE 13. Pressure coefficient and local Nusselt number on the surface of a cylinder placed near a plane surface for:
Re = 153,000 , L/D = 4.0 , d/r = 0.25

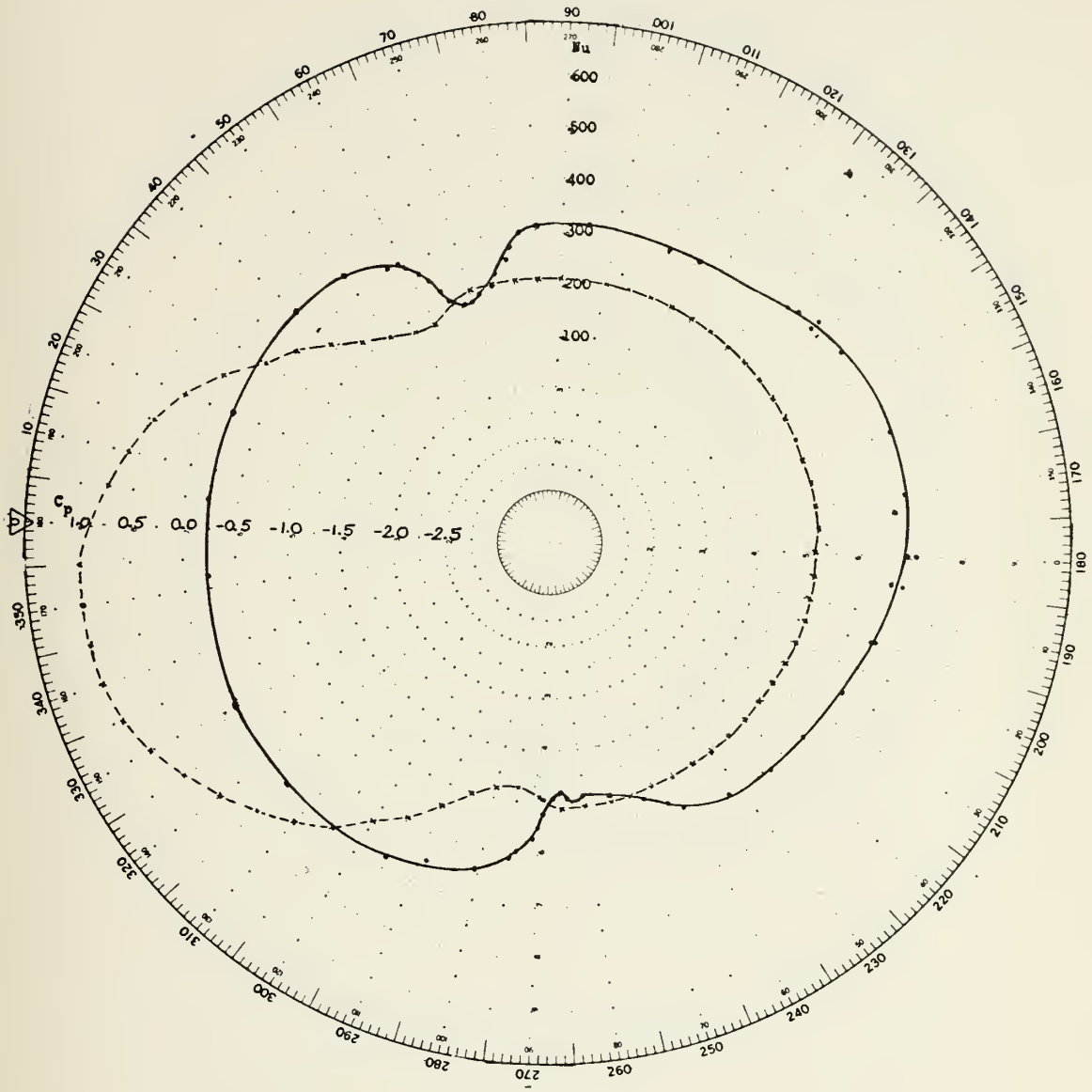

FIGURE 14. Pressure coefficient and local Nusselt number on the surface of a cylinder placed near a plane surface for:
Re = 153,000 , L/D = 4.0 , d/r = 0.5

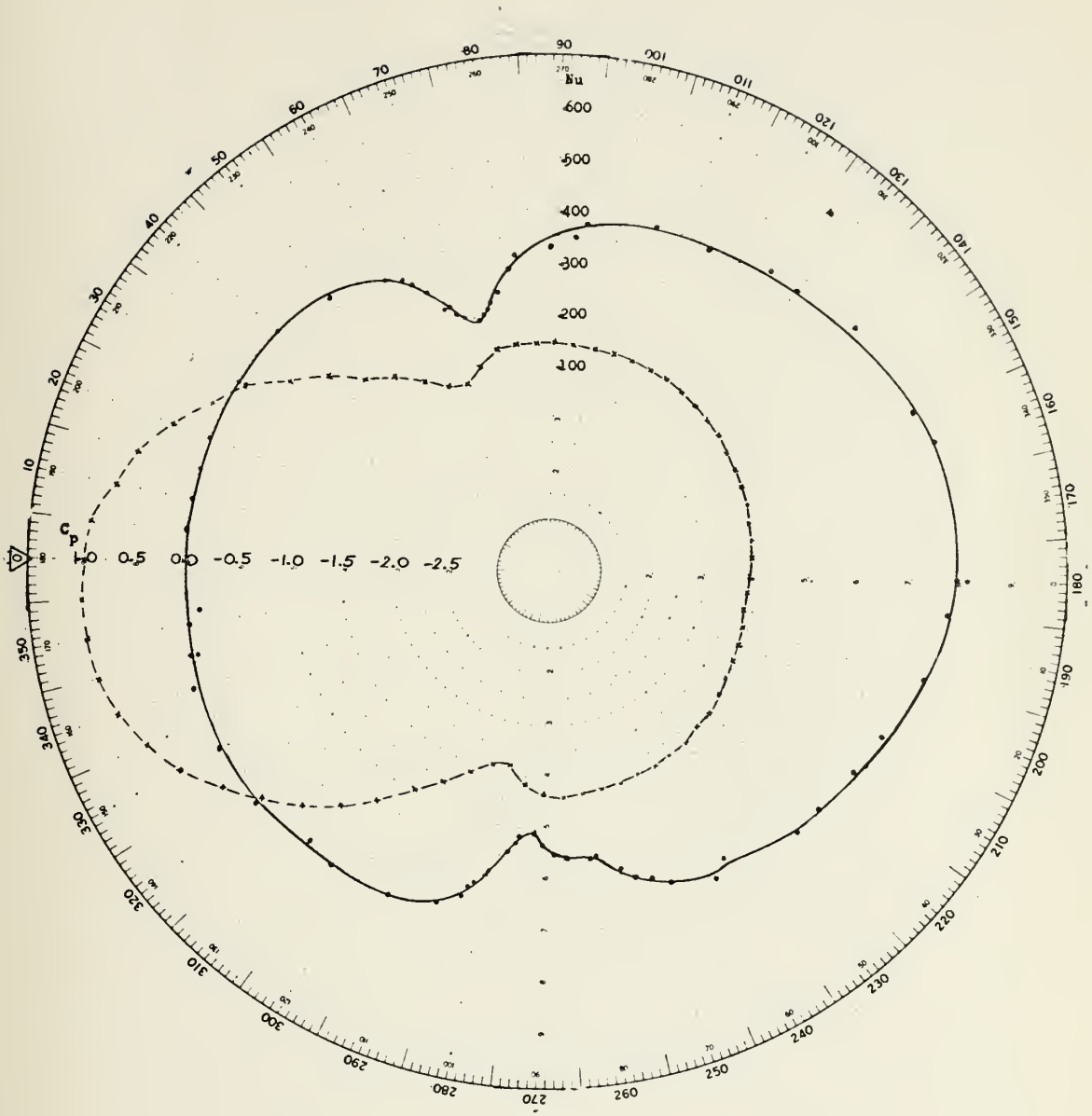

FIGURE 15. Pressure coefficient and local Nusselt number on the surface of a cylinder placed near a plane surface for:
Re = 153,000 , L/D = 4.0 , d/r = 1.0

C_p x

Nu •

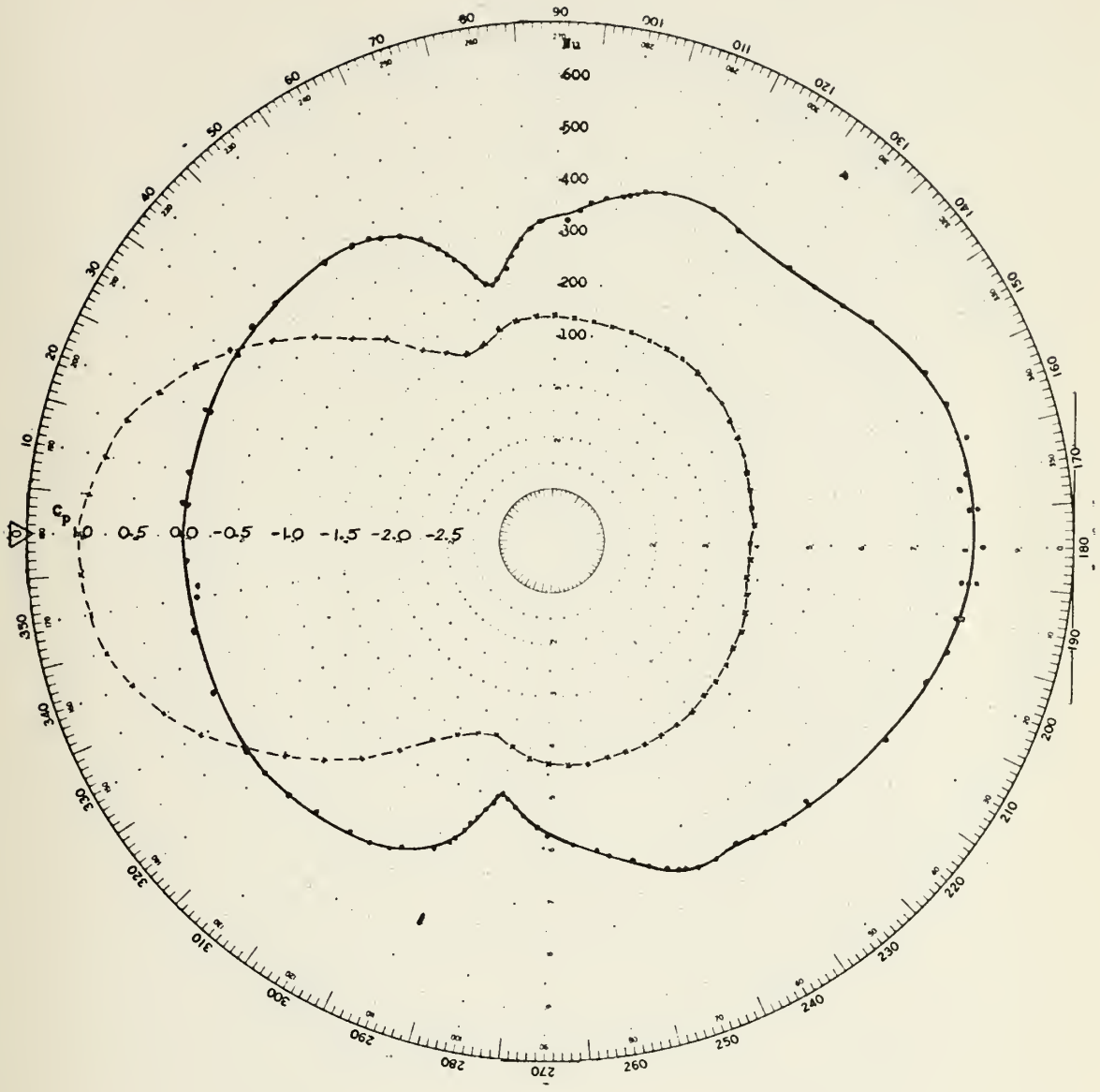

FIGURE 16. Pressure coefficient and local Nusselt number on the surface of a cylinder placed near a plane surface for:
Re = 153,000 , L/D = 4.0 , d/r = 2.0

C_p x

Nu •

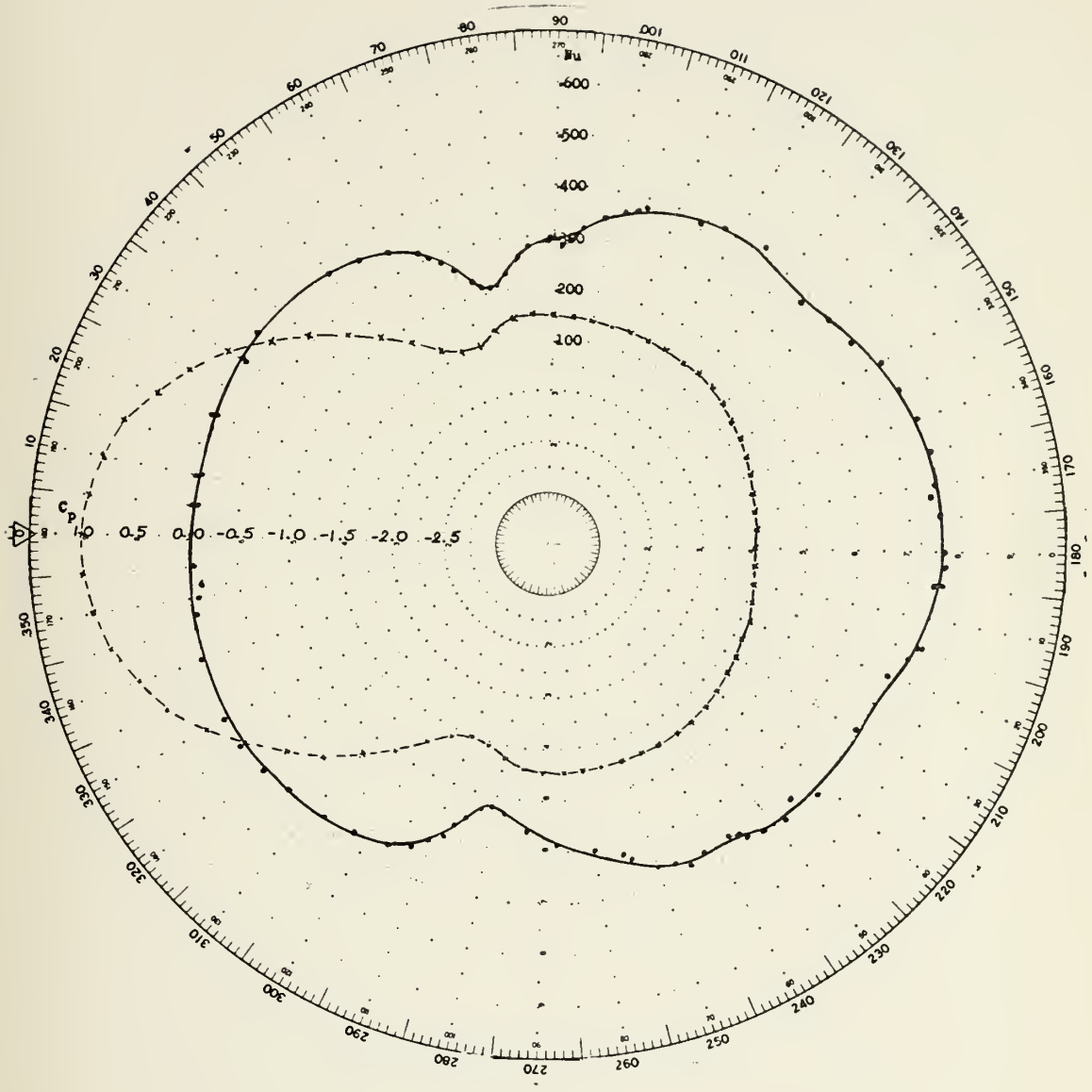

FIGURE 17. Pressure coefficient and local Nusselt number on the surface of a cylinder placed near a plane surface for:
Re = 153,000 , L/D = 4.0 , d/r = 3.0

C_p x

Nu .

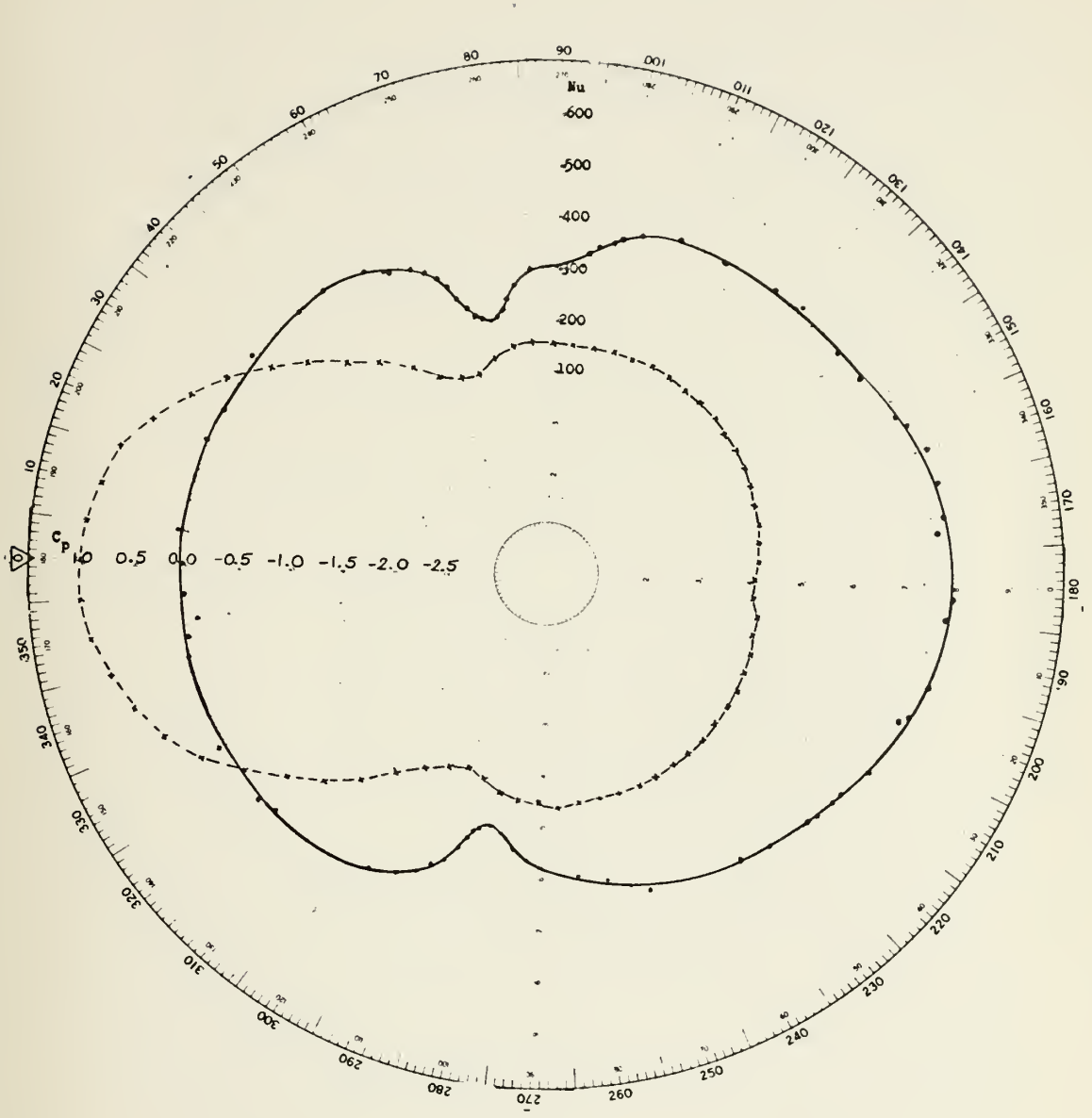

FIGURE 18. Pressure coefficient and local Nusselt number on the surface of a cylinder placed near a plane surface for:
Re = 153,000 , L/D = 4.0 , d/r = 4.0

C_p x

Nu .

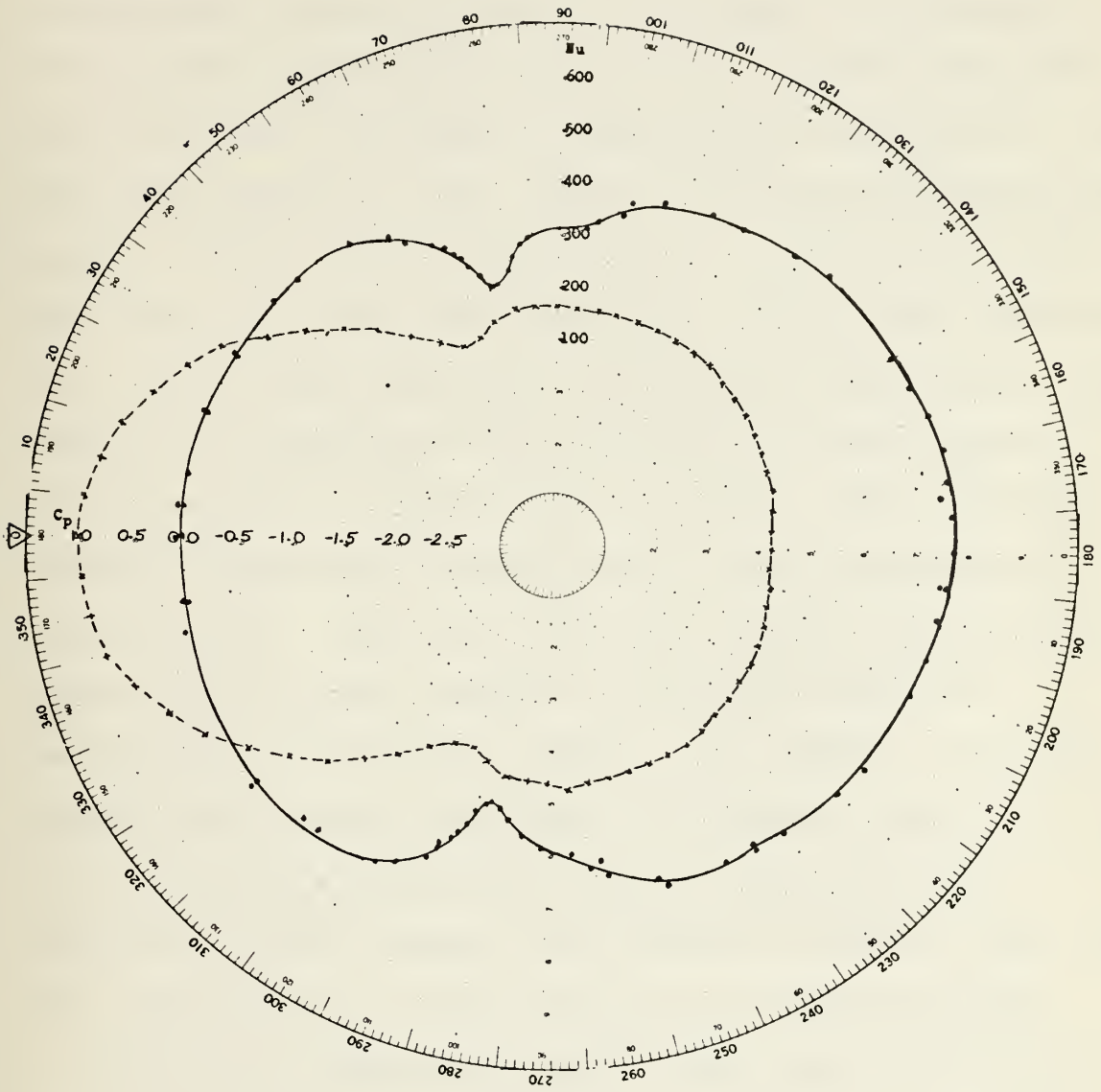

FIGURE 19. Pressure coefficient and local Nusselt number on the surface of a cylinder placed near a plane surface for:
Re = 153,000 , L/D = 4.0 , d/r = 5.33

Kösemen's [3] data were used to determine the d/r ratio associated with a change from critical to subcritical flow. The data obtained are shown in Table I. The results for a Reynolds number of 16,000 which was used by Kosemen in his investigation were included in this table for additional information. This table shows the d/r ratios where the flow undergoes a critical to subcritical transition for various Reynolds numbers and L/D ratios. For the data collection, liquid crystal thermography technique employed by Kösemen were used. In short, this technique allows visual determination of both qualitative and quantitative heat transfer and fluid flow information to be obtained on heated objects placed in forced convection environments. This technique employs cholesteric liquid crystals as the temperature-sensing agent. The liquid crystals indicate temperature by exhibiting brilliant changes in color over discrete, reproducible temperature ranges. As a result, the liquid crystal thermographic technique afforded the opportunity to visually observe the effects of flow separation, the separation bubble region, the turbulent boundary layer, and the turbulent wake on the surface of a heated cylinder.

During the experiment, uniform heat flux was applied to the cylinder surface by means of an electrical resistance paper (Temsheet). The paper was coated with S-43 liquid crystal which indicates in three distinct color bands the following event temperatures:

Re	L/D = 2.0		L/D = 4.0		L/D = 8.0	
	TOP At "d/r"	BOTTOM At "d/r"	TOP At "d/r"	BOTTOM At "d/r"	TOP At "d/r"	BOTTOM At "d/r"
16,000	0.20	1.00	0.20	0.90	0.20	0.80
90,000	0.15	0.90	0.15	0.90	0.15	0.80
153,000	0.15	1.20	0.10	1.20	0.10	1.20

TABLE I. Transition from critical to subcritical flow as a function of Reynolds number, d/r and L/D ratios

COLOR	TEMPERATURE
Red	43.2° C
Green	43.9° C
Blue	44.6° C

In the wind tunnel, the electrodes on the inner surface of the Temsheet cylinder were attached to a power supply. The power supply was energized and voltage was adjusted to bring the surface temperature of the cylinder to a temperature of approximately 50° C. This caused the S-43 liquid crystal on the surface of the cylinder to pass through its event temperature ranges. Having pre-heated the cylinder, flow was established in the wind tunnel. Immediately after flow was initiated, the cylinder started to cool. To counter this, the power supplied to the cylinder was increased to maintain the hottest point on the cylinder at about 43.2° C. This corresponded to the red point on the liquid crystal. The plate was then attached to the cylinder ($d/r = 0.0$). Adjusting the voltage to obtain the event temperature ranges on the surface of the cylinder, the following observations were made:

Due to the fact that all of the air approaching the cylinder is forced to go "up and over", the flow was found critical (See Figure 7) over the top of the cylinder with the plate attached. Also a separation bubble which manifested itself as a local cool spot (liquid crystal does not display color) bounded by two local hot spots indicated the presence of critical flow.

As soon as a space existed between the cylinder and plate ($d/r = 0.25$), the separation bubble suddenly was lost. This was the change of flow from critical to subcritical (See Figure 6) according to Reynolds numbers studied in this investigation. By alternately moving the plate and adjusting the voltage, the transition points over the top of the cylinder for various Reynolds numbers and L/D ratios were found to be within the range $0.1 \leq d/r \leq 0.2$. See Table I.

Using the same procedure of carefully adjusting spacing and voltage the transition from critical to subcritical flow on the bottom of the cylinder was found in the interval $0.8 \leq d/r \leq 1.2$ for various Reynolds numbers and L/D ratios. See Table I. One can easily see from Table I that the transition points which occurred at various d/r ratios are approximately independent of L/D ratios but dependent on Reynolds numbers. When the Reynolds number was increased, the d/r ratios for transition on the top of the cylinder decreased slightly. On the bottom of the cylinder the trend was reversed.

B. PRESSURE DRAG AND LIFT COEFFICIENTS

In order to gain further information from the pressure distribution around the cylinder, the pressure drag (C_{dp}) and the lift coefficients (C_L) were computed and are shown in Table II. Appendix B illustrates the method which was used to calculate the pressure drag and lift coefficients.

For the Reynolds numbers range used in this investigation Achenbach [6] states that the friction forces are nearly

Re	L/D	d/r	C_{dp}	C_L	Re	L/D	d/r	C_{dp}	C_L
90,000	NO PLATE		1.17	0.00	153,000	4.0	2.0	1.43	0.05
90,000	4.0	0.0	0.85	1.30	153,000	4.0	3.0	1.35	0.03
90,000	4.0	0.25	1.17	0.40	153,000	4.0	4.0	1.34	0.01
90,000	4.0	0.50	1.12	0.26	153,000	4.0	5.33	1.29	0.01
90,000	4.0	1.0	1.41	0.12	153,000	8.0	0.0	0.60	1.20
90,000	4.0	2.0	1.39	0.05	153,000	8.0	0.25	1.12	0.30
90,000	4.0	3.0	1.35	0.02	153,000	8.0	0.50	1.08	0.22
90,000	4.0	4.0	1.32	0.02	153,000	8.0	1.0	1.44	0.11
90,000	4.0	5.33	1.32	0.01	153,000	8.0	2.0	1.41	0.05
153,000	NO PLATE		1.23	0.00	153,000	8.0	3.0	1.38	0.03
153,000	2.0	0.0	0.75	1.58	153,000	8.0	4.0	1.32	0.01
153,000	2.0	0.25	1.21	0.42	153,000	8.0	5.33	1.32	0.00
153,000	2.0	0.50	1.11	0.28	250,000	NO PLATE		1.10	0.00
153,000	2.0	1.0	1.46	0.11	250,000	4.0	0.0	0.61	1.39
153,000	2.0	2.0	1.43	0.04	250,000	4.0	0.25	1.15	0.42
153,000	2.0	3.0	1.36	0.04	250,000	4.0	0.50	1.08	0.27
153,000	2.0	4.0	1.33	0.02	250,000	4.0	1.0	1.38	0.13
153,000	2.0	5.33	1.33	0.02	250,000	4.0	2.0	1.32	0.06
153,000	4.0	0.0	0.64	1.44	250,000	4.0	3.0	1.23	0.02
153,000	4.0	0.25	1.16	0.41	250,000	4.0	4.0	1.20	0.01
153,000	4.0	0.50	1.09	0.27	250,000	4.0	5.33	1.16	0.00
153,000	4.0	1.0	1.46	0.12					

TABLE II. Pressure drag and lift coefficients as a function of gap spaces for various Reynolds numbers

negligible in calculating the drag coefficient. Therefore, the skin friction drag was neglected compared to the pressure (form) drag which constitutes 98 percent or more of the total drag according to Achenbach.

The plots of the pressure drag and lift coefficients as a function of gap spacing for various Reynolds numbers and L/D ranges are shown in Figures 20 and 21. Figure 20 shows the effect of L/D ratio on C_{dp} and C_L and Figure 21 shows the effect of Reynolds numbers on C_{dp} and C_L. It is interesting to note the unexpected shapes and trends of the pressure drag versus d/r ratio curves. For all Reynolds numbers and L/D ratios, the pressure drag coefficient increases to a local maximum value, then decreases to a local minimum then increases to a maximum at $d/r = 1.0$, and finally gradually decreases to a nearly constant value as d/r approaches relative infinity. It is important to emphasize that the trends of the pressure drag coefficient versus d/r ratio curves are the same for all Reynolds numbers and L/D ratios investigated. This implies there is no effect on the trends of the curves due to changing the L/D ratio or Reynolds numbers.

A question that immediately comes to mind when examining the drag curves, Figure 20 and Figure 21, concerns the maximum value of the drag coefficient that occurs at $d/r = 1.0$. The flow visualization technique described in Section IV and hotwire anemometer measurements of the vortex shedding frequency (Section IV) were used to provide both a

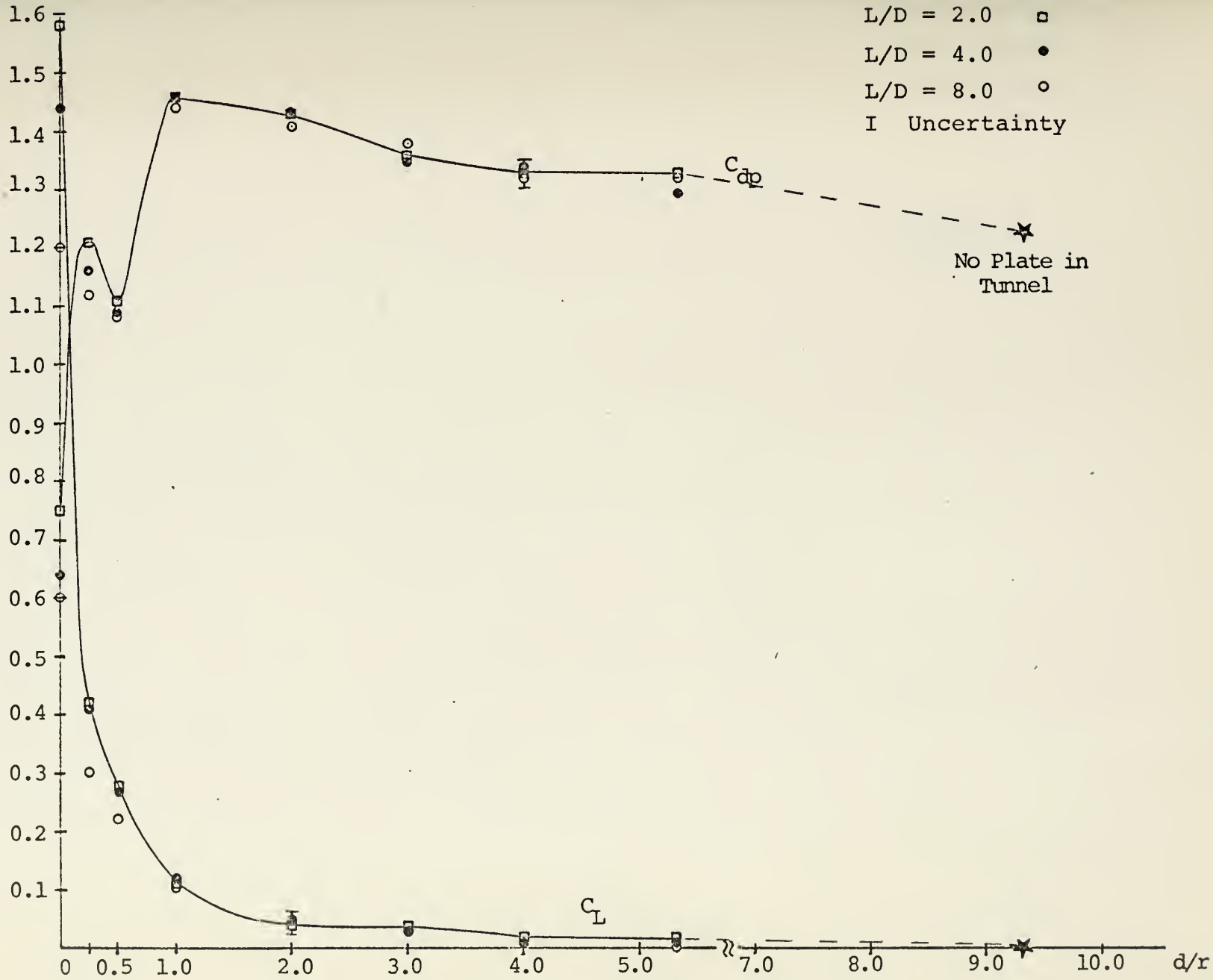

FIGURE 20. Pressure drag and lift coefficients variation as a function of plate length and gap size for a Reynolds number of 153,000

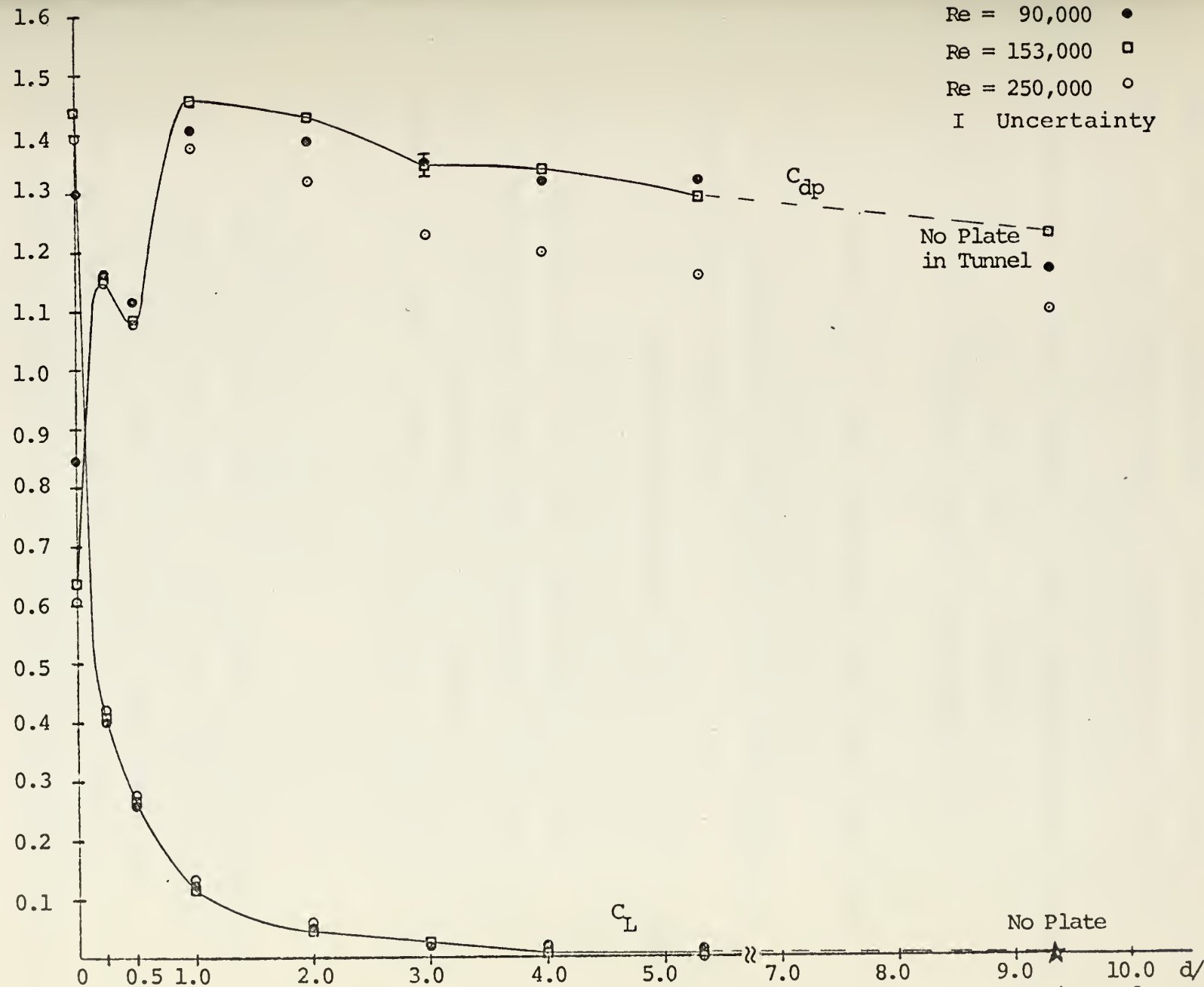

FIGURE 21. Pressure drag and lift coefficients variation as a function of gap size and Reynolds numbers for L/D = 4.0

qualitative and quantitative explanation of this phenomena. The results of this aspect of the study are shown in Part C and Part D of this section. In short, it was found that at $d/r = 1.0$ the vortex shedding frequency of the flow field reached a maximum value compared to its values at $d/r = 0.0$, 0.25, 0.5, 2.0, 3.0, 4.0 and 5.33. This caused the base pressure to exhibit a minimum value and as a result of this, the pressure drag coefficient reached its maximum value at $d/r = 1.0$.

In examining the lift coefficient as a function of gap spacing the following observations can be made:

a) The maximum lift coefficient occurs when the plate is attached to the cylinder.

b) The lift coefficient suddenly drops to a small value at $d/r = 0.25$ and then gradually decreases to an ultimate value near zero at $d/r = 5.33$. See Figures 20 and 21.

With no plate in the tunnel the lift coefficient was found to be zero as expected and the pressure drag coefficients were found to agree with literature values [6]. See Table II.

C. FLOW VISUALIZATION EXPERIMENT

In order to obtain qualitative answers to the questions which arised from the pressure (form) drag characteristics of the flow field, a flow visualization experiment was performed in the water channel (described in detail in Section III). Because of the limitation in the pump capacity,

the highest Reynolds number which could be obtained in this experiment was approximately 10,000. This was well below the Reynolds numbers range examined in the pressure experiment. However, the behavior observed agreed well with the proposed theory of vortex formation.

During the experiment the following observations were made:

1. At d/r = 0.0

Referring to Figure 22, when the gap spacing is zero there is no flow between the cylinder and plate. The flow appeared to be relatively stagnant in the downstream cavity formed by the cylinder and plate. No "trapped" vortices were observed. Indistinct vortices were observed at approximately four diameters downstream. These vortices most probably detached from the outer side of the cylinder. At the upstream cavity a series of small, circular, three-dimensional vortices were clearly evident. Also a large turbulent vortex was observed (See Figure 23). According to McComas [1], this large turbulent vortex occurs within the separated region where the flow separates from the flat plate and reattaches to the cylinder at a point just aft of the forward stagnation point. Due to the stagnant region behind the cylinder, the base pressure is found to exhibit a maximum value and thus the drag on the cylinder is decreased considerably from the free cylinder value. On the other hand, the lift force reaches its maximum value due to the plate effect. See Table II for the minimum value of the

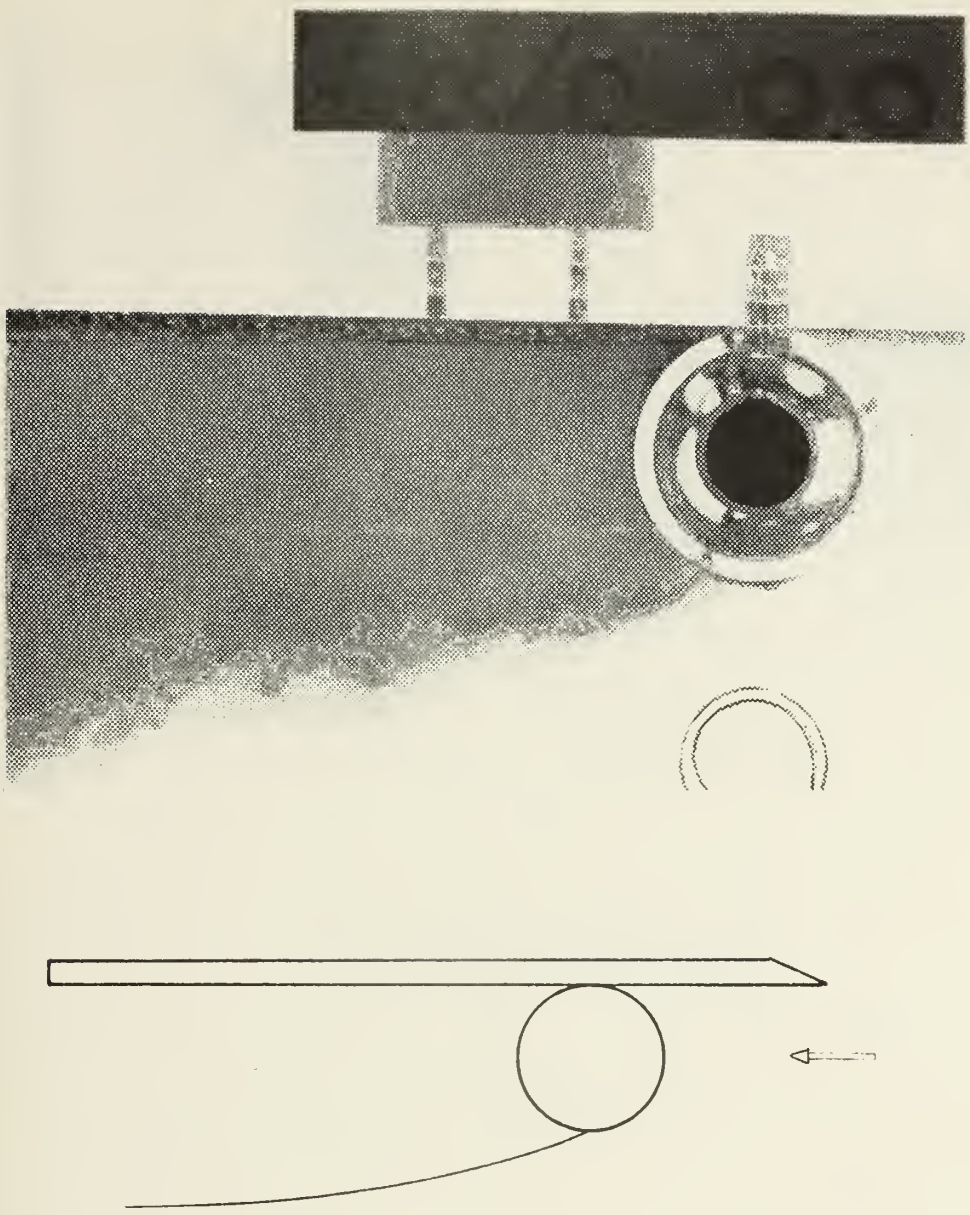

FIGURE 22. Photograph and sketch of the flow pattern at d/r = 0.0

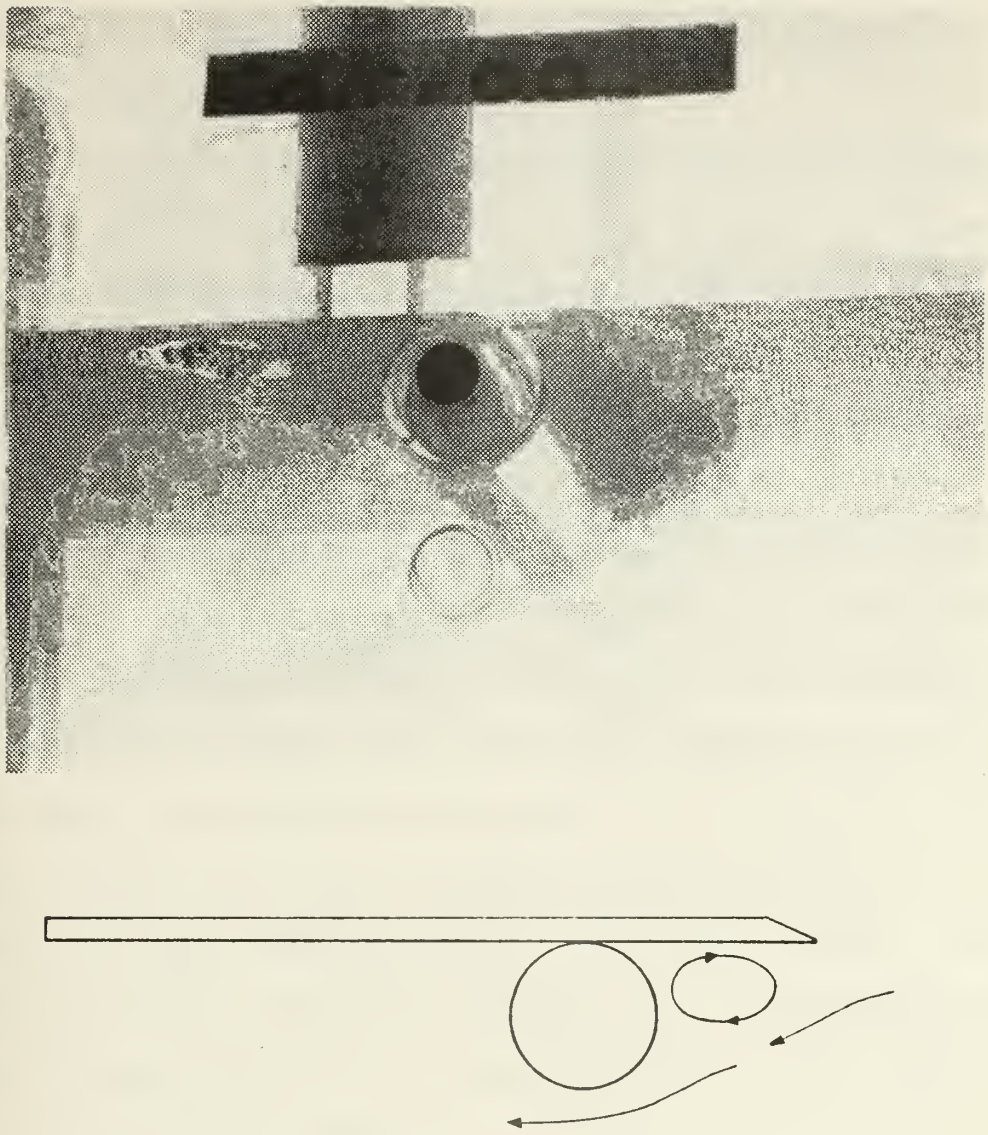

FIGURE 23. Photograph and sketch of the trapped vortices at d/r = 0.0

pressure drag coefficient and maximum value of the lift coefficient at all Reynolds numbers and L/D ranges for d/r = 0.0.

2. At d/r = 0.25

As soon as a space existed between the cylinder and plate a stable jet flow was observed between the plate and cylinder in the immediate vicinity of the gap. See Figure 24. This jet widened as it moved downstream and mixed with the flow in the wake. Vortices were not detached immediately from the top and bottom of the cylinder probably due to the effect of the jet flow. A qualitative comparison with the d/r = 0.0 case from astrength viewpoint, indicated that distinguishable vortices were observed at approximately four diameters downstream for d/r = 0.25 while only very indistinct vortices were observed for d/r = 0.0. Probably due to these vortices, the base pressure exhibited a more negative value compared to the d/r = 0.0 value. As a result of this, the drag increased to a local maximum value as indicated in Figure 20 and Figure 21 for all Reynolds numbers and L/D ranges.

3. At d/r = 0.5

As the gap further increased in size, a jet flow was still observed between the plate and cylinder. See Figure 25. In this state vortices again were observed at four diameters downstream. Compared with the d/r = 0.25 case, the vortices did not appear as strong. Due to this decrease in vortex

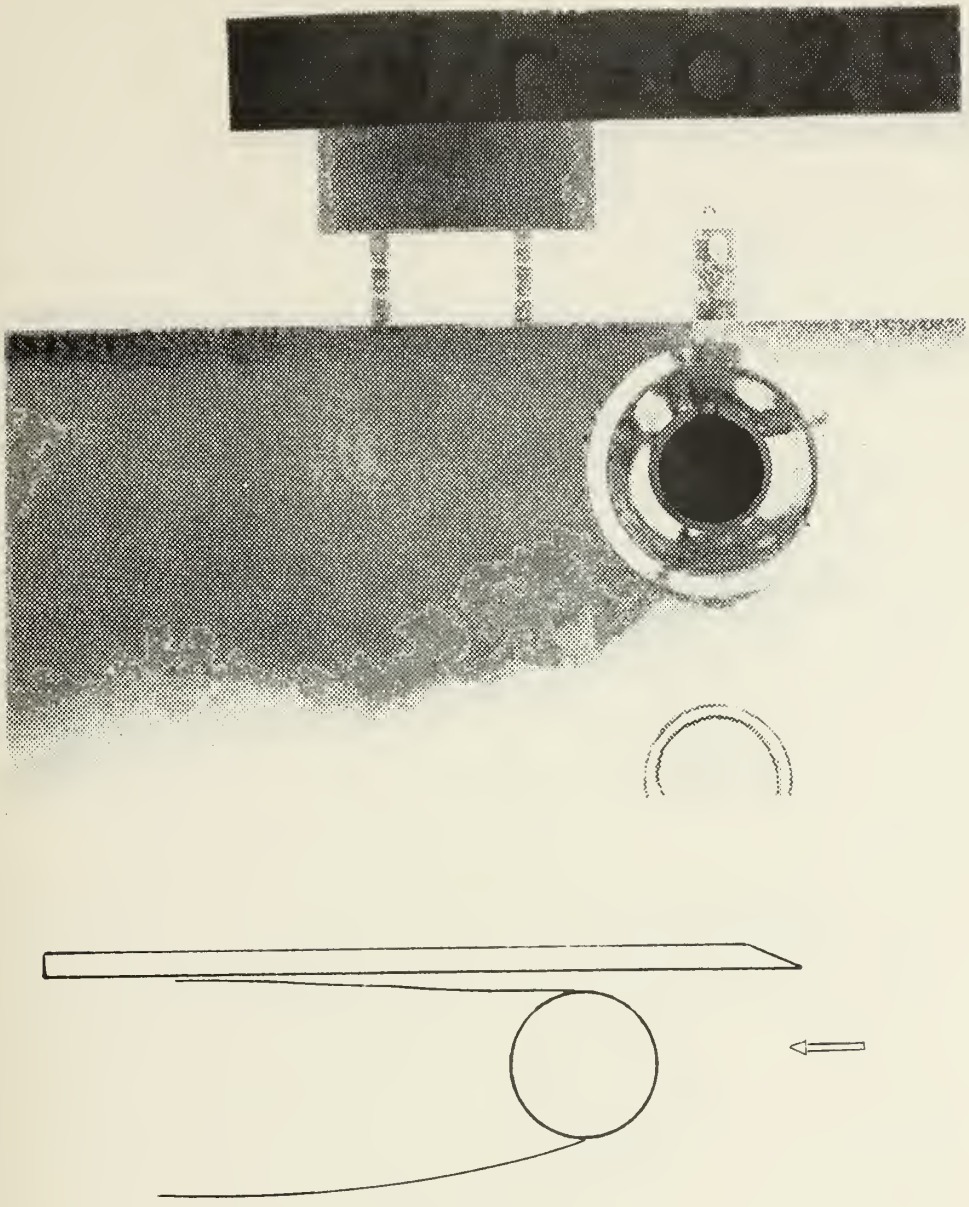

FIGURE 24. Photograph and sketch of the flow pattern at d/r = 0.25

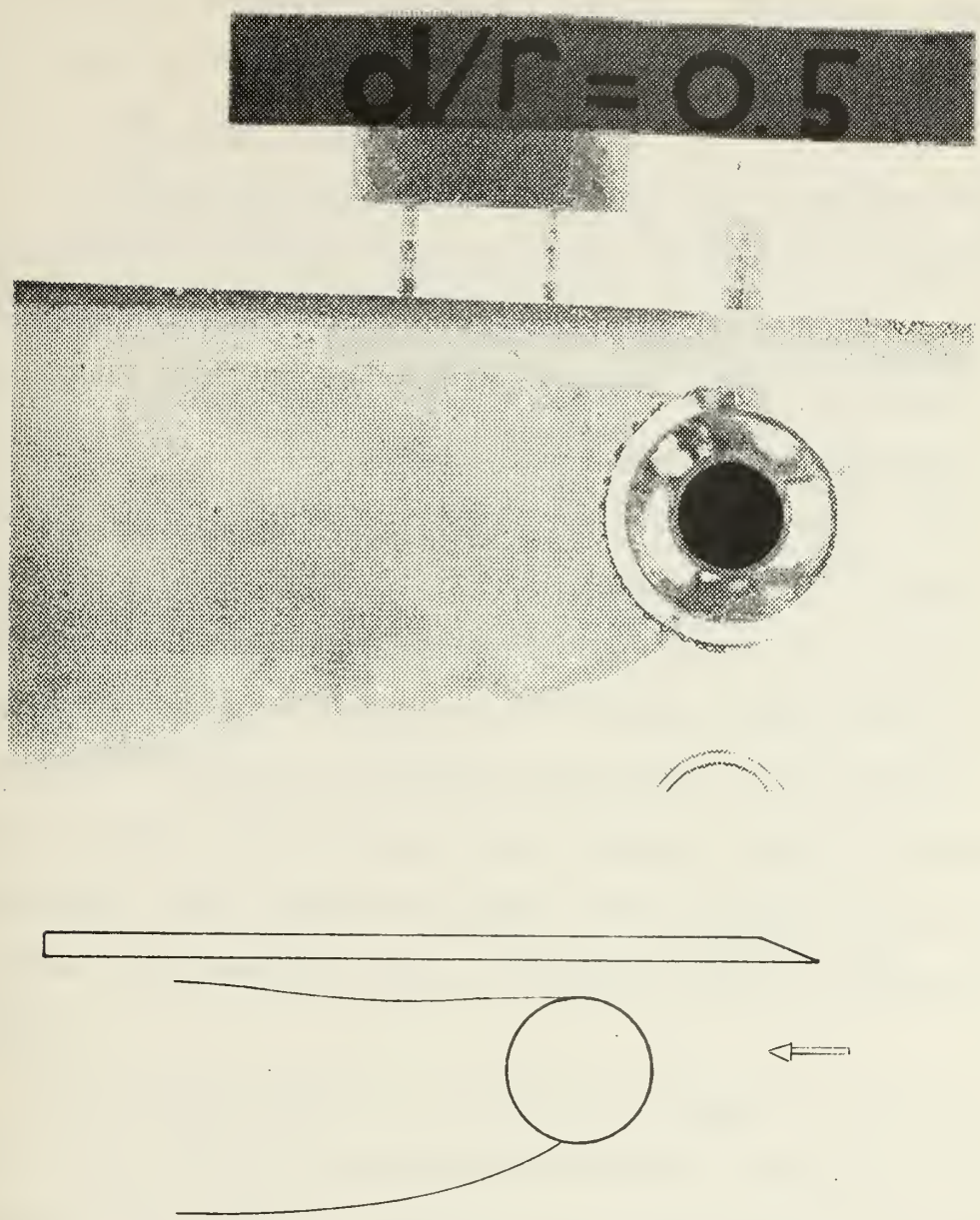

FIGURE 25. Photograph and sketch of the flow pattern at d/r = 0.5

strength, the drag decreased to a minimum value which one can see from Figures 20 and 21 for all Reynolds numbers and L/D ratio ranges which were used in this investigation.

4. At d/r = 1.0

This was the location where more distinct three-dimensional vortices were observed during the flow visualization experiment. The boundary layer appeared to separate from both the top and bottom surface of the cylinder in the form of alternating three-dimensional vortices and a very strong vortex shedding frequency was observed. Also, a rather regular, violent vortex street formed at about one-half diameter downstream. See Figure 26. Due to the formation of this strong vortex street very close to the cylinder, the base pressure decreased to its minimum value and the wake width became much greater than the cylinder diameter. As a result of this, the pressure (form) drag reached its maximum value as illustrated in Figures 20 and 21.

As the gap space was further increased to d/r = 2.0, 3.0, 4.0, 5.33 it was observed that the strength of the vortex street and shedding frequency also appeared to decrease. Therefore, the drag on the cylinder gradually decreased to its "free" cylinder value. See Figure 27.

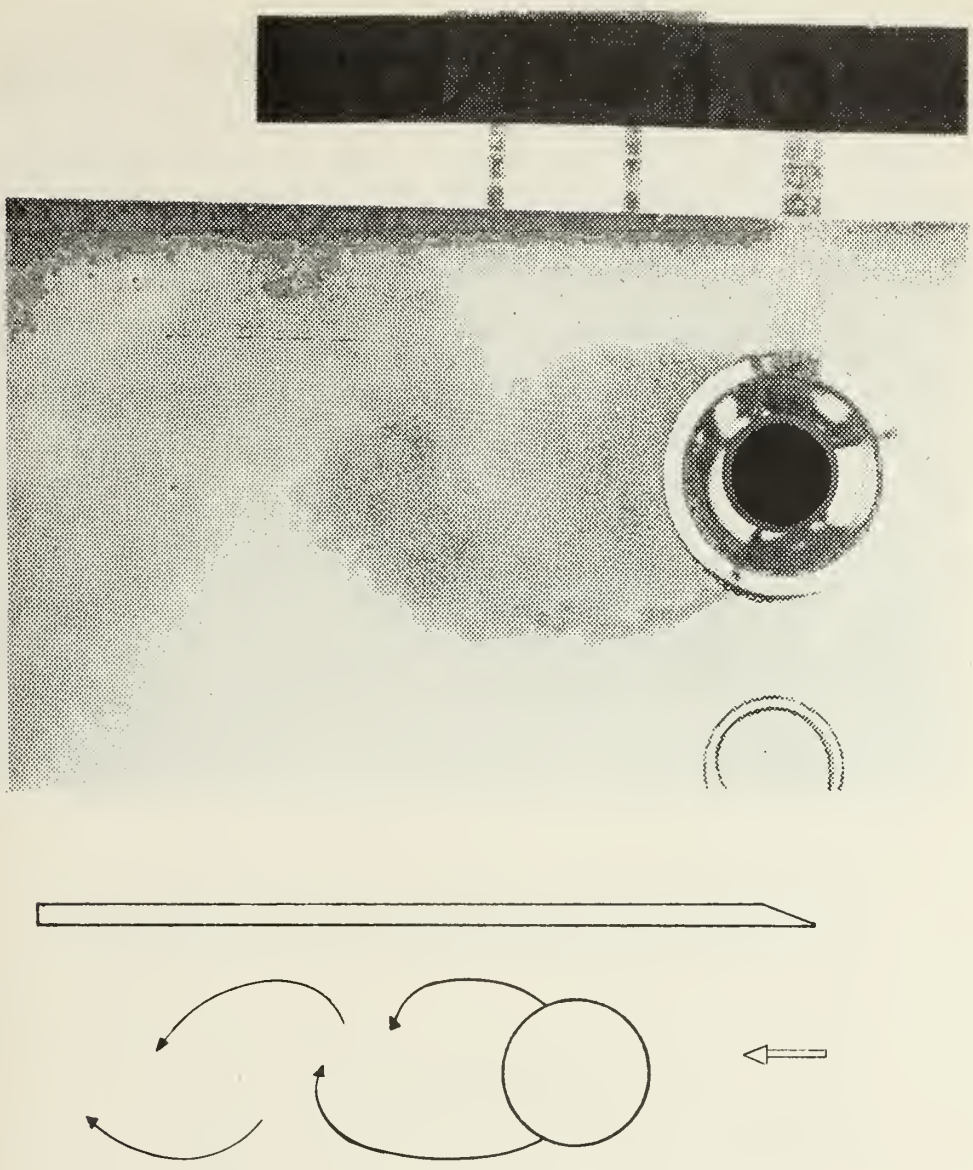

FIGURE 26. Photograph and sketch of the flow pattern at d/r = 1.0

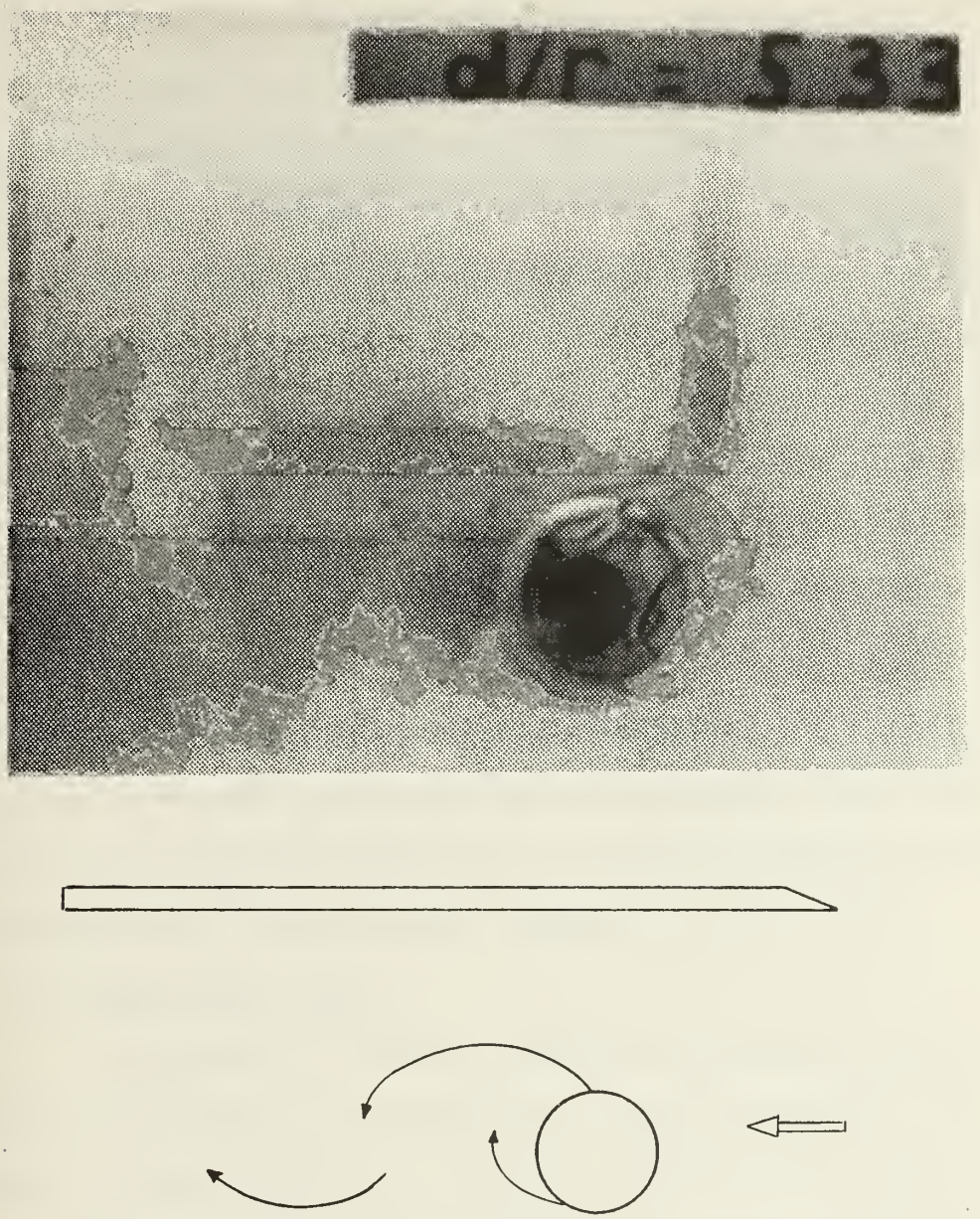

FIGURE 27. Photograph and sketch of the flow pattern at d/r = 5.33

D. VORTEX FREQUENCY EXPERIMENT

In order to obtain quantitative answers to the questions arising from the pressure drag curve characteristics, an experiment was performed to obtain the vortex shedding frequency behind the cylinder (described in detail in Section III). Because of limitations in the hotwire anemometer's transversing mechanism, the vortex shedding frequency was measured from 1 to 2.5 cylinder diameters behind the cylinder. In spite of no limitations in the vertical direction, the best results were obtained at 1.5 cylinder diameters from the center of the cylinder.

During the experiment the following results were obtained.

1. At $d/r = 0.0$

No frequency signal was observed on the display of the oscilloscope and the shedding frequency read from the counter was approximately zero. This was found to agree with the flow visualization results at $d/r = 0.0$.

2. At $d/r = 0.25$

As soon as a space existed between the cylinder and plate, two different frequencies were obtained at the top and bottom of the cylinder. The top frequency was approximately three times greater than the bottom frequency. This implied that there were no strong vortices in the gap between the cylinder and plate. This result also agrees with the flow visualization observation at $d/r = 0.25$.

3. At $d/r = 0.5$

At this gap size, two frequencies again appeared. The top frequency was about the same as the frequency which was found at $d/r = 0.25$ but the bottom frequency was less than the $d/r = 0.25$ case.

4. At $d/r = 1.0$

The maximum frequencies observed during the experiment were at this gap size. This was similar to the qualitative results observed in the flow visualization experiment and also coincides with the location at which the maximum drag coefficient was observed.

As the gap space was further increased to $d/r = 2.0$, 3.0, 4.0, and 5.33 it was found that the shedding frequency gradually decreased to its "free" cylinder value. The results, including the Strouhal number, are shown in Table III. Also, the results were found to agree qualitatively with the results which were obtained by Roshko [4] and Spivak [5].

TOP

d/r	LOCATION			n (Hz)	S
	X	Y	Z		
0.0	7.5	4.5	0.0	0.0	0.0
0.25	7.5	4.5	0.0	73	0.186
0.50	7.5	4.5	0.0	73	0.186
1.0	3.0	4.5	0.0	88	0.224
2.0	3.0	4.5	0.0	79	0.201
3.0	3.0	4.5	0.0	79	0.201
4.0	3.0	4.5	0.0	78	0.198
5.33	3.0	4.5	0.0	78	0.198
BOTTOM					
0.0	7.5	4.5	0.0	0.0	0.00
0.25	7.5	-0.88	0.0	23	0.058
0.50	7.5	-1.24	0.0	20	0.050
1.0	3.0	-2.0	0.0	81	0.206
2.0	3.0	-3.5	0.0	79	0.201
3.0	3.0	-3.9	0.0	79	0.201
4.0	3.0	-4.5	0.0	78	0.198
5.33	3.0	-4.5	0.0	78	0.198

TABLE III. The vortex shedding frequency, n, and Strouhal number, $S = nD/U_S$, as a function of gap size at a Reynolds number of 153,000 with L/D = 4.0

X = Distance measured downstream from the center of the cylinder (inch)

Y = Vertical distance from the center of the cylinder (inch)

VI. SUMMARY

The experimental investigation described in this thesis was conducted to gain an understanding of the fluid flow surrounding a right circular cylinder placed near a plane surface. Surface pressure coefficients were measured around the cylinder circumference for various plate to cylinder spacings, plate lengths and Reynolds numbers. Drag and lift coefficients were obtained from these data by numerical integration.

An unexpected trend which was observed in the plots of drag versus cylinder to plate separation prompted a flow visualization experiment and hotwire anemometer measurements of the vortex shedding frequency in the cylinder wake. Based on these observations and measurements, it was concluded that the structure of the vortex pattern that develops in the wake of the cylinder exerts a controlling influence on the shape of the drag curve. For a range of plate to cylinder spacings on the order of one cylinder radius, it was found that the plate interferes with the formation of the vortex street in the wake of the cylinder. This interference significantly affected the cylinder base pressure which, in turn, influenced the drag on the cylinder.

APPENDIX A

PRESSURE DATA AND DATA REDUCTION

The values of the pressure coefficient were determined from the formula

$$C_p = \frac{P_\theta - P_s}{\frac{1}{2}\rho U_s^2} = \frac{P_\theta - P_s}{P_{ps} - P_s}$$

where

C_p = Pressure coefficient

ρ = Density of air, lb/ft^3

U_s = Air stream velocity, ft/sec

P_θ = Pressure on the cylinder surface at angular location θ, $in\text{-}H_2O$

P_s = Air stream pressure in the wind tunnel test section, $in\text{-}H_2O$

P_{ps} = Pressure in the wind tunnel stilling chamber, $in\text{-}H_2O$

A sample calculation for data obtained at Re = 250,000, d/r = 0.25 and L/D = 4.0 is shown below

$\theta = 235°$ $P_\theta = 14.10$ $P_s = 8.00$ $P_{ps} = 1.90$.

$$C_p = \frac{14.10 - 8.00}{1.90 - 8.00}$$

$$C_p = -1.00$$

PRESSURE DATA

Air Speed = 0.76 in - H_2O
= 57.6 ft/sec

Air Temp = 61 °F

d/r = 0.25

Date : AUGUST - 23 - 1975
Time : 22.40 PM

Re = 90,000

L/D = 4.0

θ	Ps	Pps	Pe	Cp
0	3.68	2.75	2.90	0.232
5			3.02	0.709
10			3.19	0.526
15			3.32	0.367
20			3.55	0.139
25			3.78	-0.107
30			3.95	-0.290
35			4.20	-0.559
40			4.39	-0.763
45			4.58	-0.967
50			4.68	-1.075
55			4.78	-1.182
60			4.78	-1.182
65			4.68	-1.075
70			4.60	-0.989
75			4.59	-0.978
80			4.59	-0.978
85	↓	↓	4.59	-0.978
90	3.68	2.75	4.60	-0.989
95			4.60	-0.989
100			4.60	
105			4.60	
110			4.60	
115			4.60	
120			4.60	
125			4.60	
130			4.60	
135			4.60	
140			4.60	
145			4.60	
150			4.60	
155			4.60	
160			4.60	
165			4.60	
170			4.60	
175	↓	↓	4.60	↓

θ	Ps	Pps	Pe	Cp
180	3.68	2.75	4.60	-0.989
185			4.60	
190			4.60	
195			4.60	
200			4.60	
205			4.60	
210			4.60	
215			4.60	
220			4.60	
225			4.60	
230			4.60	↓
235			4.62	-1.010
240			4.62	-1.010
245			4.62	-1.010
250			4.62	-1.010
255			4.61	-1.000
260			4.61	-1.000
265	↓	↓	4.68	-1.075
270	3.68	2.75	4.82	-1.230
275			4.75	-1.150
280			4.55	-0.935
285			4.30	-0.666
290			4.00	-0.344
295			3.77	-0.096
300			3.60	0.086
305			3.40	0.301
310			3.27	0.440
315			3.13	0.591
320			3.05	0.677
325			2.93	0.806
330			2.83	0.914
335			2.78	0.967
340			2.75	1.000
345			2.75	1.000
350			2.77	0.978
355	↓	↓	2.62	0.924

PRESSURE DATA

Air Speed = 2.2 in. H_2O
= 98 ft/sec

Air Temp = 78°F

d/r = 0.25

Date : JULY-29-1975
Time : 16 20 PM

Re = 153,000

L/D = 4.0

θ	Ps	Pps	Pe	Cp
0	4.40	2.00	2.50	0.791
5			2.75	0.687
10			3.25	0.479
15			3.62	0.322
20			4.20	0.083
25			4.80	-0.166
30			5.20	-0.333
35			5.78	-0.575
40			6.25	-0.770
45			6.70	-0.956
50			7.05	-1.104
55			7.25	-1.187
60			7.25	-1.187
65			6.90	-1.041
70			6.85	-1.020
75			6.80	-1.000
80			6.80	-1.000
85	↓	↓	6.80	-1.000
90	4.40	2.00	6.80	-1.000
95			6.84	-1.016
100			6.85	-1.020
105			6.80	-1.000
110			6.77	-0.989
115			6.77	-0.989
120			6.80	-1.000
125			6.80	
130			6.80	
135			6.80	
140			6.80	
145			6.80	
150			6.80	↓
155			6.75	-0.979
160			6.75	
165			6.75	
170			6.75	
175	↓	↓	6.75	↓

θ	Ps	Pps	Pe	Cp
180	4.40	2.00	6.75	-0.979
185			6.80	-1.000
190			6.80	
195			6.80	
200			6.80	
205			6.80	
210			6.80	
215			6.80	
220			6.80	
225			6.80	↓
230			6.85	-1.020
235			6.85	-1.020
240			6.85	-1.020
245			6.82	-1.010
250			6.82	-1.010
255			6.82	-1.010
260			6.80	-1.000
265	↓	↓	6.85	-1.020
270	4.40	2.00	7.35	-1.229
275			7.20	-1.166
280			6.62	-0.927
285			6.06	-0.691
290			5.40	-0.416
295			4.60	-0.083
300			4.20	0.083
305			3.70	0.291
310			3.30	0.458
315			2.95	0.604
320			2.65	0.729
325			2.35	0.854
330			2.20	0.916
335			2.10	0.958
340			2.05	0.979
345			2.05	0.979
350			2.10	0.958
355	↓	↓	2.20	0.916

PRESSURE DATA

Air Speed = 5.85 in-H_2O
= 160 ft/sec

Air Temp = 66 °F

Date : AUGUST-31-1975
Time : 9.30 AM

Re = 250,000

d/r = 0.25

L/D = 4.0

θ	Ps	Pps	Pe	Cp
0	8.00	1.90	3.00	0.819
5			3.78	0.691
10			4.87	0.513
15			5.88	0.347
20			7.25	0.122
25			9.70	-0.114
30			9.90	-0.311
35			11.38	-0.554
40			12.80	-0.786
45			14.00	-0.983
50			14.90	-1.131
55			15.70	-1.262
60			15.75	-1.270
65			14.65	-1.090
70			14.30	-1.032
75			14.30	-1.032
80			14.30	-1.032
85	↓	↓	14.40	-1.049
90	8.00	1.90	14.30	-1.032
95			14.10	-1.000
100			14.10	-1.000
105			14.00	-0.983
110			14.00	-0.983
115			14.00	-0.983
120			14.00	-0.983
125			14.00	-0.983
130			14.05	-0.991
135			14.00	-0.983
140			14.05	-0.991
145			14.05	-0.991
150			14.00	-0.983
155			14.00	-0.983
160			14.00	-0.983
165			14.00	-0.983
170			13.90	-0.967
175	↓	↓	13.95	-0.975

θ	Ps	Pps	Pe	Cp
180	8.00	1.90	14.00	-0.983
185			13.90	-0.967
190			14.00	-0.983
195			13.99	-0.981
200			13.99	-0.981
205			13.99	-0.981
210			14.00	-0.983
215			14.00	-0.983
220			14.05	-0.991
225			14.00	-0.983
230			14.05	-0.991
235			14.10	-1.000
240			14.15	-1.008
245			14.20	-1.016
250			14.20	-1.016
255			14.15	-1.008
260			14.05	-0.991
265	↓	↓	14.30	-1.032
270	8.00	1.90	15.70	-1.262
275			15.10	-1.163
280			13.60	-0.918
285			11.95	-0.647
290			10.10	-0.344
295			8.50	-0.081
300			7.38	0.101
305			6.15	0.303
310			5.20	0.459
315			4.30	0.606
320			3.70	0.704
325			3.00	0.819
330			2.58	0.891
335			2.00	0.983
340			1.89	1.001
345			1.90	1.000
350			2.08	0.970
355	↓	↓	2.49	0.903

APPENDIX B

CALCULATION OF PRESSURE DRAG AND LIFT COEFFICIENTS

The pressure drag coefficient and lift coefficient were calculated from the following formulas.

$$C_{dp} = \frac{1}{2} \int_0^{2\pi} C_p(\theta) \cos \theta \, d\theta$$

$$C_L = -\frac{1}{2} \int_0^{2\pi} C_p(\theta) \sin \theta \, d\theta$$

where

C_{dp} = Pressure drag coefficient
C_L = Lift coefficient
C_p = Pressure coefficient
$d\theta$ = Angular increment (5-degree)

Pressure drag and lift coefficients were obtained by numerically integrating the above formulas using the computer (IBM 360) and Simpson's Rule of Quadrature with a step size of five degrees. The results are shown in Table II in Section V.

APPENDIX C

UNCERTAINTY ANALYSIS

Since uncertainties existed in our measured variables, an uncertainty analysis was performed in order to ascertain the degree of uncertainty in the experimental results. The method of Kline and McClintock [7] was used.

Uncertainties existed in the following variables:

Wall manometer	Z	± 0.05 inch	(20:1)
Manometer bank	H	± 0.05 inch	(20:1)

The uncertainties associated with the properties of air were considered negligible.

REYNOLDS NUMBER, Re:

The Reynolds number was calculated from the equation

$$Re = \frac{U_s \cdot D}{\nu}$$

Therefore,

$$\frac{\omega_{Re}}{Re} = \sqrt{\left(\frac{\omega_{U_s}}{U_s}\right)^2 + \left(\frac{\omega_D}{D}\right)^2 + \left(\frac{\omega_\nu}{\nu}\right)^2}$$

The value of U_s is directly proportional to the square root of the wall manometer reading Z; hence

$$\frac{\omega_{U_s}}{U_s} = 0.5 \frac{\omega_Z}{Z}$$

Again, since the uncertainty in the kinematic viscosity of air and in the cylinder diameter are negligible,

$$\frac{\omega_{Re}}{Re} = 0.5 \frac{\omega_Z}{Z}$$

Therefore at various Reynolds number ranges the uncertainties were calculated as follows:

a) At a Reynolds number of 90,000

$Z = 0.76$ in-H_2O $\omega_Z = \pm 0.05$ in-H_2O

$$\frac{\omega_{Re}}{Re} = 0.5(0.05/0.76)$$

$$\frac{\omega_{Re}}{Re} = 0.0328 \quad \text{or} \quad \omega_{Re} = 2968 \approx 3000$$

$$Re = 90{,}000 \pm 3000 \quad (20:1)$$

b) At a Reynolds number of 153,000

$Z = 2.20$ $\omega_Z = \pm 0.05$ in-H_2O

$$\frac{\omega_{Re}}{Re} = 0.5(0.05/2.20)$$

$$\frac{\omega_{Re}}{Re} = 0.011 \qquad \text{or} \qquad \omega_{Re} = 1738 \approx 2000$$

$$Re = 153{,}000 \pm 2000 \qquad (20:1)$$

c) At a Reynolds number of 250,000

$$Z = 5.85 \text{ in-}H_2O \qquad \omega_Z = 0.05 \text{ in-}H_2O$$

$$\frac{\omega_{Re}}{Re} = 0.5(0.05/5.85)$$

$$\frac{\omega_{Re}}{Re} = 0.004 \qquad \text{or} \qquad \omega_{Re} = 1000$$

$$Re = 250{,}000 \pm 1000 \qquad (20:1)$$

PRESSURE COEFFICIENT, C_p:

The pressure coefficient was calculated from the equation

$$C_p = \frac{P_\theta - P_s}{P_{ps} - P_s} = \frac{\Delta P_1}{\Delta P_2}$$

Therefore,

$$\frac{\omega_{C_p}}{C_p} = \sqrt{\left(\frac{\omega_{\Delta P_1}}{\Delta P_1}\right)^2 + \left(\frac{\omega_{\Delta P_2}}{\Delta P_2}\right)^2}$$

Since both pressure differences were measured on the same manometer bank they shared the same uncertainty which is shown on page 75. Therefore, for the various Reynolds numbers the uncertainties were calculated for the pressure coefficient as follows.

a) At a Reynolds number of 90,000 and an angular location of 270 degrees,

$d/r = 0.25 \quad L/D = 4.0 \quad P_\theta = 4.82 \quad P_s = 3.68 \quad P_{ps} = 2.75$

$$\frac{\omega_{C_p}}{C_p} = 0.069 \qquad \text{or} \qquad \omega_{C_p} = 0.08$$

$$C_p = -1.23 \pm 0.08 \qquad (20:1)$$

b) At a Reynolds number of 153,000 and an angular location of 270 degrees,

$d/r = 0.25 \quad L/D = 4.0 \quad P_\theta = 7.35 \quad P_s = 4.40 \quad P_{ps} = 2.00$

$$\frac{\omega_{C_p}}{C_p} = 0.026 \qquad \text{or} \qquad \omega_{C_p} = 0.03$$

$$C_p = -1.23 \pm 0.03 \qquad (20:1)$$

c) At a Reynolds number of 250,000 and an angular location of 270 degrees

$d/r = 0.25 \quad L/D = 4.0 \quad P_\theta = 15.7 \quad P_s = 8.00 \quad P_{ps} = 1.90$

$$\frac{\omega_{C_p}}{C_p} = 0.01 \qquad \text{or} \qquad \omega_{C_p} = 0.01$$

$$C_p = -1.26 \pm 0.01 \qquad (20:1)$$

PRESSURE DRAG AND LIFT COEFFICIENTS, C_{dp} , C_L

Since the pressure drag and lift coefficients were obtained integrating the pressure coefficient, it seems reasonable to assume that the drag and lift coefficients exhibit the same uncertainty as the pressure coefficient. Therefore,

a) At a Reynolds number of 90,000, d/r = 0.25, and L/D = 4.0

$$C_{dp} = 1.17 \pm 0.08$$

(20:1)

$$C_L = 0.40 \pm 0.08$$

b) At a Reynolds number of 153,000, d/r = 0.25, and L/D = 4.0

$$C_{dp} = 1.16 \pm 0.03$$

(20:1)

$$C_L = 0.41 \pm 0.03$$

c) At a Reynolds number of 250,000, d/r = 0.25, and L/D = 4.0

$$C_{dp} = 1.15 \pm 0.01$$

(20:1)

$$C_L = 0.42 \pm 0.01$$

APPENDIX D

POLAR PLOTS OF PRESSURE COEFFICIENT VERSUS ANGULAR LOCATION

The polar plots for Reynolds numbers of 90,000 and 250,000 with plate L/D = 4.0 and d/r ranging from 0.0 to 5.33 are shown in Figures 28 through 43. Also this Appendix includes the polar plots for Reynolds number of 153,000 with plate L/D = 2.0, 8.0 and d/r ranging from 0.0 to 5.33. See Figures 44 through 59.

C_p x

Nu •

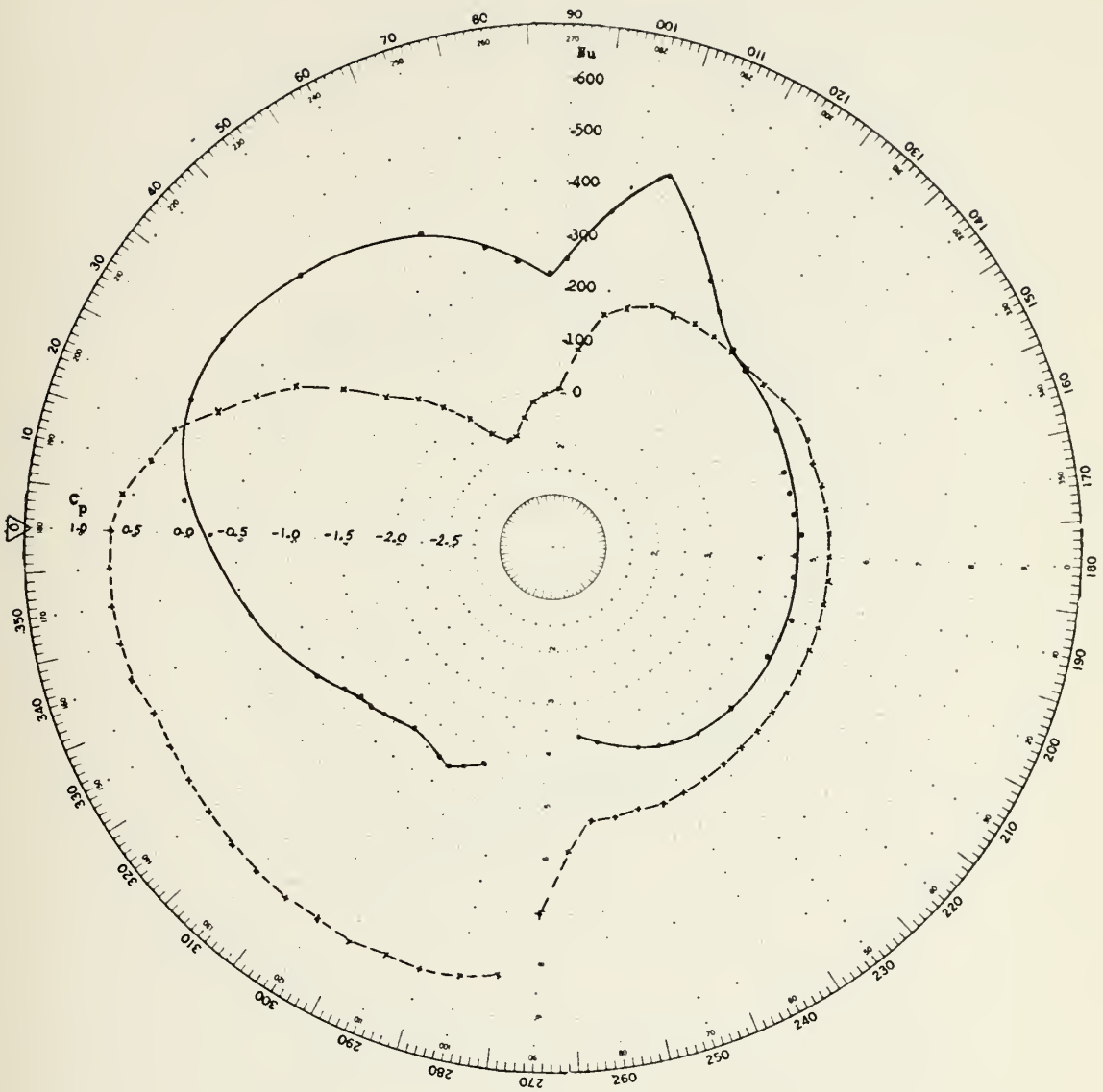

FIGURE 28. Pressure coefficient and local Nusselt number on the surface of a cylinder placed near a plane surface for:
Re = 90,000, L/D = 4.0, d/r = 0.0

C_p x

Nu •

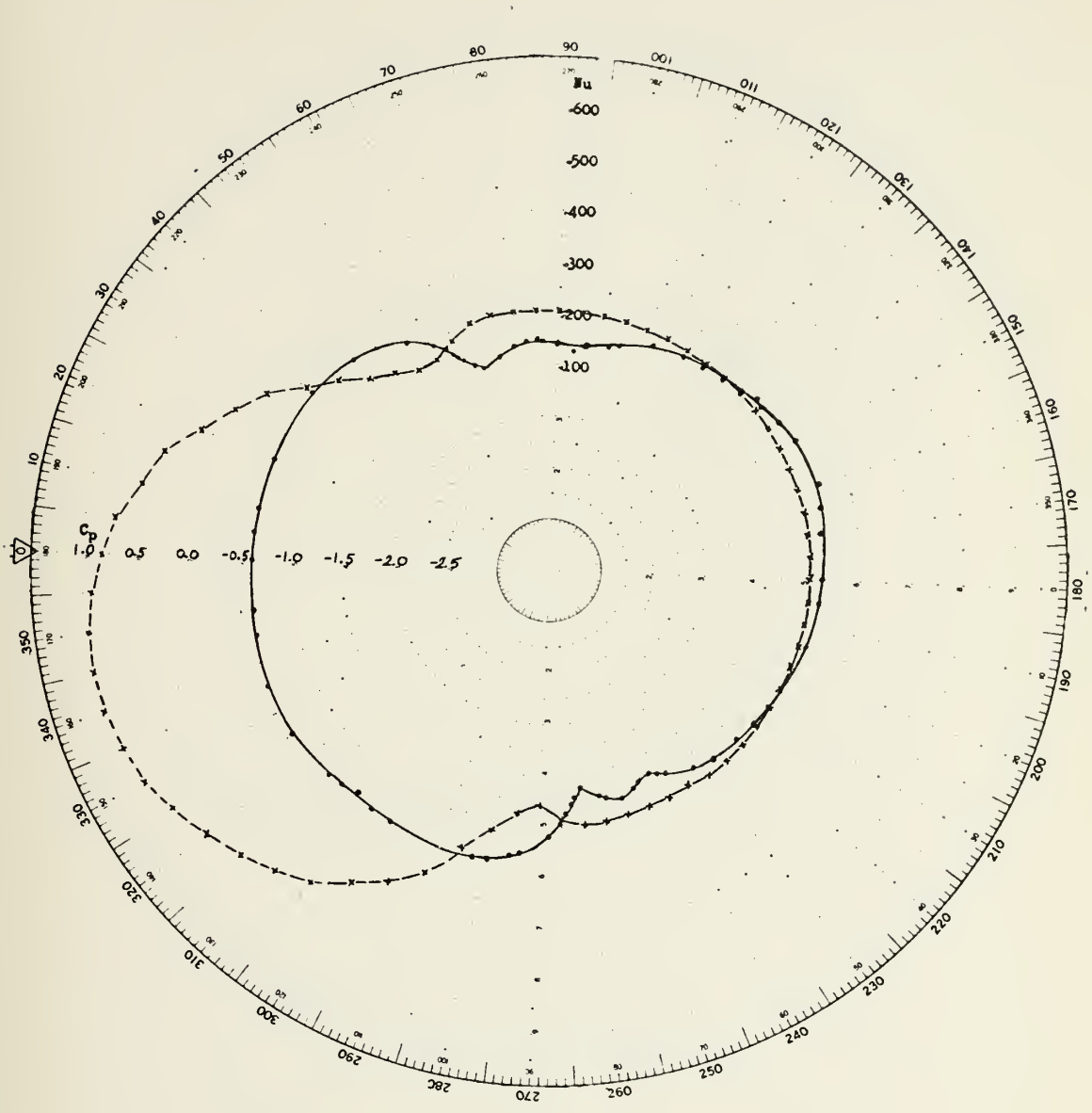

FIGURE 29. Pressure coefficient and local Nusselt number on the surface of a cylinder placed near a plane surface for:
Re = 90,000 , L/D = 4.0 , d/r = 0.25

C_p x

Nu .

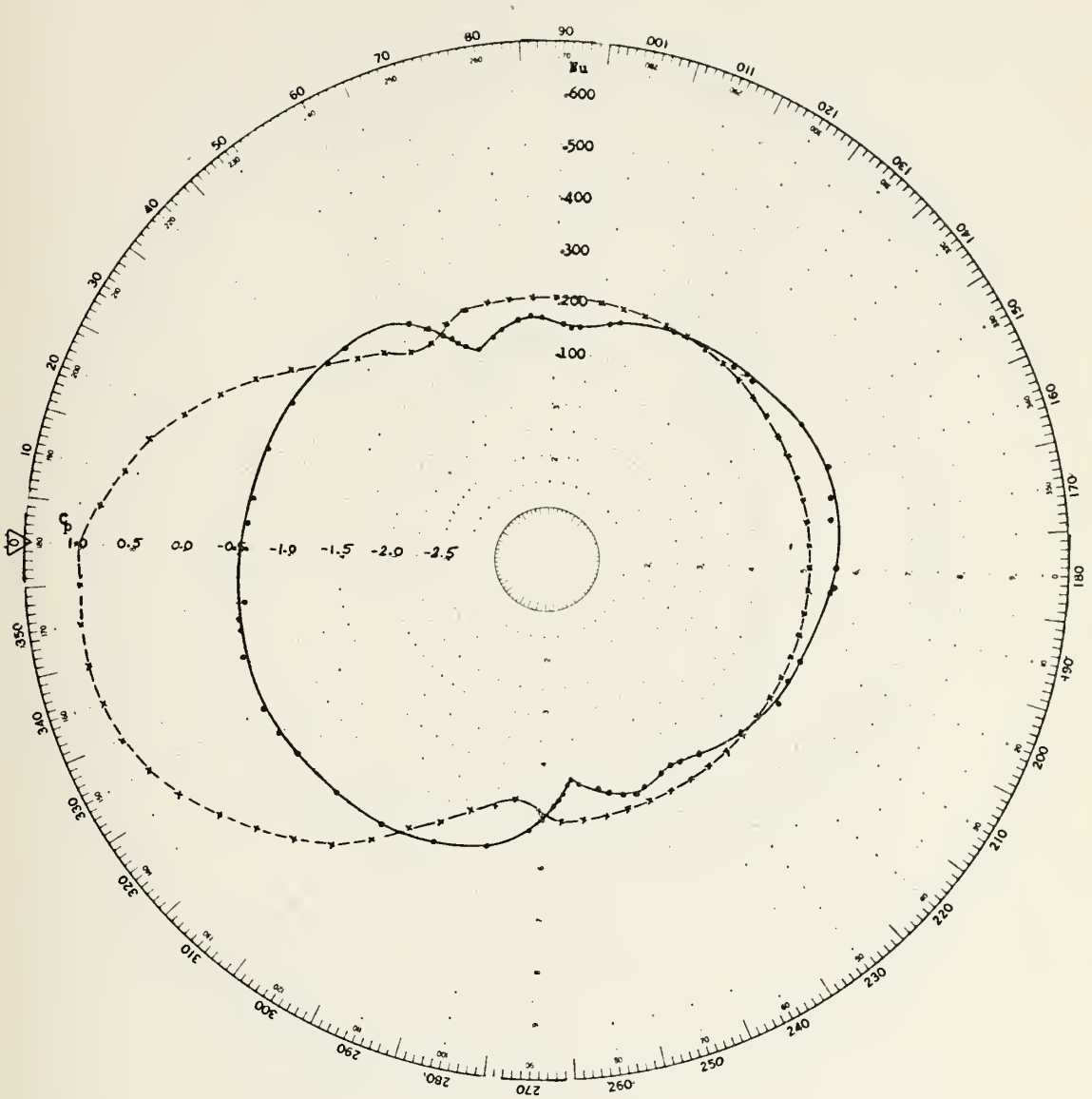

FIGURE 30. Pressure coefficient and local Nusselt number on the surface of a cylinder placed near a plane surface for:
Re = 90,000 , L/D = 4.0 , d/r = 0.5

C_p x

Nu .

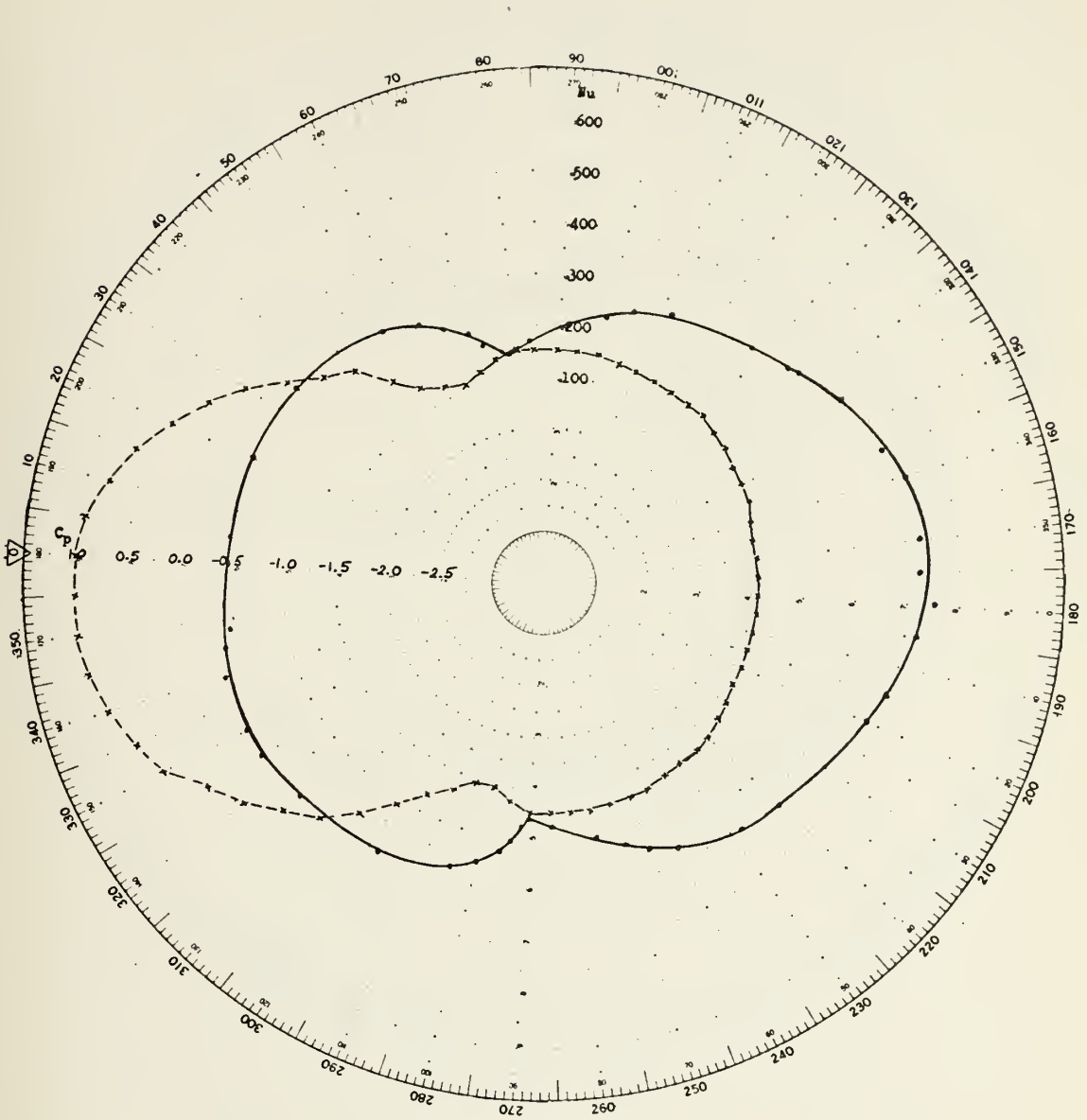

FIGURE 31. Pressure coefficient and local Nusselt number on the surface of a cylinder placed near a plane surface for:
Re = 90,000 , L/D = 4.0 , d/r = 1.0

C_p x

Nu .

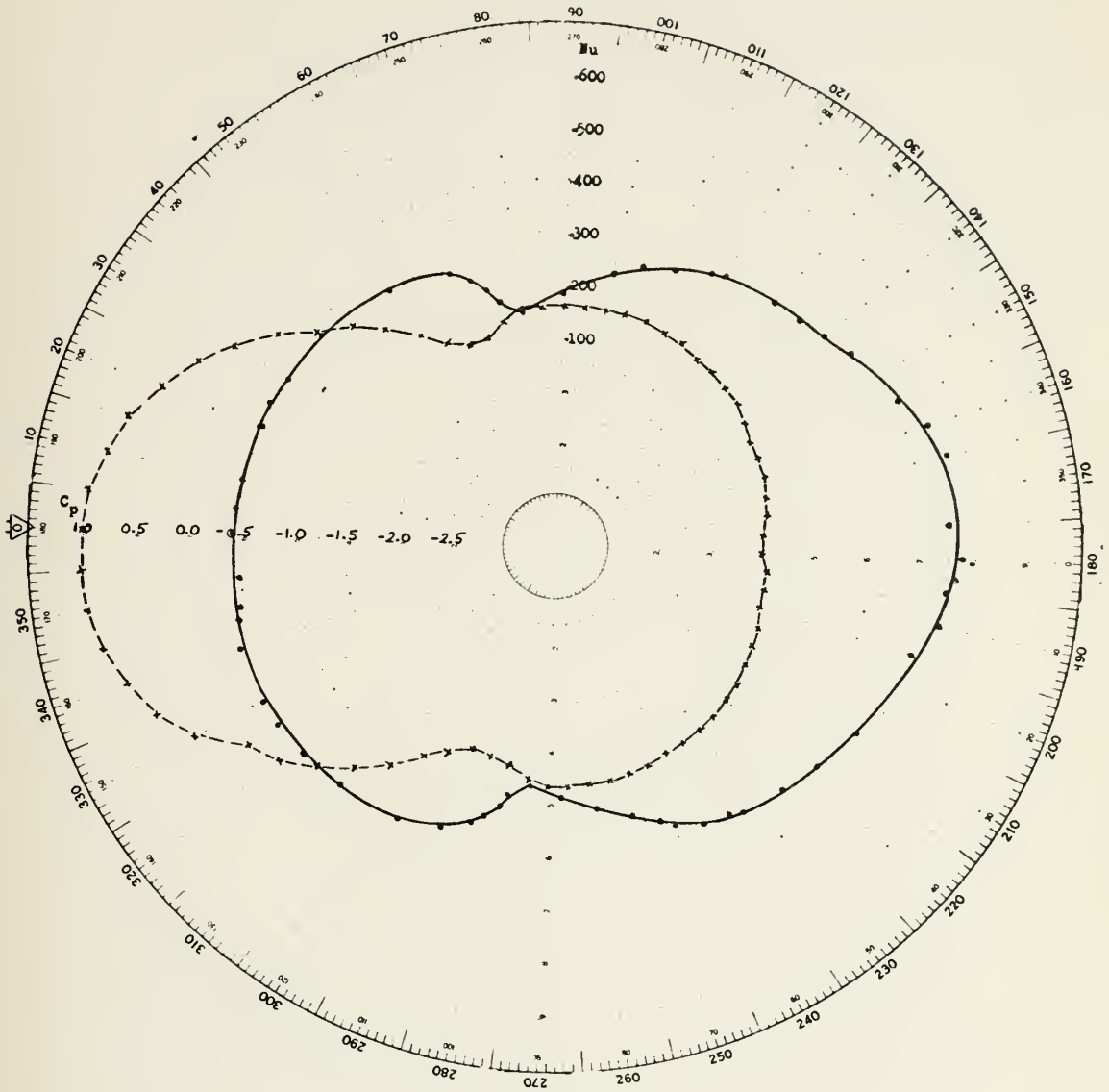

FIGURE 32. Pressure coefficient and local Nusselt number on the surface of a cylinder placed near a plane surface for:
Re = 90,000 , L/D = 4.0 , d/r = 2.0

C_p x

Nu .

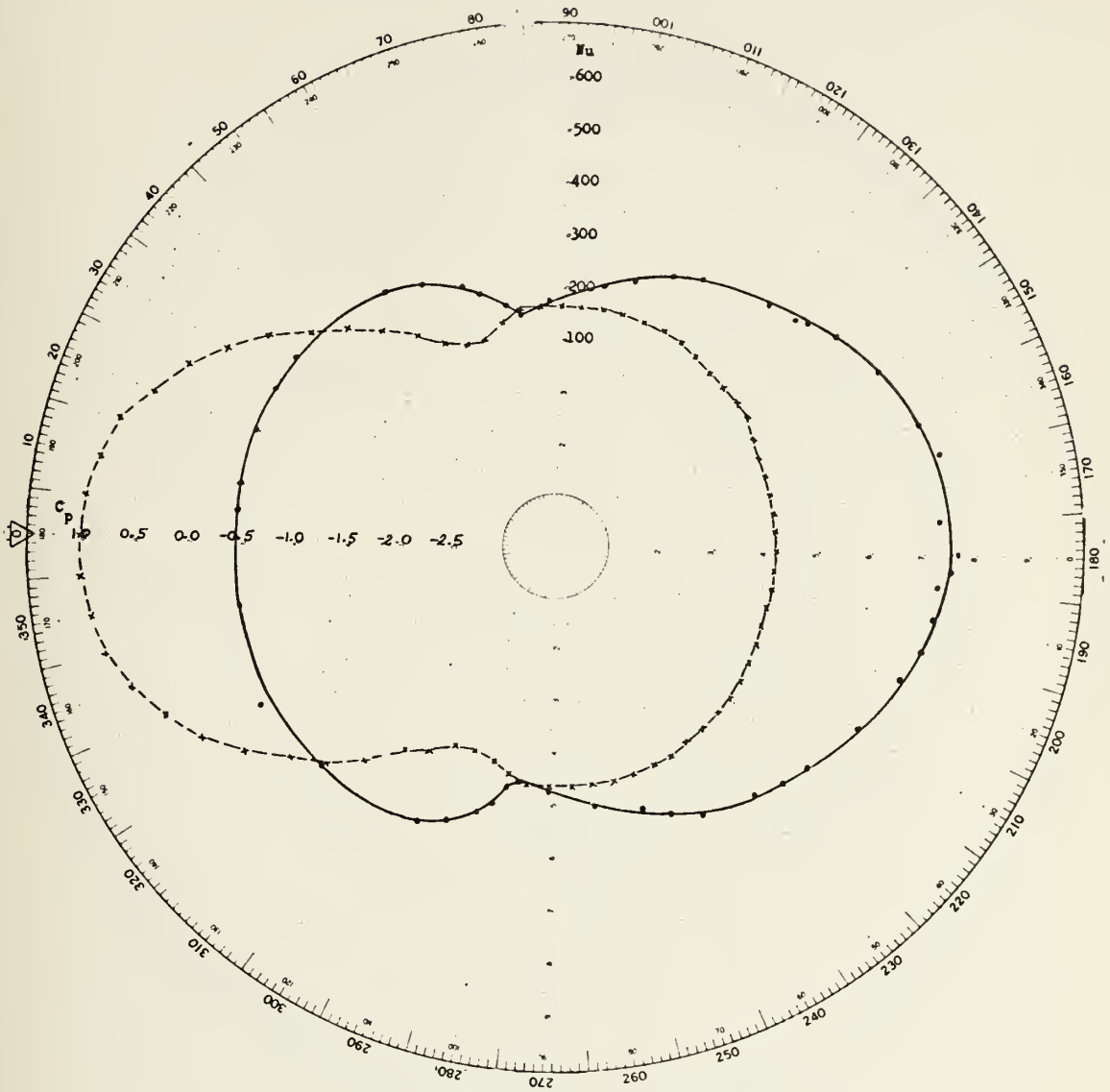

FIGURE 33. Pressure coefficient and local Nusselt number on the surface of a cylinder near a plane surface for:
Re = 90,000 , L/D = 4.0 , d/r = 3.0

C_p x

Nu .

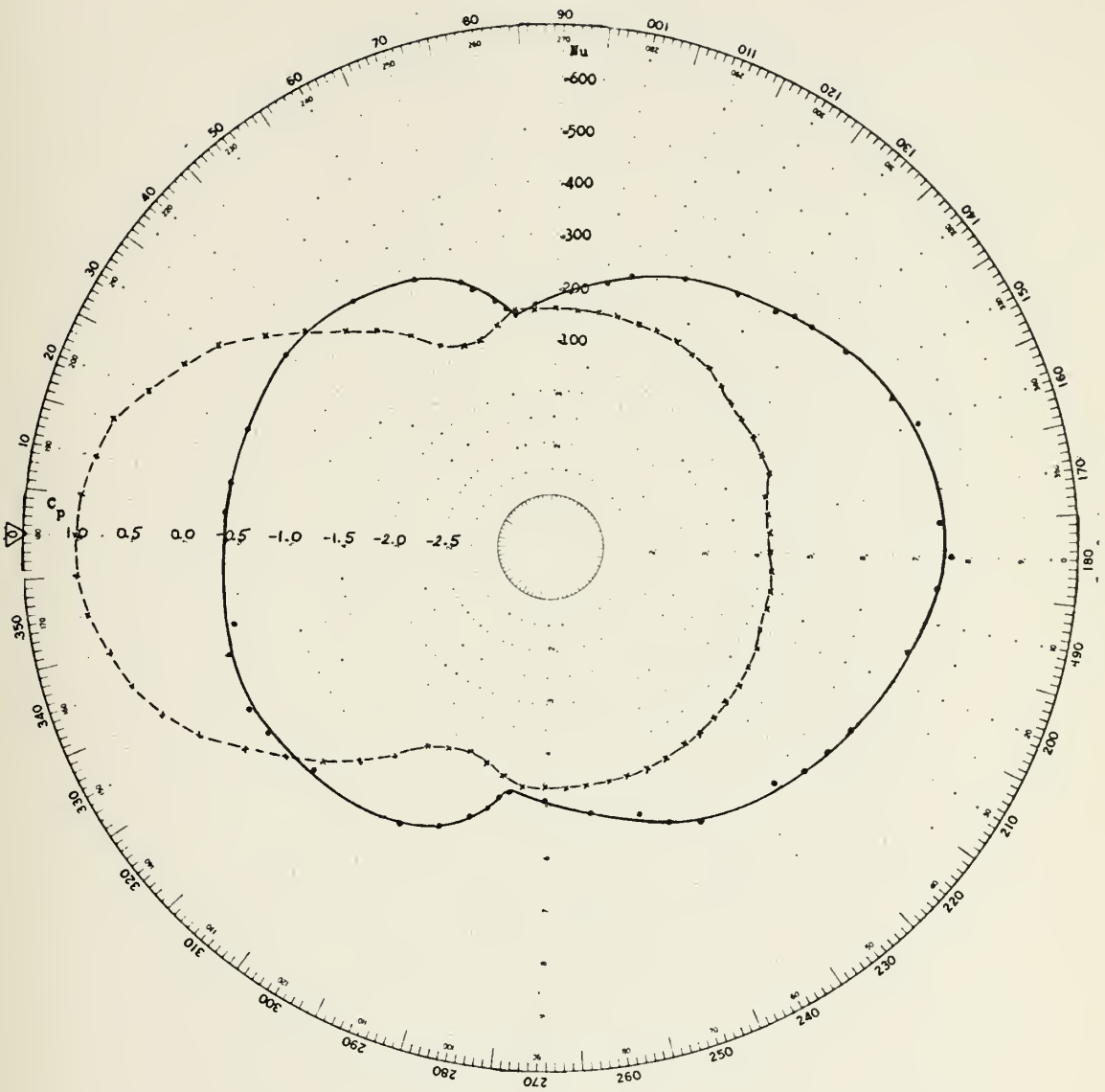

FIGURE 34. Pressure coefficient and local Nusselt number on the surface of a cylinder placed near a plane surface for:
Re = 90,000 , L/D = 4.0 , d/r = 4.0

C_p x

Nu .

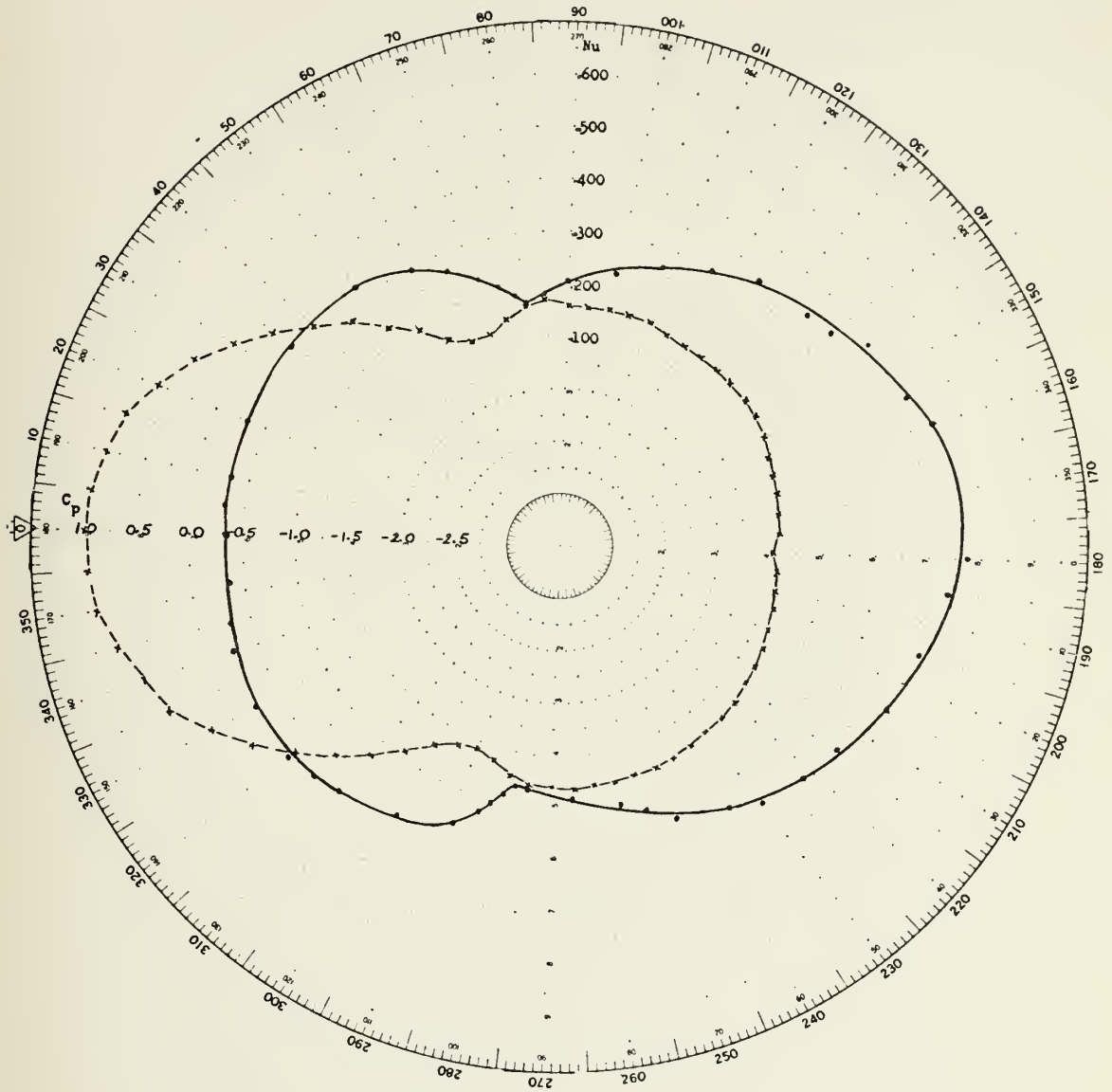

FIGURE 35. Pressure coefficient and local Nusselt number on the surface of a cylinder placed near a plane surface for:
Re = 90,000 , L/D = 4.0 , d/r = 5.33

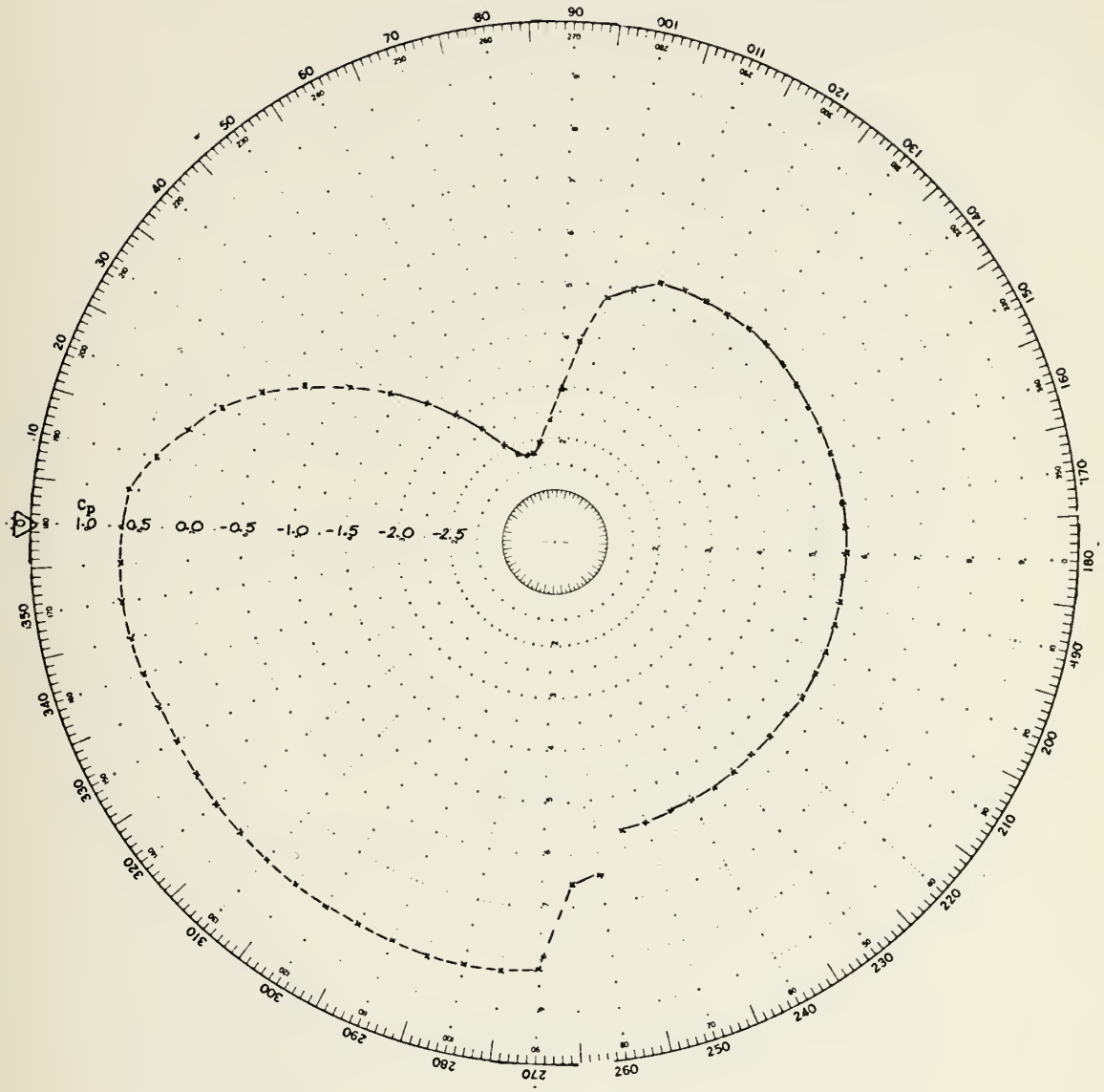

FIGURE 36. Pressure coefficient on the surface of a cylinder placed near a plane surface for: Re = 250,000, L/D = 4.0, d/r = 0.0

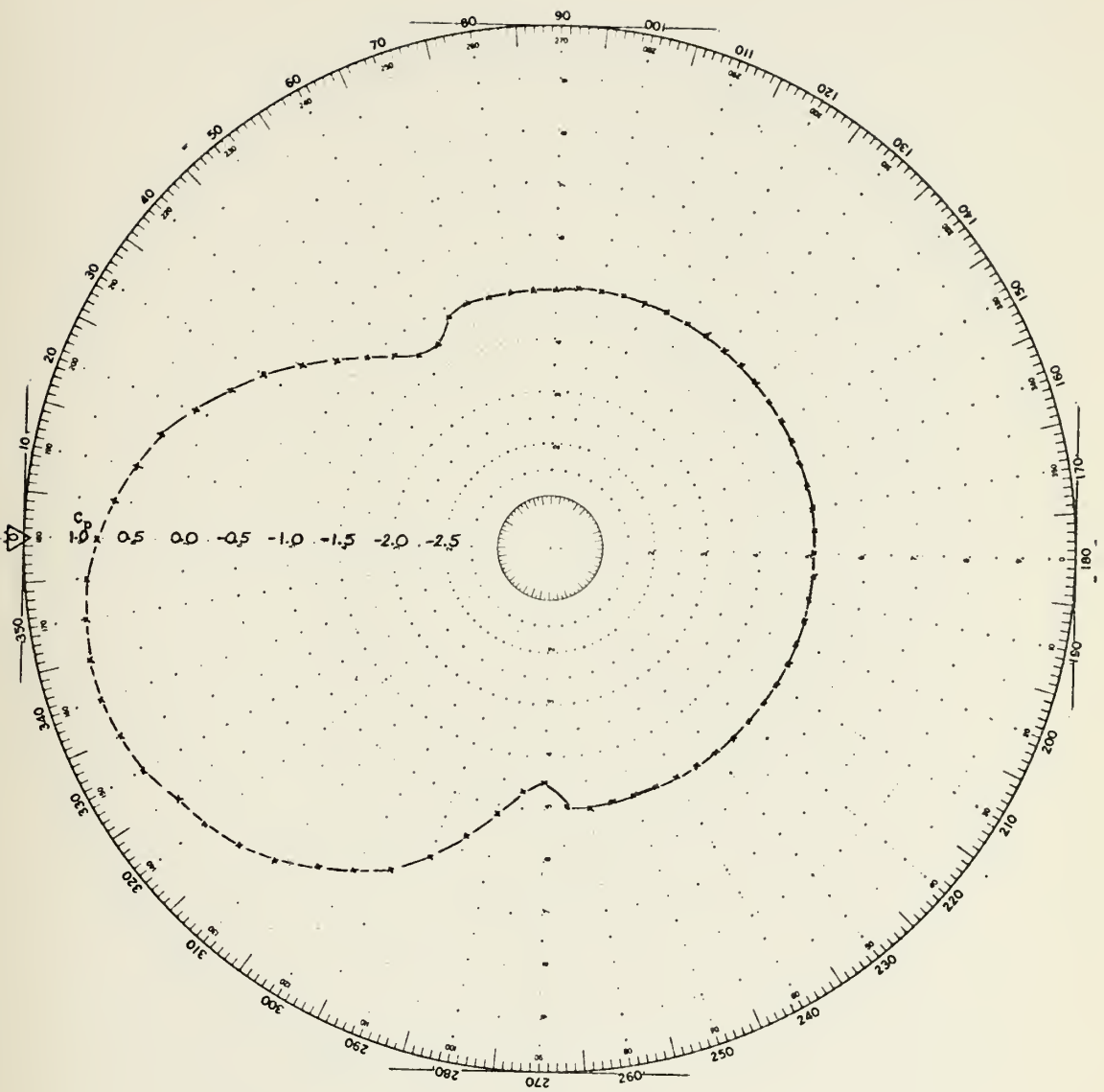

FIGURE 37. Pressure coefficient on the surface of a cylinder placed near a plane surface for: Re = 250,000 , L/D = 4.0 , d/r = 0.25

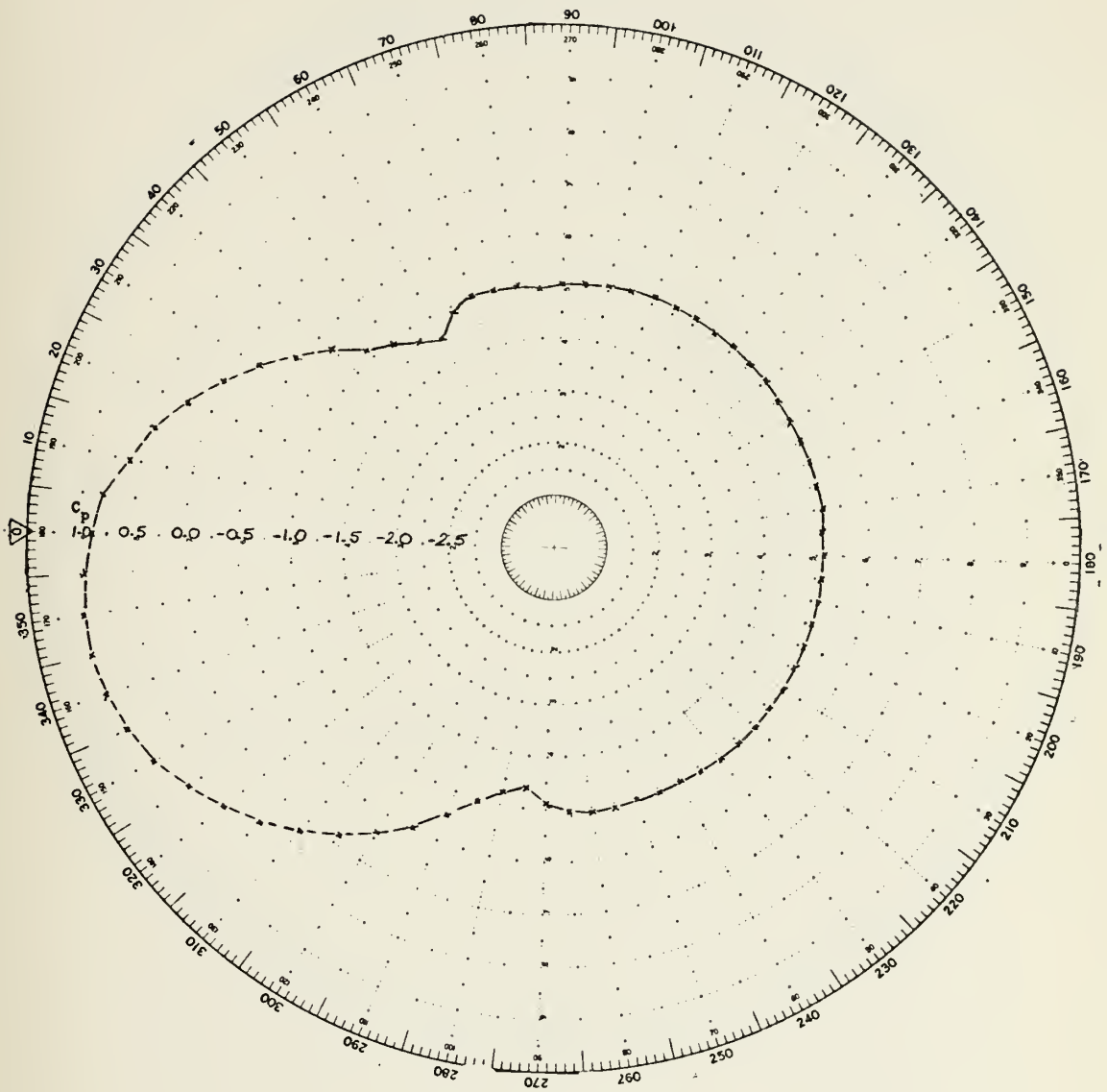

FIGURE 38. Pressure coefficient on the surface of a cylinder placed near a plane surface for: Re = 250,000 , L/D = 4.0 , d/r = 0.5

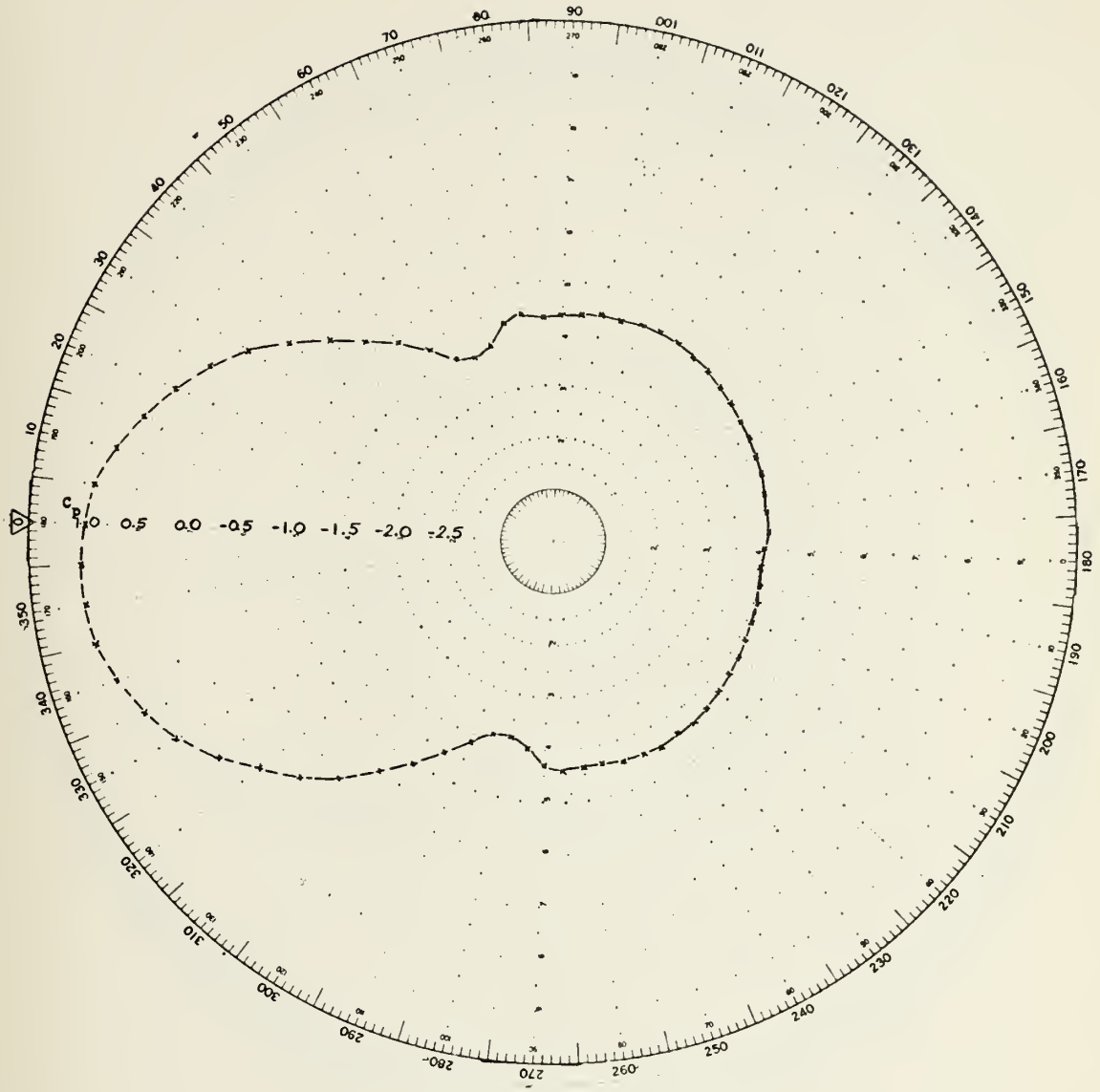

FIGURE 39. Pressure coefficient on the surface of a cylinder placed near a plane surface for: Re = 250,000 , L/D = 4.0 , d/r = 1.0

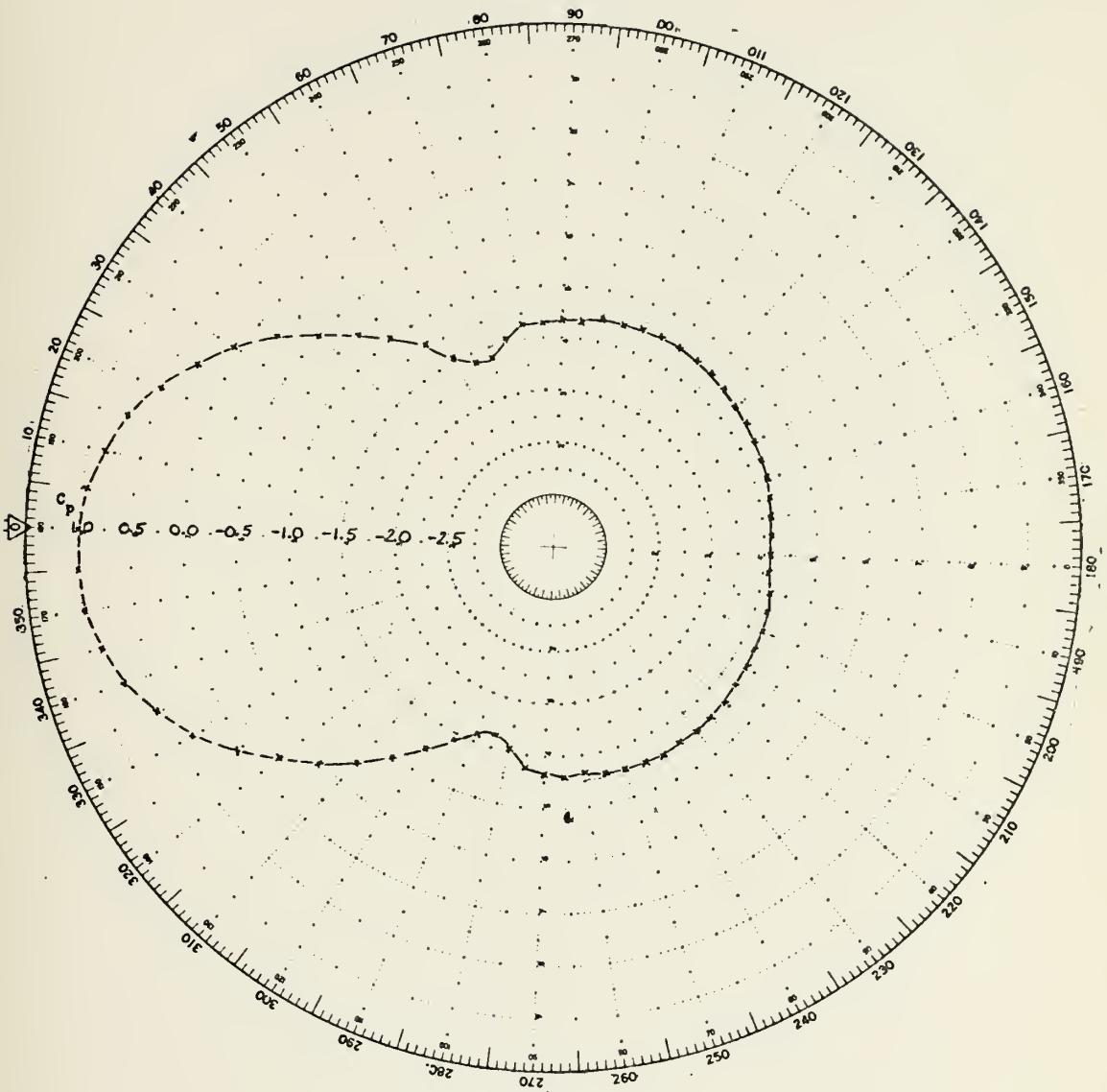

FIGURE 40. Pressure coefficient on the surface of a cylinder placed near a plane surface for: Re = 250,000 , L/D = 4.0 , d/r = 2.0

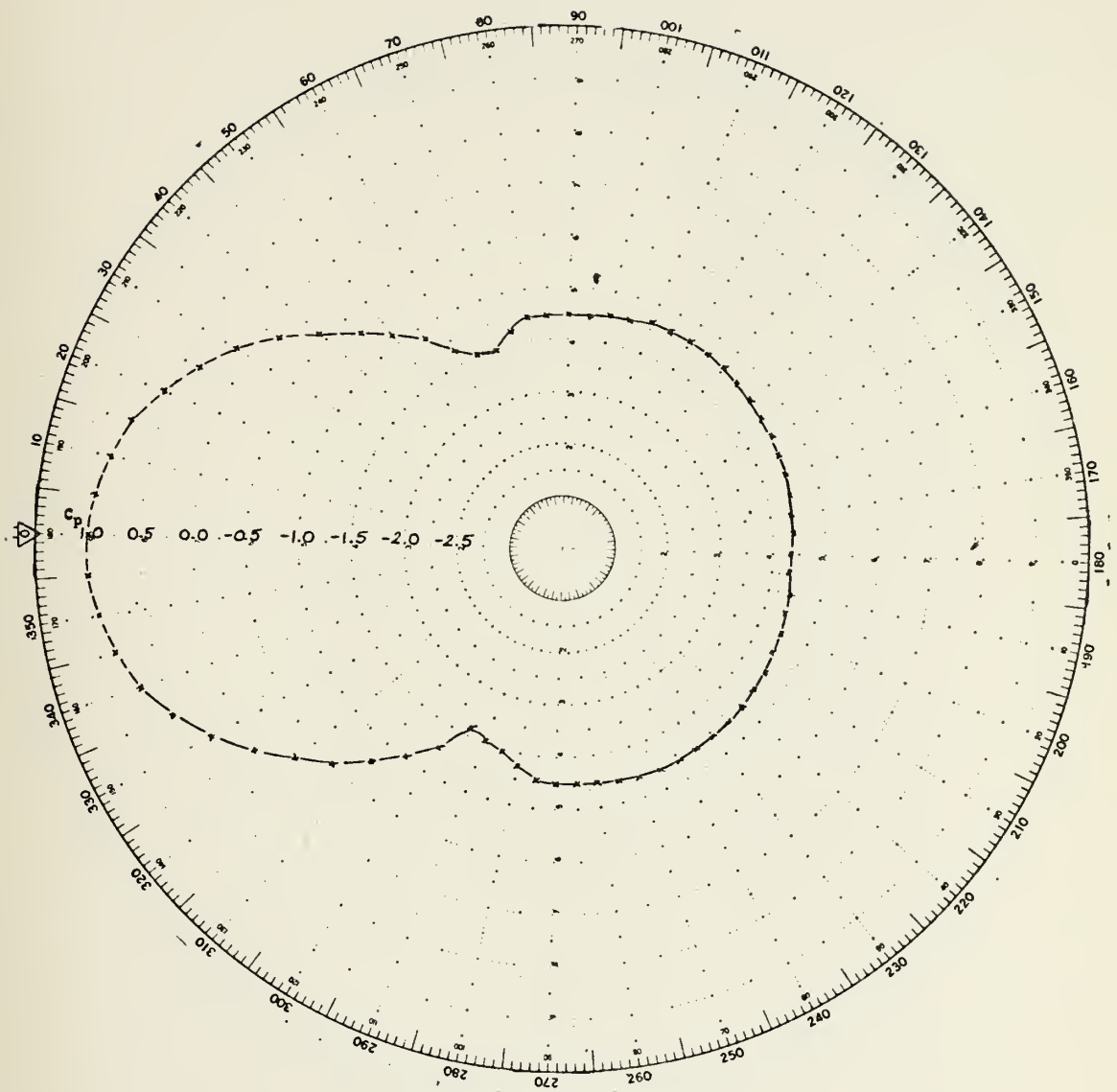

FIGURE 41. Pressure coefficient on the surface of a cylinder placed near a plane surface for: Re = 250,000 , L/D = 4.0 , d/r = 3.0

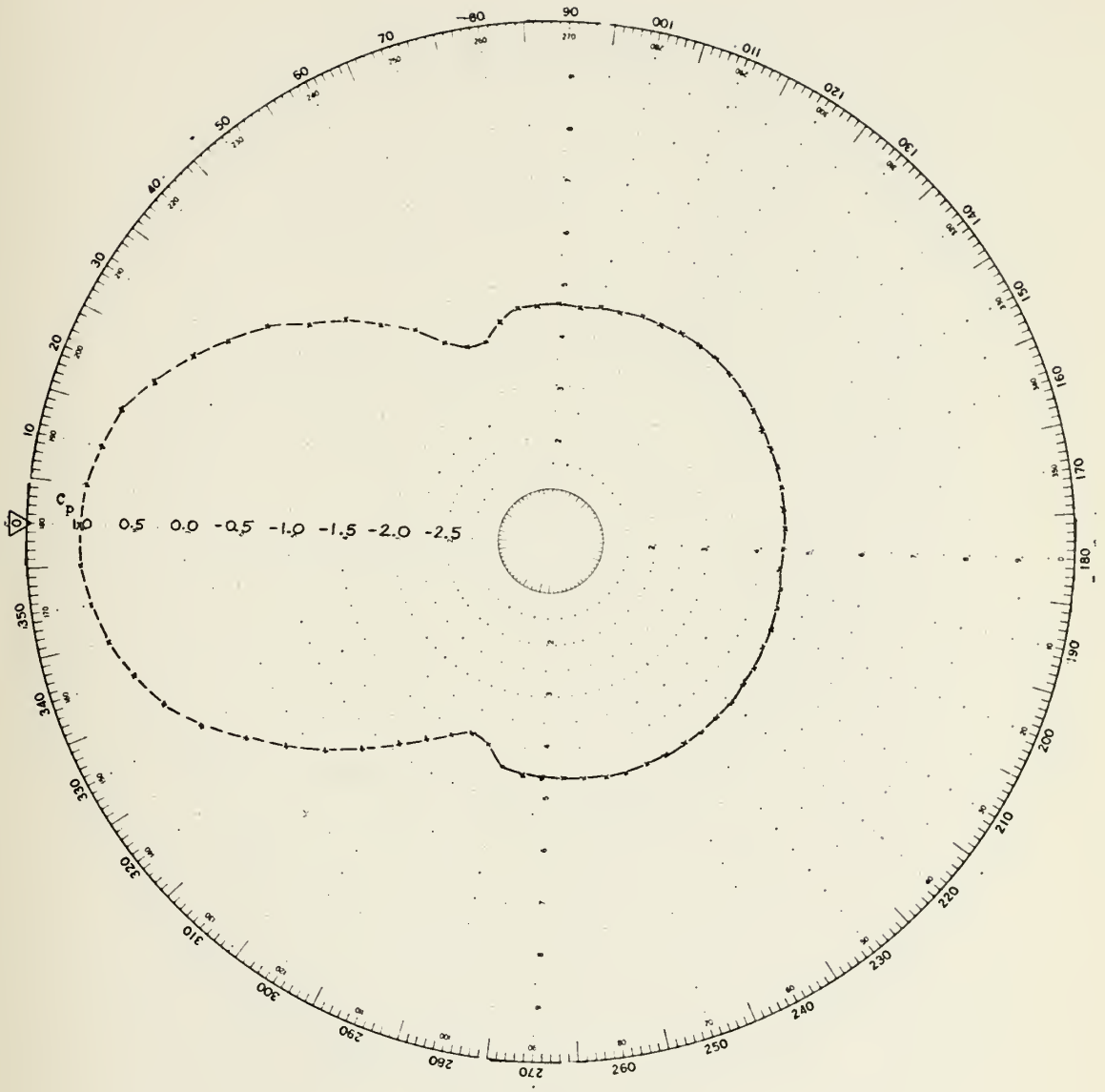

FIGURE 42. Pressure coefficient on the surface of a cylinder placed near a plane surface for: Re = 250,000 , L/D = 4.0 , d/r = 4.0

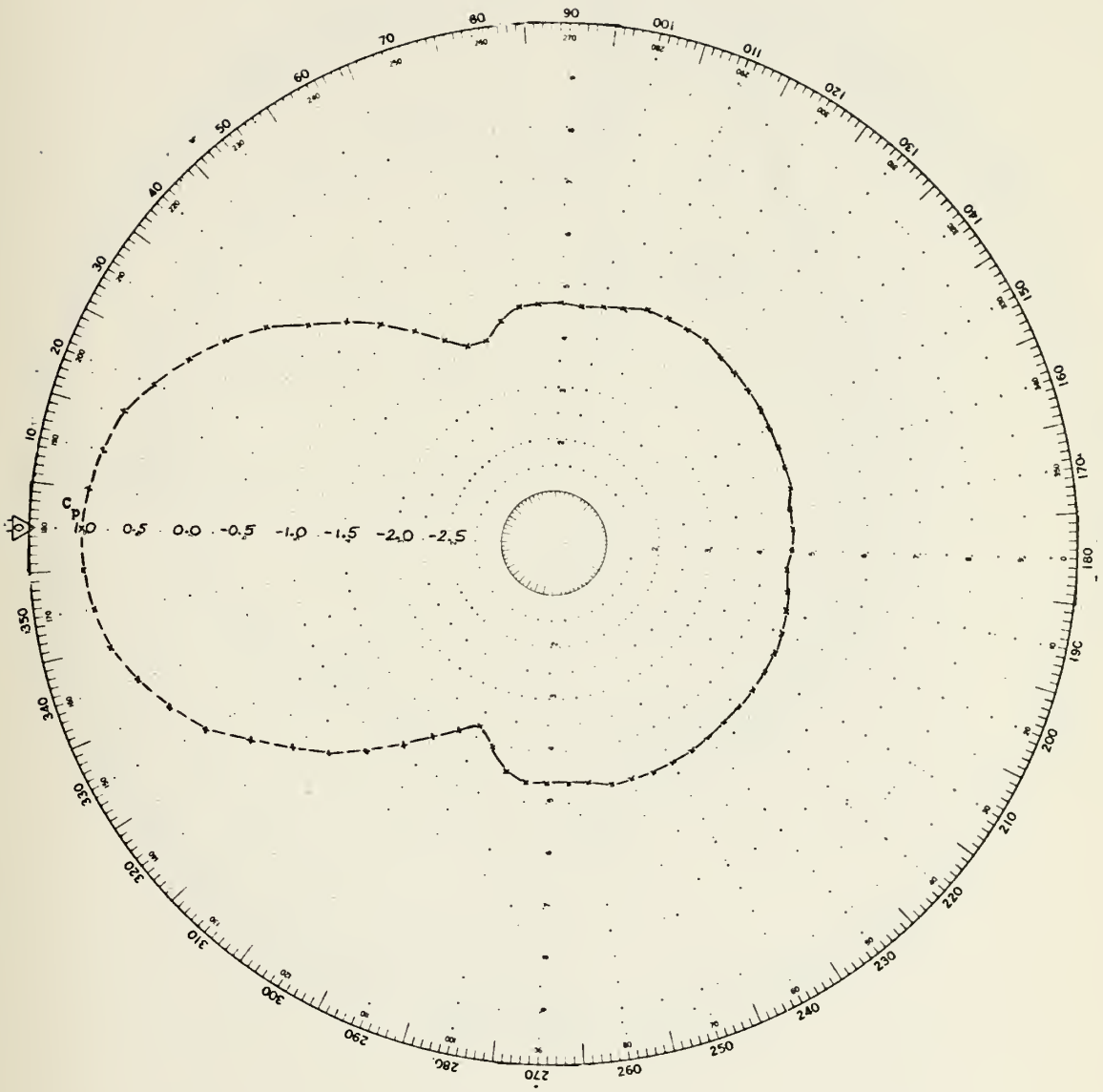

FIGURE 43. Pressure coefficient on the surface of a cylinder placed near a plane surface for: Re = 250,000 , L/D = 4.0 , d/r = 5.33

C_p x

Nu .

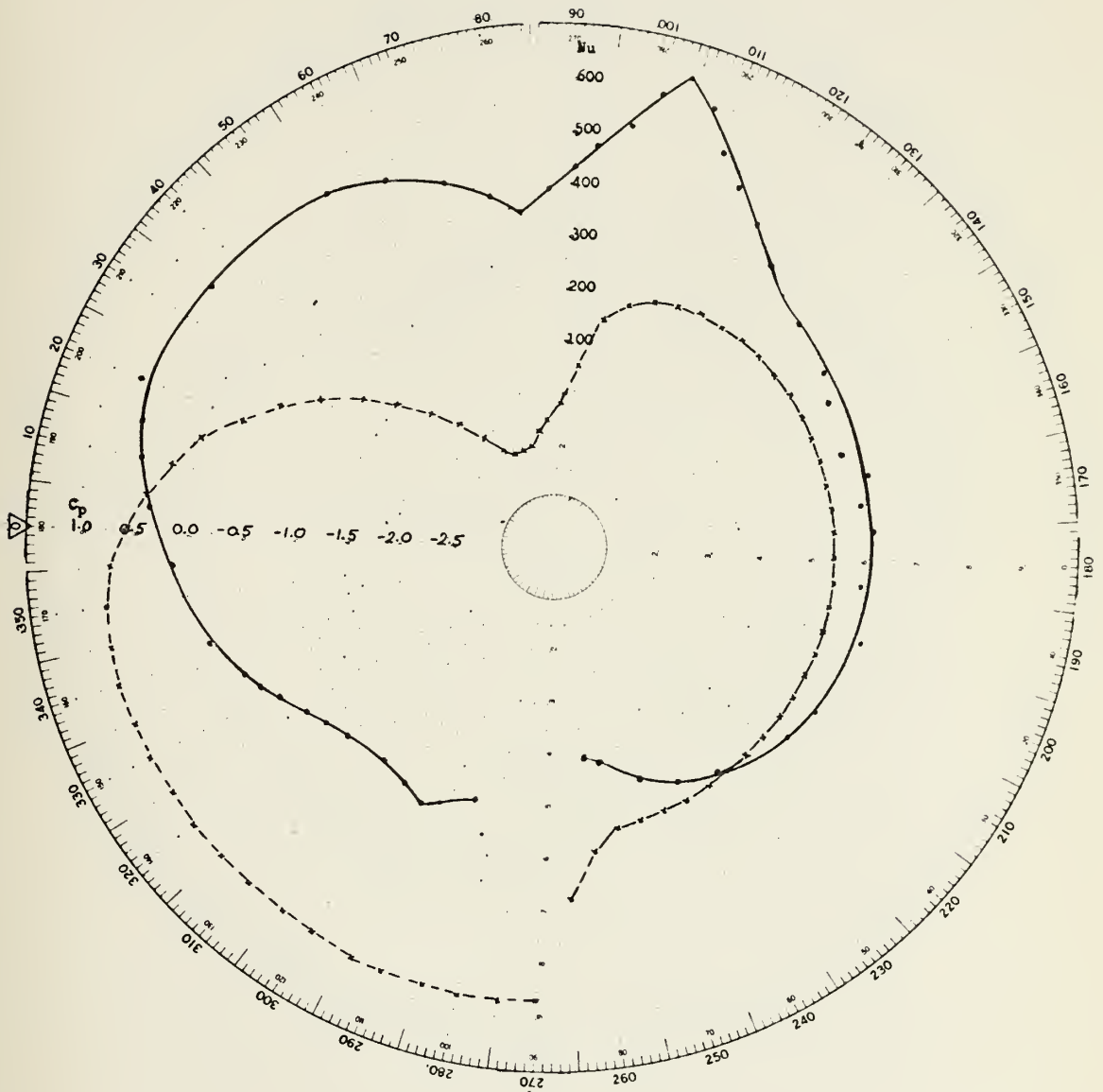

FIGURE 44. Pressure coefficient and local Nusselt number on the surface of a cylinder placed near a plane surface for:
Re = 153,000 , L/D = 2.0 , d/r = 0.0

C_p x

Nu .

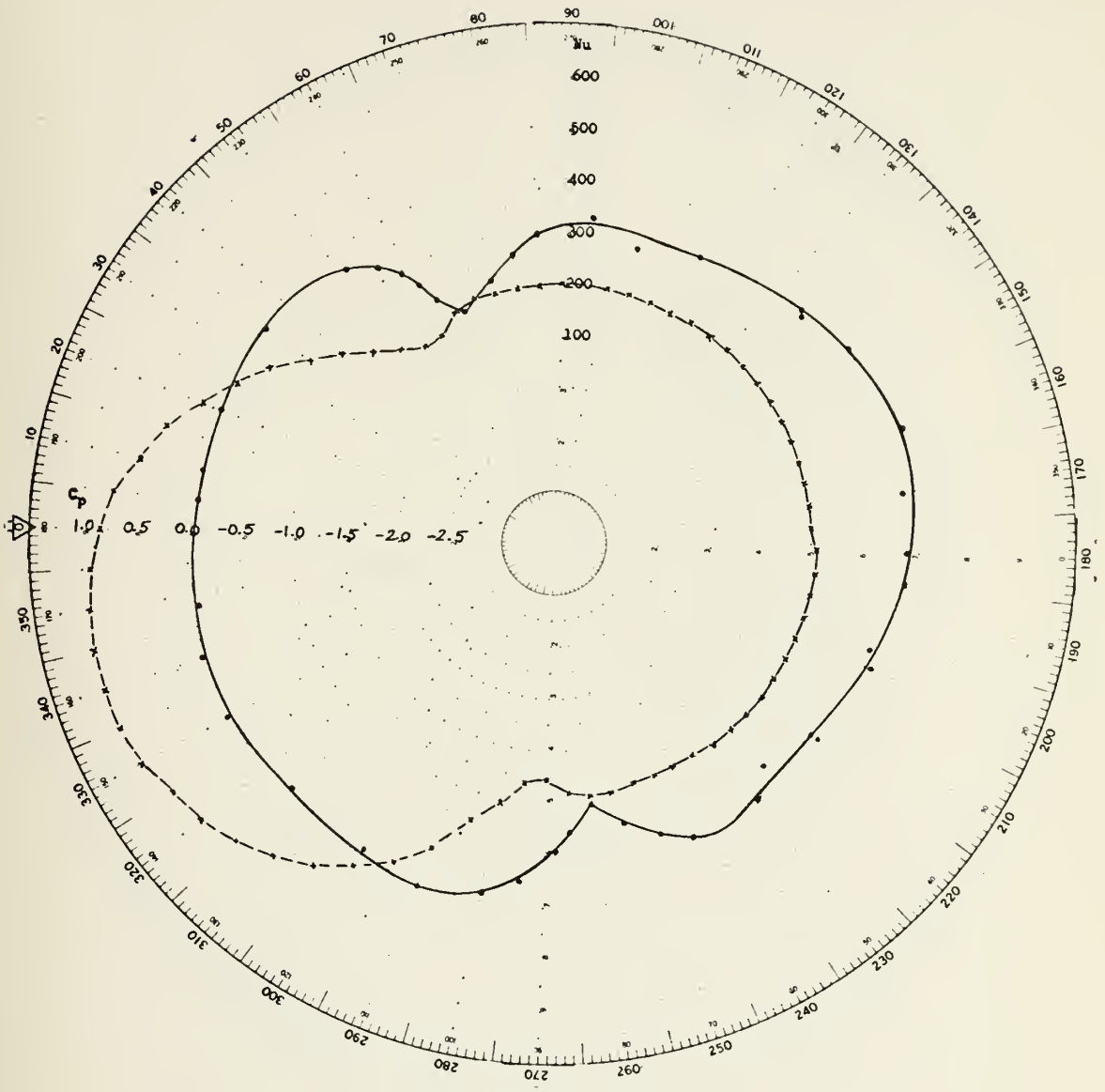

FIGURE 45. Pressure coefficient and local Nusselt number on the surface of a cylinder placed near a plane surface for:
Re = 153,000 , L/D = 2.0 , d/r = 0.25

C_p x

Nu .

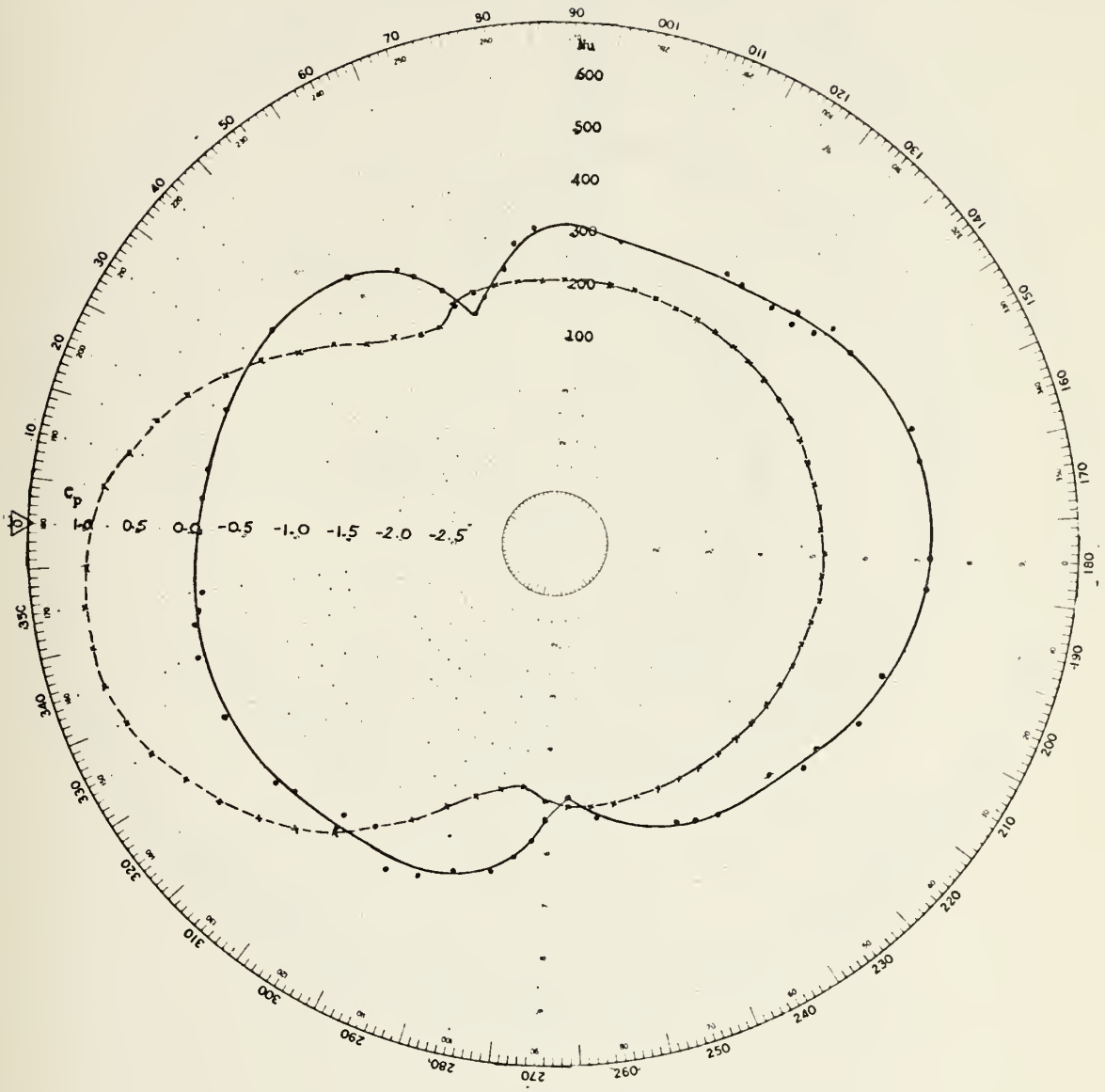

FIGURE 46. Pressure coefficient and local Nusselt number on the surface of a cylinder placed near a plane surface for:
Re = 153,000 , L/D = 2.0 , d/r = 0.5

C_p x

Nu .

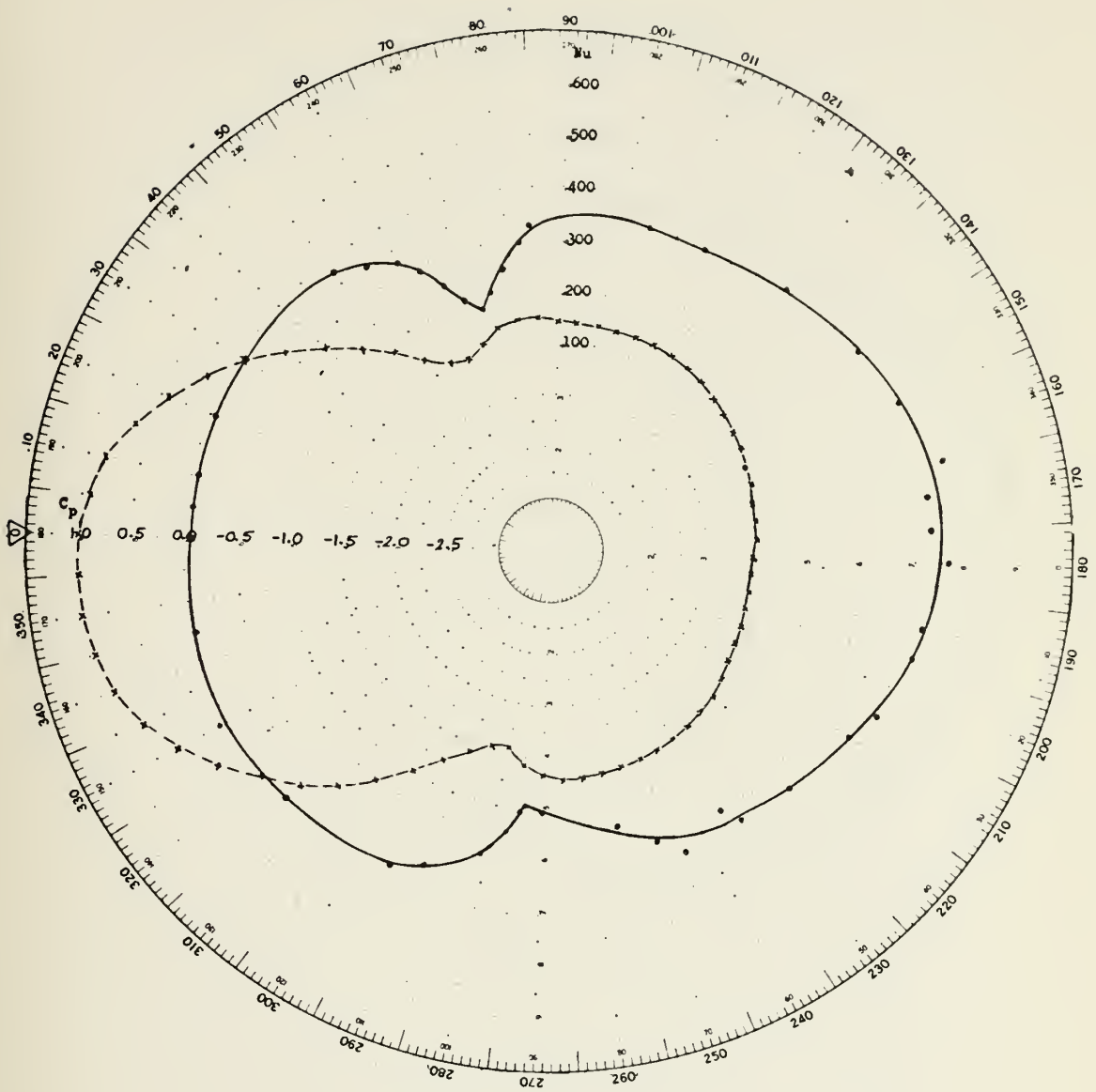

FIGURE 47. Pressure coefficient and local Nusselt number on the surface of a cylinder placed near a plane surface for:
Re = 153,000 , L/D = 2.0 , d/r = 1.0

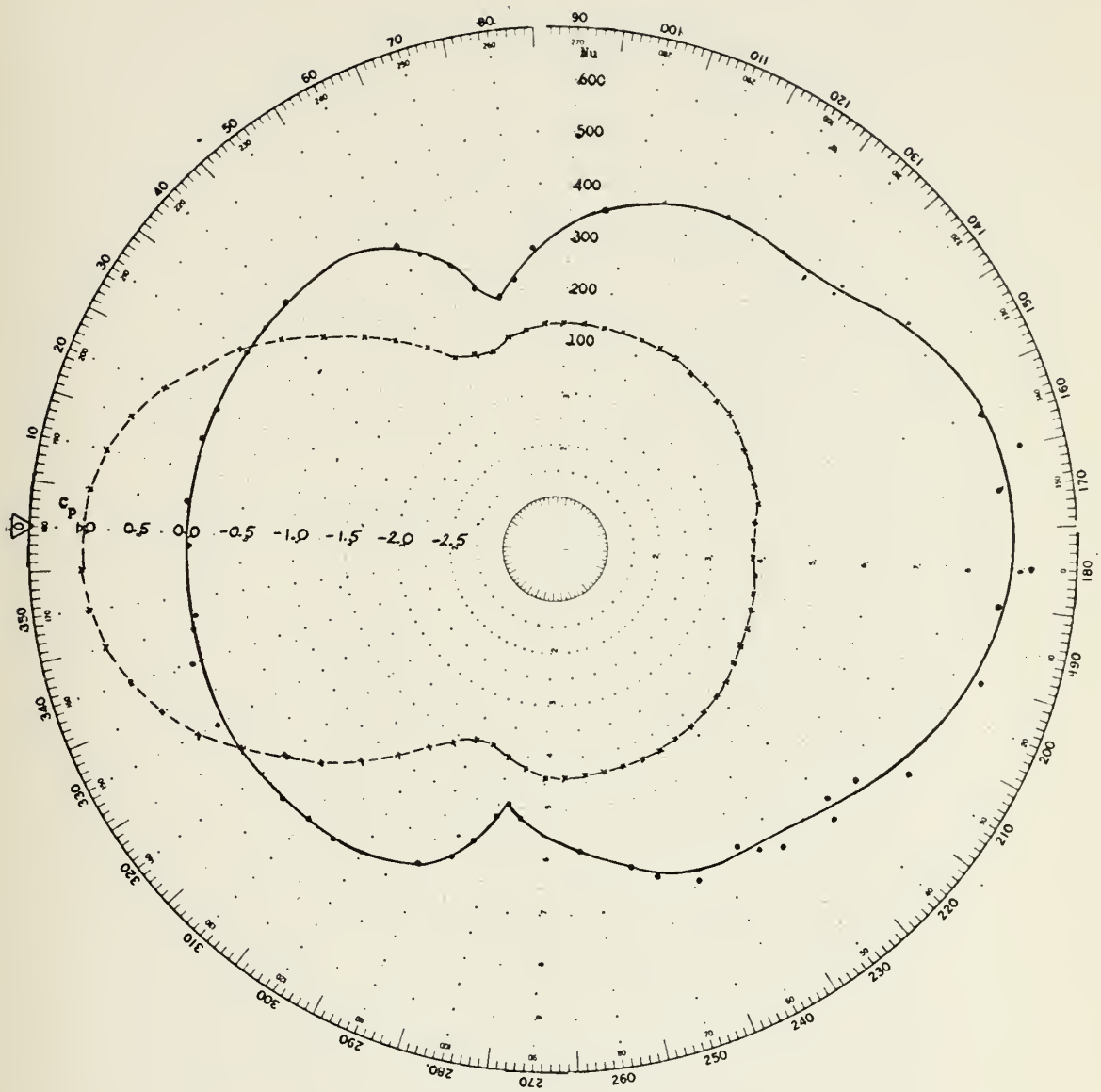

FIGURE 48. Pressure coefficient and local Nusselt number on the surface of a cylinder placed near a plane surface for:
Re = 153,000 , L/D = 2.0 , d/r = 2.0

C_p x

Nu .

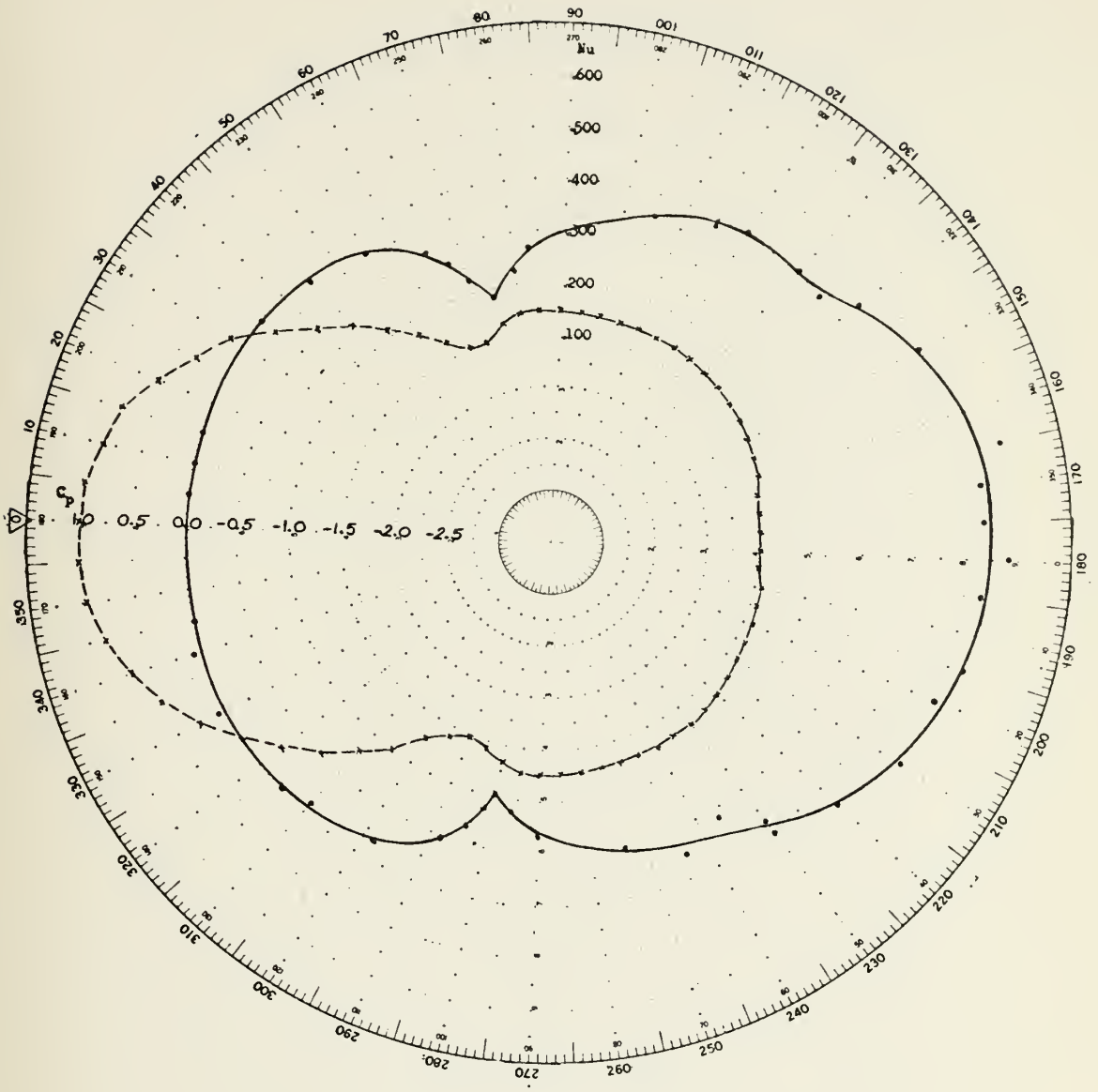

FIGURE 49. Pressure coefficient and local Nusselt number on the surface of a cylinder placed near a plane surface for:
Re = 153,000 , L/D = 2.0 , d/r = 3.0

C_p x

Nu .

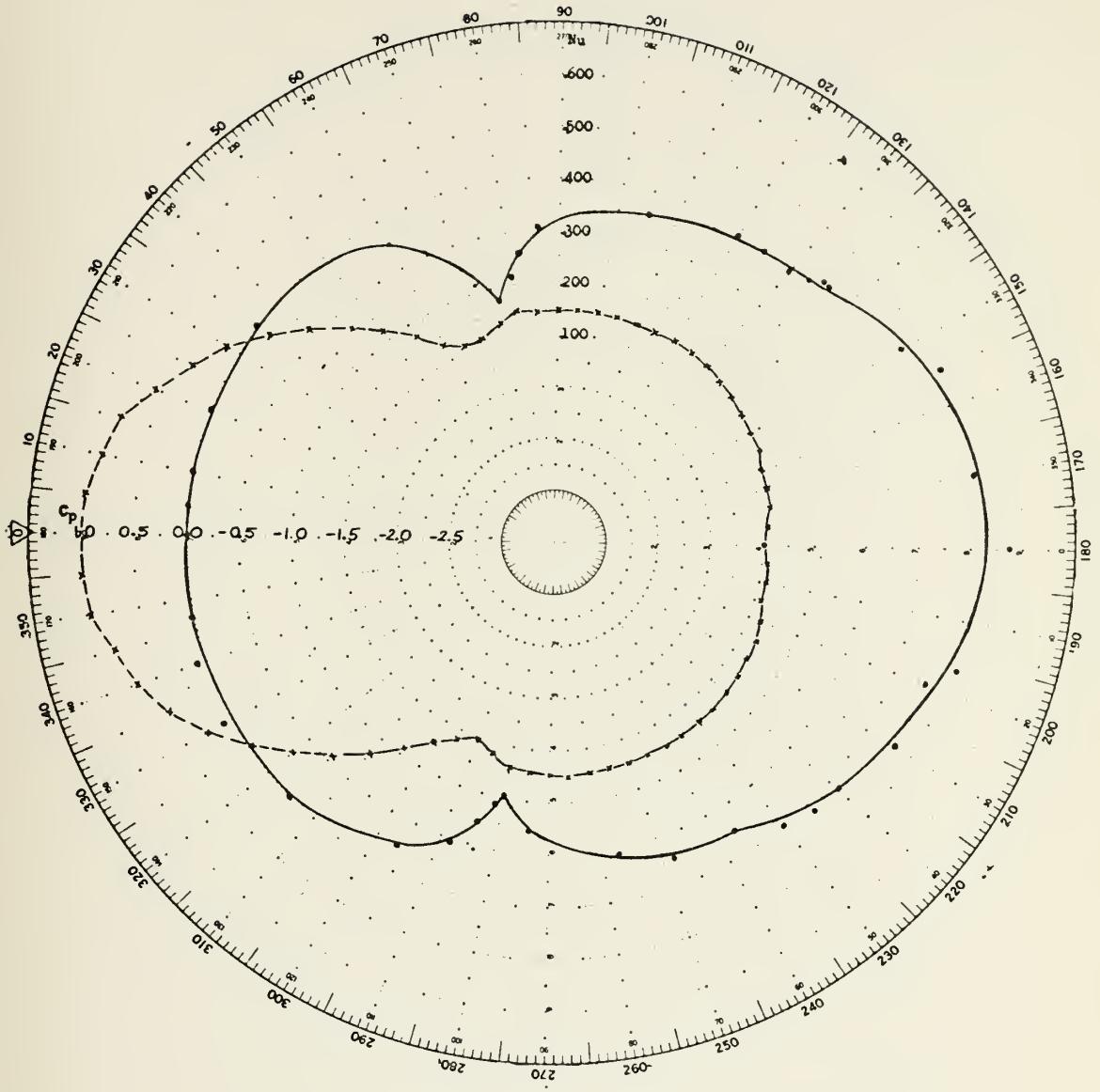

FIGURE 50. Pressure coefficient and local Nusselt number on the surface of a cylinder placed near a plane surface for:
Re = 153,000 , L/D = 2.0 , d/r = 4.0

C_p x

Nu .

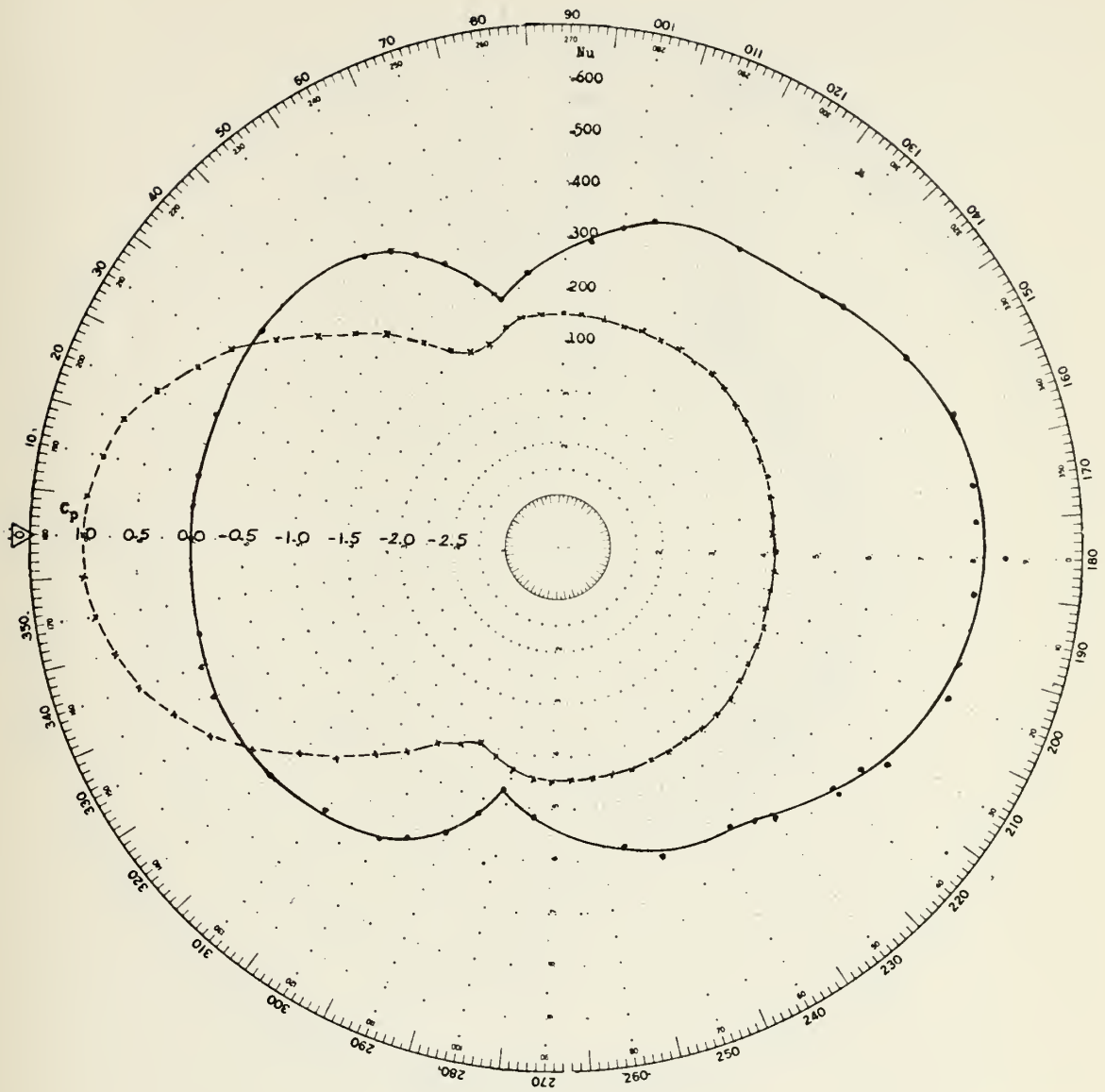

FIGURE 51. Pressure coefficient and local Nusselt number on the surface of a cylinder placed near a plane surface for:
Re = 153,000 , L/D = 2.0 , d/r = 5.33

C_p x

Nu .

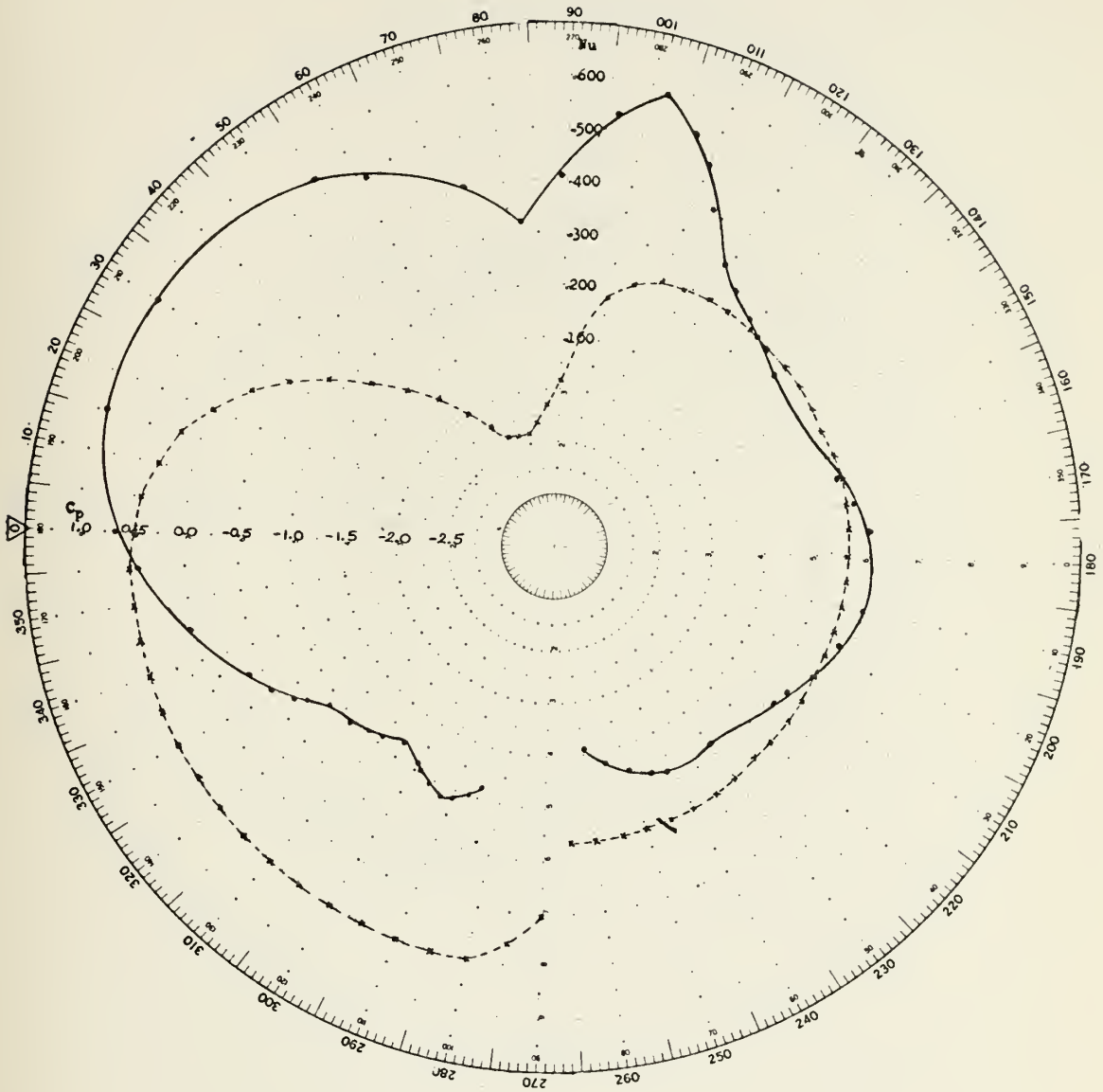

FIGURE 52. Pressure coefficient and local Nusselt number on the surface of a cylinder placed near a plane surface for:
Re = 153,000 , L/D = 8.0 , d/r = 0.0

C_p x

Nu .

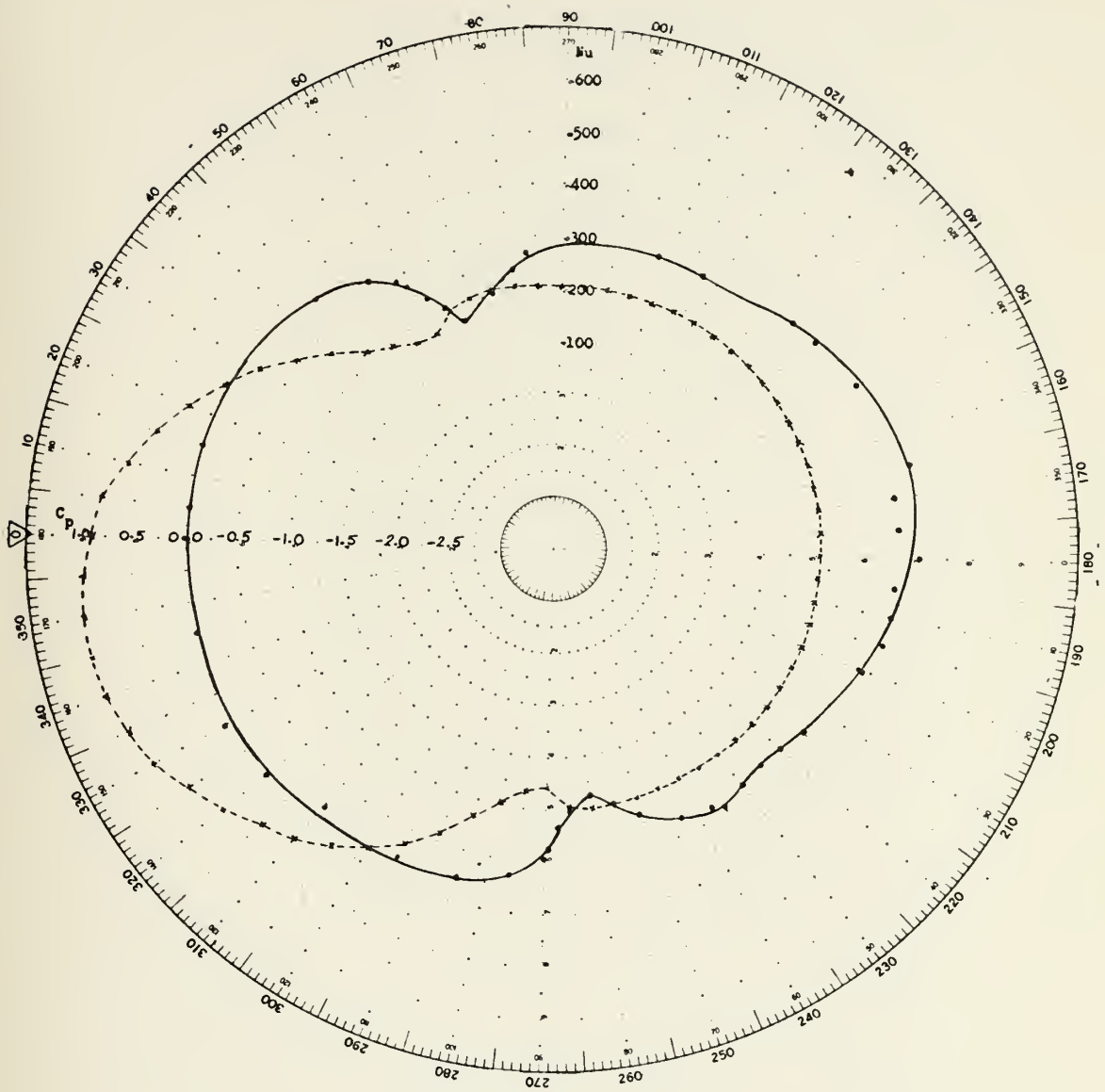

FIGURE 53. Pressure coefficient and local Nusselt number on the surface of a cylinder placed near a plane surface for:
Re = 153,000 , L/D = 8.0 , d/r = 0.25

C_p x

Nu .

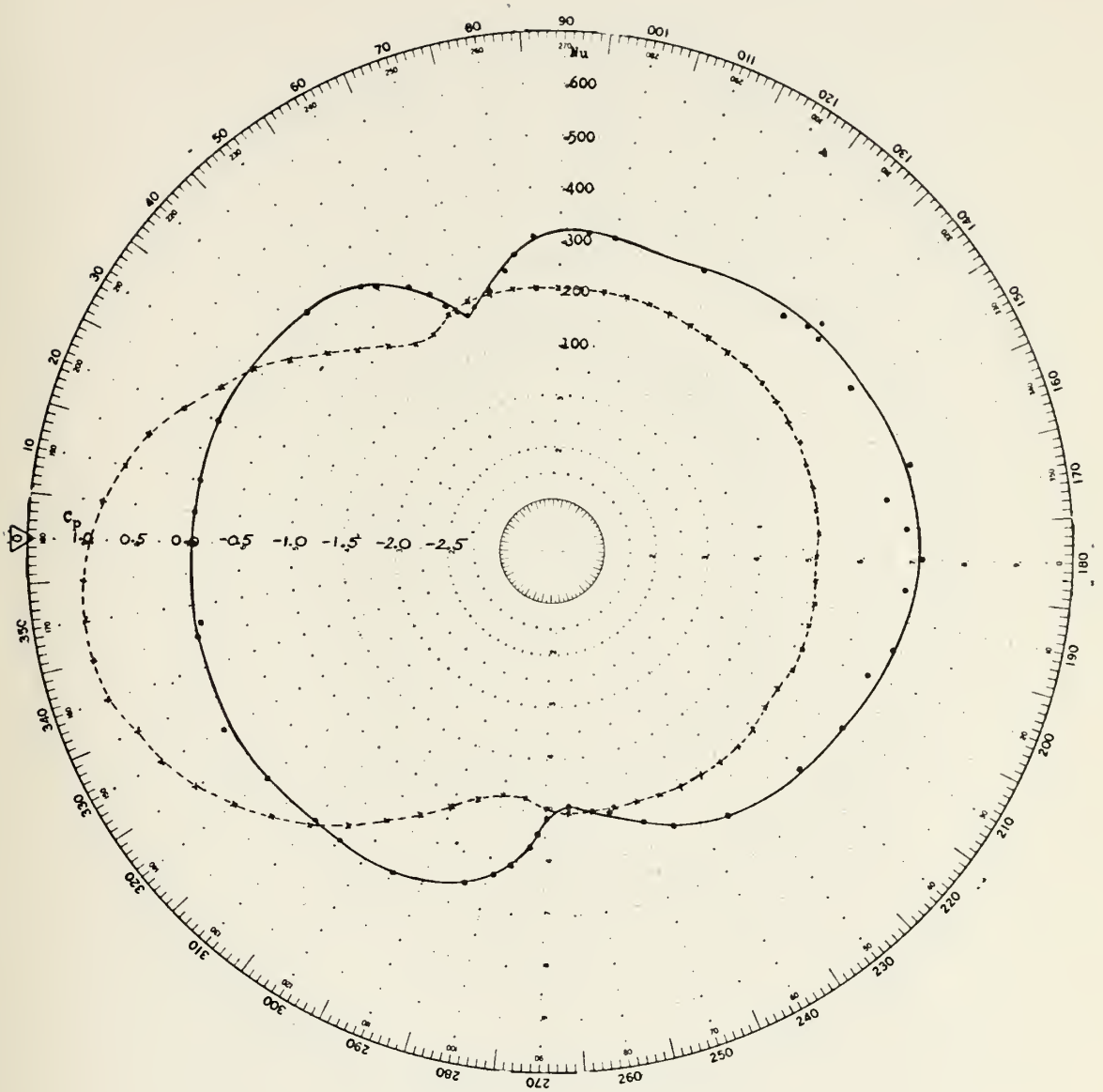

FIGURE 54. Pressure coefficient and local Nusselt number on the surface of a cylinder placed near a plane surface for:
Re = 153,0-0 , L/D = 8.0 , d/r = 0.5

C_p x

Nu .

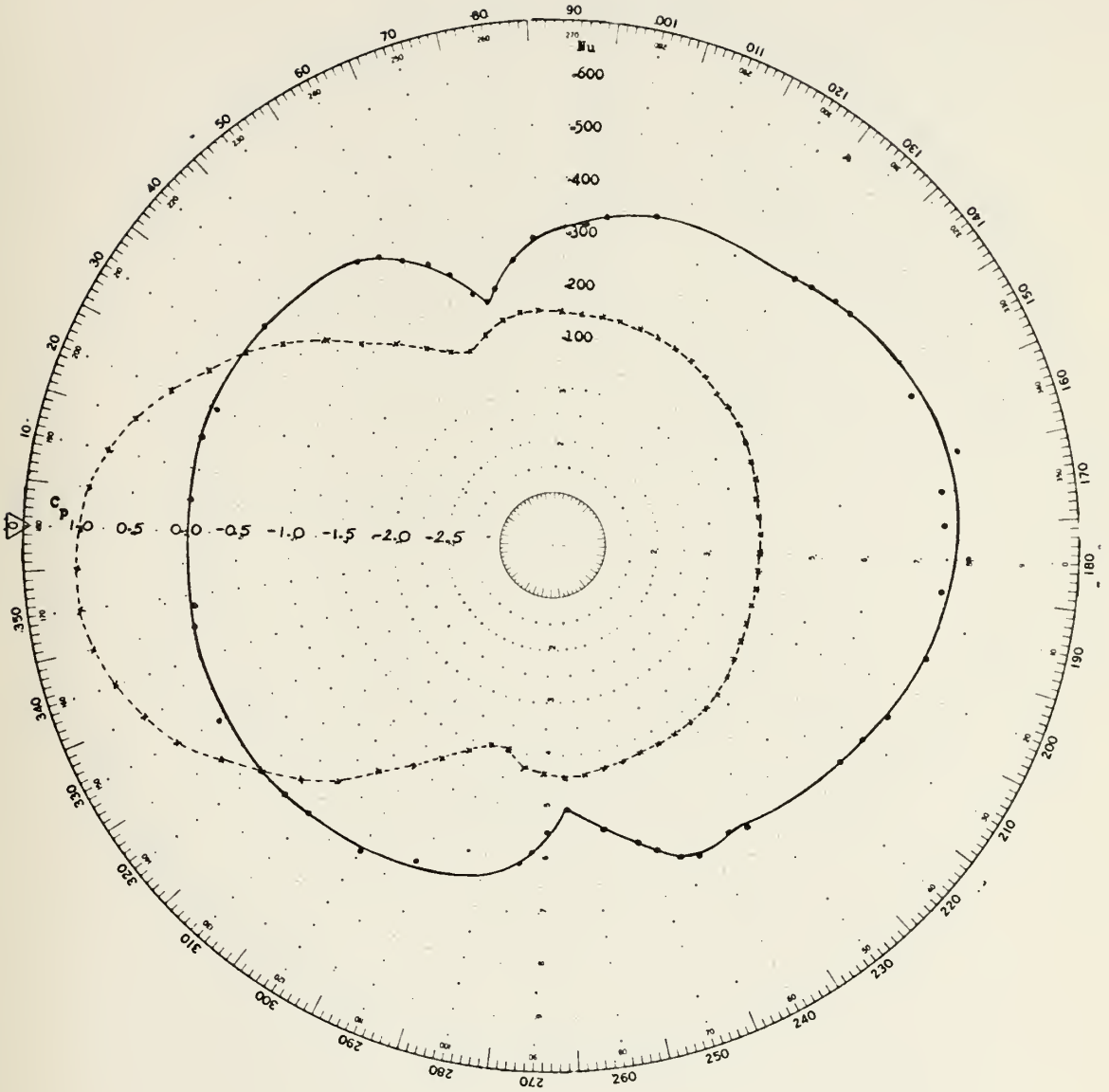

FIGURE 55. Pressure coefficient and local Nusselt number on the surface of a cylinder placed near a plane surface for:
Re = 153,000 , L/D = 8.0 , d/r = 1.0

C_p x

Nu .

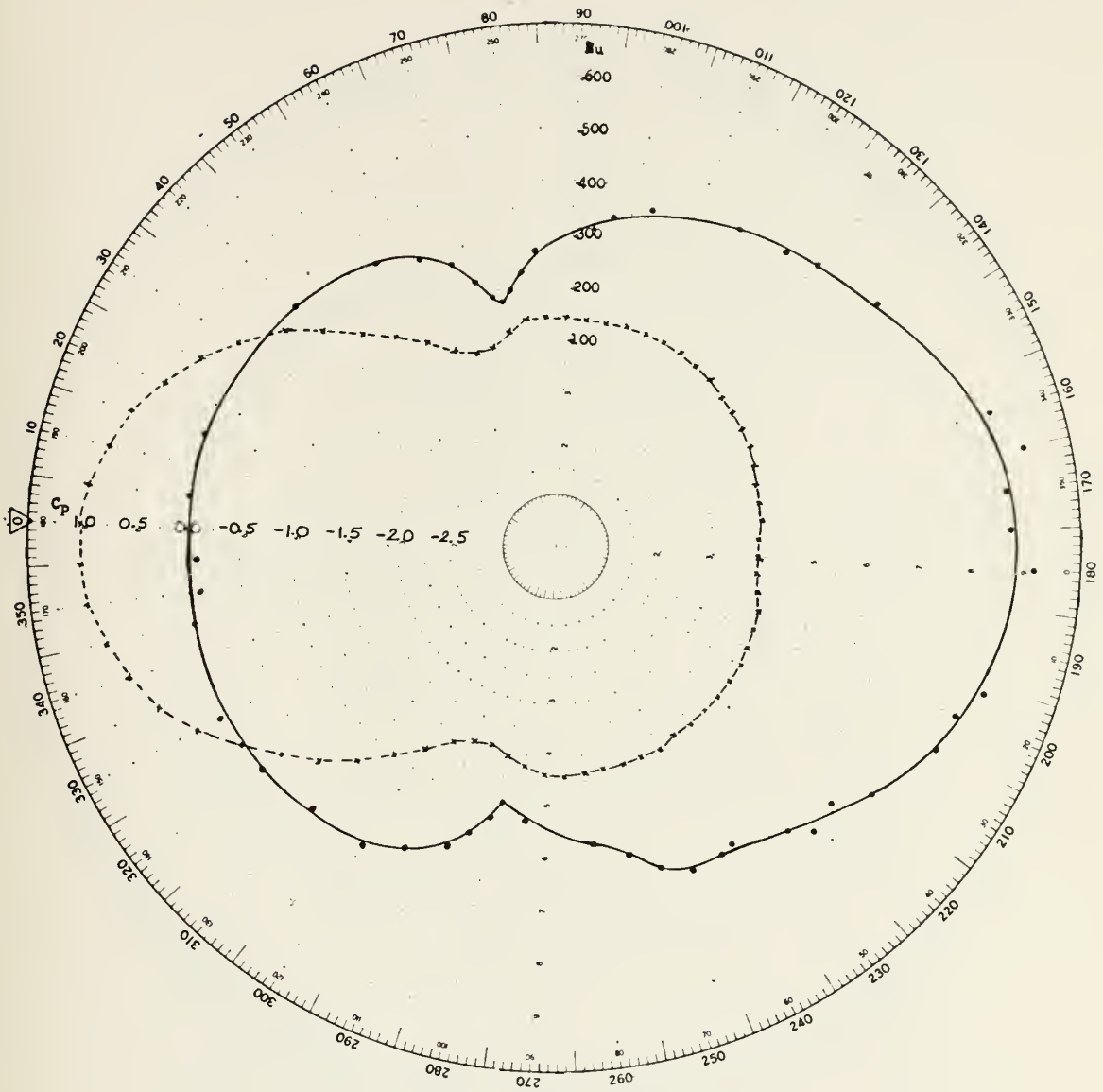

FIGURE 56. Pressure coefficient and local Nusselt number on the surface of a cylinder placed near a plane surface for:
Re = 153,000 , L/D = 8.0 , d/r = 2.0

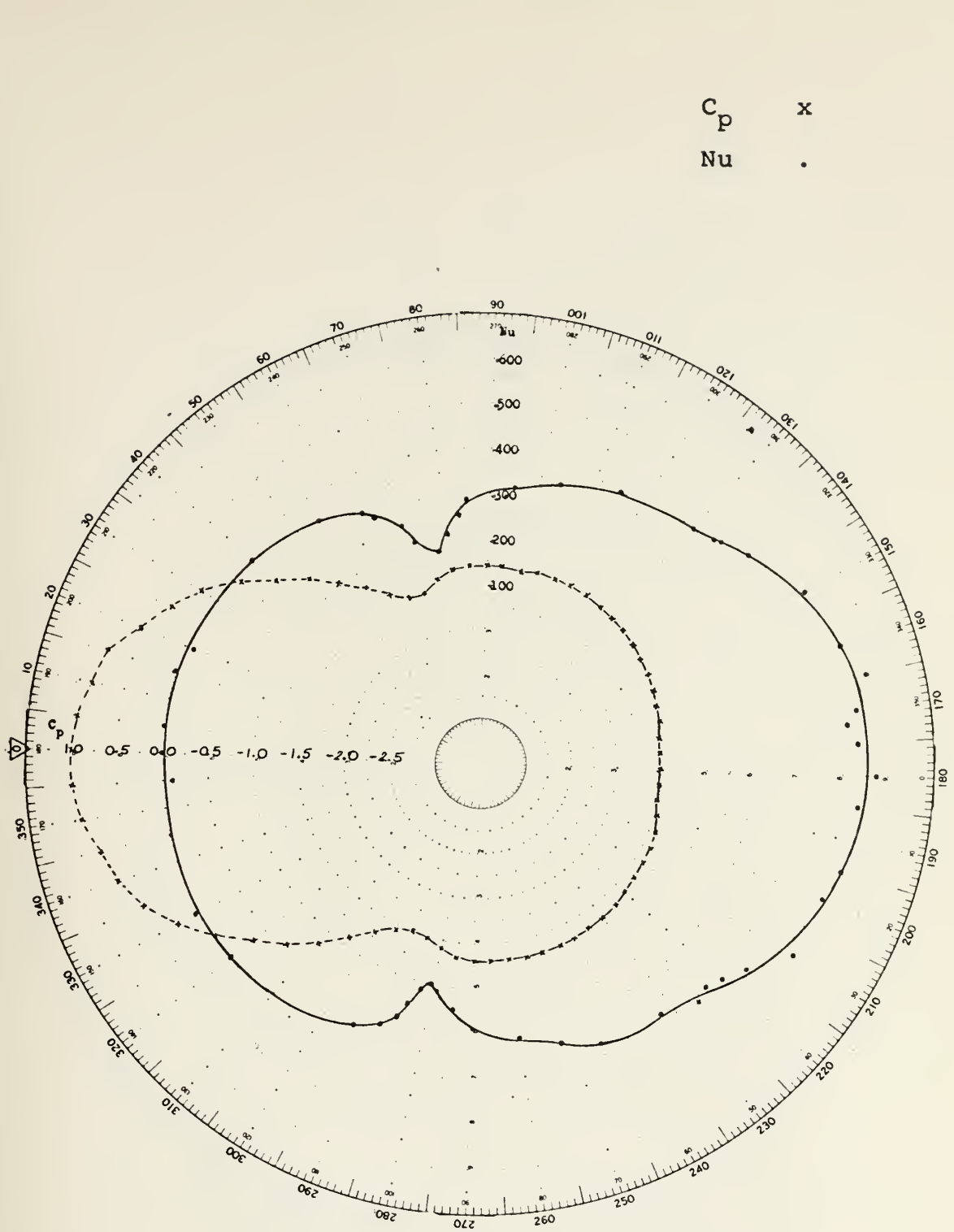

FIGURE 57. Pressure coefficient and local Nusselt number on the surface of a cylinder placed near a plane surface for:
Re = 153,000 , L/D = 8.0 , d/r = 3.0

C_p x

Nu .

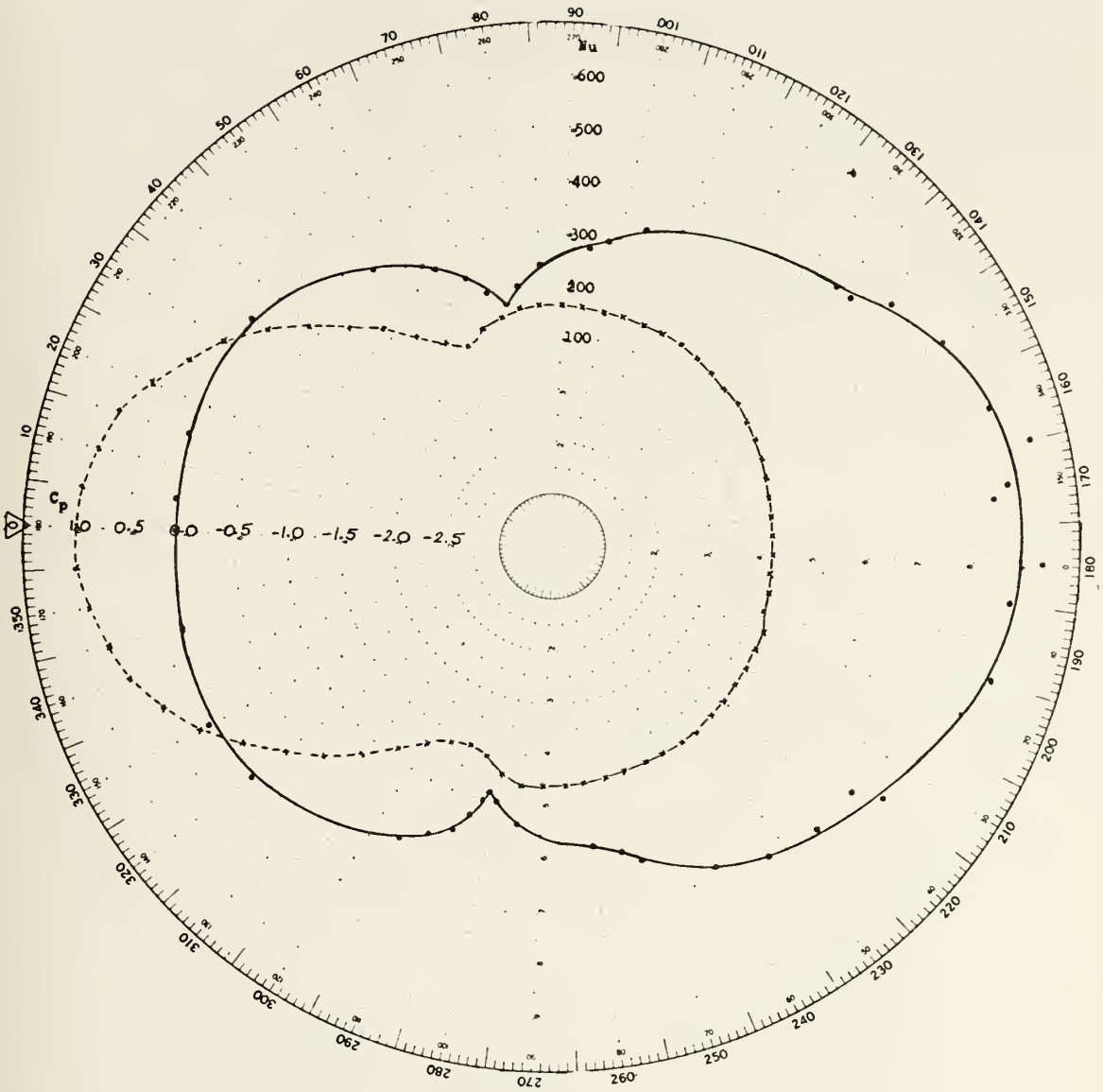

FIGURE 58. Pressure coefficient and local Nusselt number on the surface of a cylinder placed near a plane surface for:
Re = 153,000 , L/D = 8.0 , d/r = 4.0

C_p x

Nu .

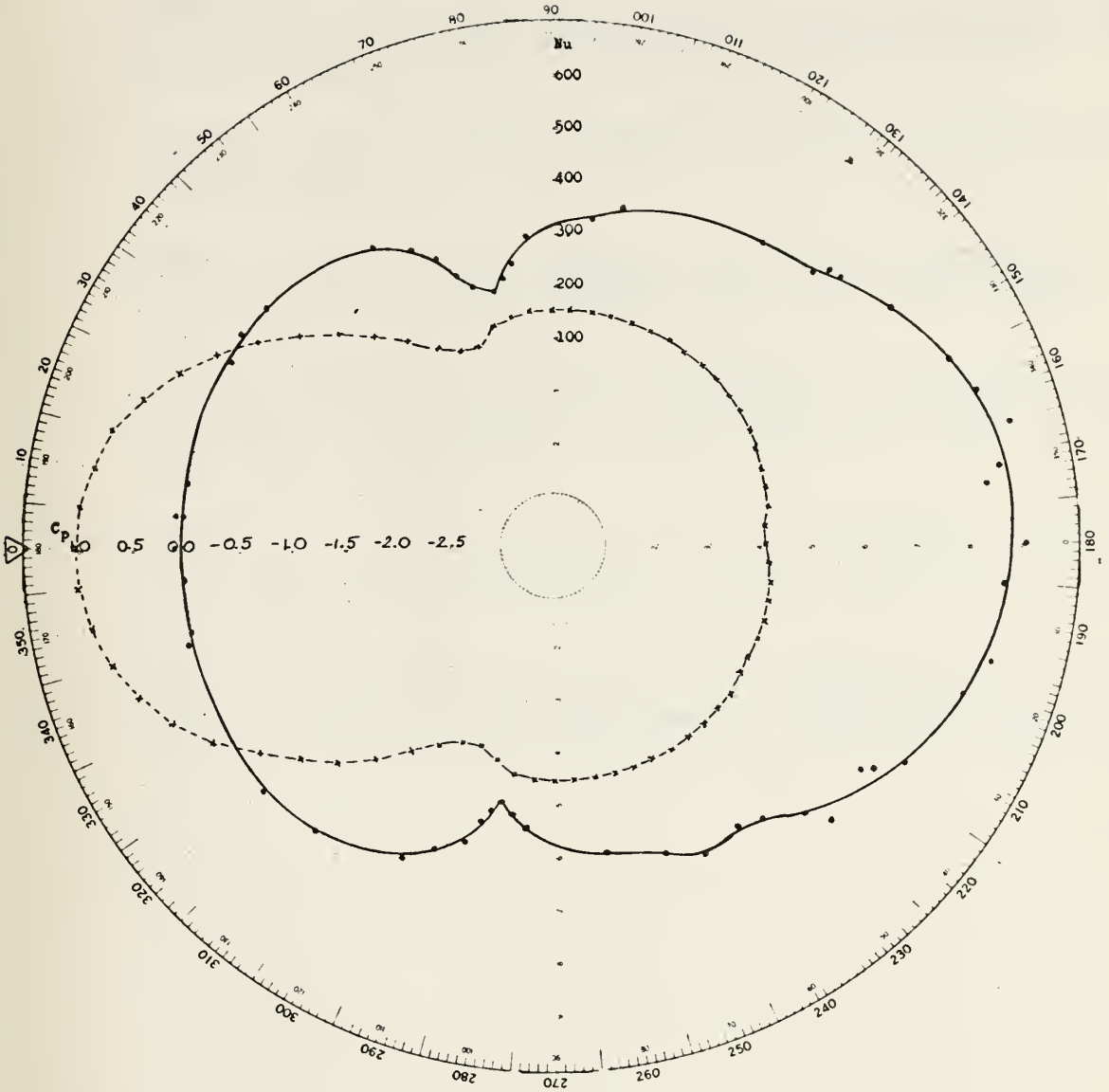

FIGURE 59. Pressure coefficient and local Nusselt number on the surface of a cylinder placed near a plane surface for:
Re = 153,000 , L/D = 8.0 , d/r = 5.33

LIST OF REFERENCES

1. McComas, J. P., Experimental Investigation of Ground Effects on a Heated Cylinder in Crossflow, M.S.M.E. Thesis, Naval Postgraduate School, 1974.

2. Gnerlich, C. H., The Convective Heat Transfer Behavior of a Heated Cylinder Located Near a Plane Surface, M.S.M.E. Thesis, Naval Postgraduate School, 1975.

3. Kosemen, Ender, Thermal Study of a Heated Cylinder Near a Plane Surface, M.S.M.E. Thesis, Naval Postgraduate School, 1975.

4. Roshko, Anatol, On the Drag and Shedding Frequency of Two Dimensional Bluff Bodies, Nat. Adv. Comm. Aero., Washington, Tech. Note 3169, 1954.

5. Spivack, Hermann N., "Vortex Frequency and Flow Pattern in the Wake of Two Parallel Cylinders at Varied Spacing Normal to an Air Stream," Jour. Aero Sci., vol. 13, no. 6, June 1946, pp. 289-301.

6. Achenbach, E., "Distribution of Local Pressure and Skin Friction Around a Circular Cylinder in Cross-Flow up to $Re = 5 \times 10^6$," J. Fluid Mech., (1968), vol. 34, part 4, pp. 625-639.

7. Kline, S. J. and McClintock, F. A., "Describing Uncertainties in Single-Sample Experiments," Mechanical Engineering, vol. 75, pp. 3-8, January 1953.

INITIAL DISTRIBUTION LIST

		No. Copies
1.	Defense Documentation Center Cameron Station Alexandria, VA 22314	2
2.	Library, Code 0212 Naval Postgraduate School Monterey, California 93940	2
3.	Department Chairman, Code 59 Department of Mechanical Engineering Naval Postgraduate School Monterey, California 93940	1
4.	T. E. Cooper, Code 59Cg Department of Mechanical Engineering Naval Postgraduate School Monterey, California 93940	5
5.	C. F. Markarian Code 4061 Naval Weapons Center China Lake, California 93555	1
6.	LT Selahattin Goktun, Turkish Navy Harmanlik Sokak No:7 Kartal-Istanbul Turkey	1
7.	Istanbul Teknik Universitesi Makina Fakultesi Taskisla, Istanbul Turkey	1